RHEOLOGICAL AND ELECTRICAL PROPERTIES OF AQUEOUS LITHIUM IRON PHOSPHATE SUSPENSION ELECTRODES

A THESIS SUBMITTED TO
THE GRADUATE SCHOOL OF NATURAL AND APPLIED SCIENCES
OF
MIDDLE EAST TECHNICAL UNIVERSITY

BY

BAYRAM YILDIZ

IN PARTIAL FULFILLMENT OF THE REQUIREMENTS
FOR
THE DEGREE OF DOCTOR OF PHILOSOPHY
IN
METALLURGICAL AND MATERIALS ENGINEERING

JANUARY 2024

Approval of the thesis:

RHEOLOGICAL AND ELECTRICAL PROPERTIES OF AQUEOUS LITHIUM IRON PHOSPHATE SUSPENSION ELECTRODES

submitted by **BAYRAM YILDIZ** in partial fulfillment of the requirements for the degree of **Doctor of Philosophy** in **Metallurgical and Materials Engineering, Middle East Technical University** by,

Prof. Dr. Halil Kalıpçılar
Dean, **Graduate School of Natural and Applied Sciences** _____

Prof. Dr. Ali Kalkanlı
Head of the Department, **Metallurgical and Materials Eng., METU** _____

Assoc. Prof. Dr. Simge Çınar Aygün
Supervisor, **Metallurgical and Materials Eng., METU** _____

Prof. Dr. Bora Maviş
Co-Supervisor, **Mechanical Eng., Hacettepe University** _____

Examining Committee Members:

Prof. Dr. Mehmet Kadri Aydınol
Metallurgical and Materials Eng., METU _____

Assoc. Prof. Dr. Simge Çınar Aygün
Metallurgical and Materials Eng., METU _____

Prof. Dr. Hüsnü Emrah Ünalan
Metallurgical and Materials Eng., METU _____

Assoc. Prof. Dr. Burak Ülgüt
Department of Chemistry, Bilkent Uni. _____

Assist. Prof. Dr. Recep Yüksel
Department of Chemistry, Eskişehir Osmangazi Uni. _____

Date: 26.01.2024

I hereby declare that all information in this document has been obtained and presented in accordance with academic rules and ethical conduct. I also declare that, as required by these rules and conduct, I have fully cited and referenced all material and results that are not original to this work.

Name Last name : Bayram Yıldız

Signature :

ABSTRACT

RHEOLOGICAL AND ELECTRICAL PROPERTIES OF AQUEOUS LITHIUM IRON PHOSPHATE SUSPENSION ELECTRODES

Yıldız, Bayram
Doctor of Philosophy, Metallurgical and Materials Engineering
Supervisor: Assoc. Prof. Dr. Simge Çınar Aygün
Co-Supervisor: Prof. Dr. Bora Maviş

January 2024, 145 pages

Developing homogeneous suspension electrodes characterized by low viscosity and high electrochemical performance is critical for the feasibility of suspension-based electrochemical energy storage technologies. One of the essential criteria for obtaining a homogeneous suspension is to use non-agglomerated particles. However, the use of agglomerated particles is unexpectedly common in most studies. This dissertation is focused on addressing the current gap in understanding the impact of the agglomeration characteristics of electroactive materials on the microstructure, flow, and electrical-electrochemical response of aqueous suspension electrodes and used lithium iron phosphate ($LiFePO_4$, LFP) as a model system. First, a procedure was developed to synthesize individual LFP particles. The results highlighted the significance of post-synthesis processes not only on the agglomeration state of particles but also showed its influence on their electrochemical response. Second, the suspension formulation was optimized to obtain homogeneous suspension electrodes capable of long-term stability. This optimization was a priori to acquiring stable and reproducible electrochemical impedance spectroscopy results. Third, the

influence of the particles' agglomeration state on the electrode characteristics was compared regarding its impact on suspensions' microstructure, percolation characteristics, flow behavior, and electrical conductivity. This study showed that utilizing individual particles enabled an increase of 50% in the solids content in the suspensions while preserving their flowability and electrical conductivity. Lastly, fructose was used for the first time in an aqueous suspension electrode. Adding fructose noticeably enhanced the suspension electrode's discharge capacity and polarization. Although the underlying mechanisms of these improvements are yet to be studied, using the optimum amount of fructose increased the initial discharge capacity of LFP particles from 129 mAh/g to 151 mAh/g in an aqueous electrolyte.

Keywords: Suspension Electrode, Agglomeration State, Flow-Assisted Energy Storage, Lithium Iron Phosphate, Suspension Microstructure

ÖZ

SULU LİTYUM DEMİR FOSFAT SÜSPANSİYON ELEKTROTLARININ REOLOJİK VE ELEKTRİKSEL ÖZELLİKLERİ

Yıldız, Bayram
Doktora, Metalurji ve Malzeme Mühendisliği
Tez Yöneticisi: Doç. Dr. Simge Çınar Aygün
Ortak Tez Yöneticisi: Prof. Dr. Bora Maviş

Ocak 2024, 145 sayfa

Düşük viskozite ve yüksek elektrokimyasal performansa sahip homojen süspansiyon elektrotların geliştirilmesi, süspansiyon bazlı elektrokimyasal enerji depolama teknolojilerin uygulanabilirliği için kritik öneme sahiptir. Homojen bir süspansiyon elde etmek için önemli bir kriter aglomere olmayan parçacıklar kullanmaktır. Ancak, beklenmedik bir şekilde aglomere parçacıkların kullanımı çoğu çalışmada yaygındır. Bu tez, elektroaktif malzemelerin aglomerasyon özelliklerinin sulu süspansiyon elektrotlarının mikroyapısı, akışı ve elektriksel-elektrokimyasal tepkisi üzerindeki etkisini anlamadaki mevcut boşluğu ele almaya odaklanmış ve model sistem olarak lityum demir fosfat ($LiFePO_4$, LFP) kullanmıştır. İlk olarak, tekil LFP parçacıkların sentezlenmesi için bir prosedür geliştirilmiştir. Sonuçlar, sentez sonrası işlemlerin sadece parçacıkların aglomerasyon durumu üzerindeki önemini vurgulamakla kalmamış, aynı zamanda elektrokimyasal tepkileri üzerindeki etkisini de göstermiştir. İkinci olarak, uzun süreli stabiliteye sahip homojen süspansiyon elektrotları elde etmek için süspansiyon formülasyonu optimize edilmiştir. Bu optimizasyon, kararlı ve tekrarlanabilir elektrokimyasal empedans spektroskopisi sonuçları elde etmek için bir önceliğe sahiptir. Üçüncü olarak, parçacıkların

aglomerasyon durumunun elektrot özellikleri üzerindeki etkisi, süspansiyonların mikroyapısı, perkolasyon özellikleri, akış davranışı ve elektriksel iletkenliği üzerindeki etkisi açısından karşılaştırılmıştır. Bu çalışma, tekil parçacık kullanılmasının, akışkanlık ve elektrik iletkenliği koruyacak şekilde, süspansiyon içerisindeki katı madde içeriğinde %50'lik bir artış sağladığını göstermiştir. Son olarak, ilk kez sulu bir süspansiyon elektrodunda fruktoz kullanılmıştır. Fruktoz eklenmesi, süspansiyon elektrodunun deşarj kapasitesini ve polarizasyonunu belirgin şekilde iyileştirmiştir. Bu gelişmelerin altında yatan mekanizmalar henüz araştırılmamış olsa da optimum fruktoz miktarının kullanılması, LFP parçacıklarının başlangıç deşarj kapasitesini sulu bir elektrolitte 129 mAh/g'dan 151 mAh/g'a yükseltmiştir.

Anahtar Kelimeler: Süspansiyon Elektrot, Aglomerasyon Durumu, Akış Destekli Enerji Depolama, Lityum Demir Fosfat, Süspansiyon Mikroyapısı

To Aysun and Çınar Ege…

ACKNOWLEDGEMENTS

I would like to express my endless gratitude to Assoc. Prof. Dr. Simge Çınar Aygün, my supervisor, and Prof. Dr. Bora Maviş, my co-supervisor, who did not spare their support and efforts in this process, who enabled me to gain a different perspective on the events and with whom I will always be proud to work and be their student.

I want to thank Prof. Dr. M. Kadri Aydınol, Assoc. Prof. Dr. Burak Ülgüt, Prof. Dr. H. Emrah Ünalan, and Assist. Prof. Dr. Recep Yüksel for their scientific contributions and guidance in the progress of my thesis studies, as well as for opening the laboratory doors to me whenever needed and sharing all their facilities with me.

I am grateful to Yusuf Tutel, a dear friend whose support I have felt since the beginning of my Ph.D. program, and to his precious family for their support throughout this journey.

I greatly appreciate you, my dear friends, Kerim Sert, Sedat Türker, and Burak Cengiz. Thank you for always being there for me and for being a constant source of support and encouragement.

I would like to thank my dear friends Elif Çoşkun and Yasemin Aşkar for their outstanding contributions to my thesis on particle synthesis.

It was a pleasure to work with my laboratory colleagues Oğuz Gözcü, Utkucan Kayacı, Doğu Şeyda, Duygu İnce, Ekin Kurşun, Murat Tuna Pamuk, Orçun Dinçer and Mert Ulusel.

Special thanks to Serkan Koylan, Mustafa Utku Yıldırım, Hasan Çelikli, Mustafa Alp Yıldırım, Doruk Bahtiyar, Nevzat Karaduman, Serkan Yılmaz, Süha Tirkeş, and Ayşenur İrfanoğlu for their support in various ways in this process.

This work was supported financially by the Scientific Research Projects Coordination Unit of Middle East Technical University with project numbers HDESP-308-2021-10814 and GAP-308-2022-10858. The Scientific and Technological Research Council of Turkey (TÜBİTAK) also supported the present research under a project with grant no 122M310.

Lastly, I would like to express my heartfelt appreciation to my wife, Aysun Yıldız, for her endless love, encouragement, patience, advice, support, and caring companionship throughout my thesis journey. To my son, Çınar Ege Yıldız, your patience and understanding have been my source of strength and motivation. I am truly blessed to have both of you by my side. I am endlessly grateful to both of you.

TABLE OF CONTENTS

LIST OF TABLES

TABLES

LIST OF FIGURES

FIGURES

LIST OF ABBREVIATIONS

ABBREVIATIONS

EES: Electrochemical Energy Storage

FAES: Flow-assisted Electrochemical Systems

RFB: Redox Flow Battery

VRFB: Vanadium Redox Flow Battery

EAM: Electroactive Material

SFAS: Suspension-based Flow-Assisted Systems

CA: Conductive Additive

Wh/L: Watt·Hour per Liter

LIBs: Lithium-ion Batteries

Na: Sodium

$LiCoO_2$: Lithium Cobalt Oxide

LMFP: $LiMn_{0.7}Fe_{0.3}PO_4$

KB: Ketjen Black

LFP: Lithium Iron Phosphate, $LiFePO_4$

Ah/L: Ampere·Hour per Liter

LTP: $LiTi_2(PO_4)_3$

LTO: $Li_4Ti_5O_{12}$

AC: Activated Carbon

TX: Triton X-100

PVP: Polyvinylpyrrolidone

DIW: Deionized Water

EtOH: Ethanol

EG: Ethylene Glycol

LiOH: Lithium Hydroxide

H_3PO_4: Ortho-phosphoric Acid

$FeSO_4 \cdot 7H_2O$: Iron (II) Sulfate Heptahydrate

PVDF: Polyvinylidene Fluoride

NMP: N-methyl-2-pyrrolidone

Li_2SO_4: Lithium Sulfate

XRD: X-Ray Diffraction

SEM: Scanning Electron Microscopy

HRTEM: High-Resolution Transmission Electron Microscope

DLS: Dynamic Light Scattering

LD: Laser Diffraction

SSA: Specific Surface Area

BET: Brunauer-Emmett-Teller

FTIR: Fourier Transform Infrared

EC: Ethylene Carbonate

DMC: Dimethyl Carbonate

CV: Cyclic Voltammetry

mAh/g: Miliampere·Hour per Gram

LFP-A: Agglomerated $LiFePO_4$

LFP-D: Dispersible $LiFePO_4$

EDS: Energy-dispersive X-Ray Spectroscopy

LVER: Linear Viscoelastic Region

EIS: Electrochemical Impedance Spectroscopy

LIST OF SYMBOLS

SYMBOLS

ζ - Potential: Zeta Potential

Ω: Ohm

CHAPTER 1

INTRODUCTION

The global energy demand continues to rise steadily due to the natural consequences of rapid population growth, the desire for high-quality goods, increased prosperity, and the ongoing modernization of societies [1,2]. The overuse of fossil fuels, their limited reserves, rising energy prices, and energy security raise concerns about energy demand. Therefore, government policies and incentives support the shift to renewable energy [3,4]. Since renewable energy resources exhibit seasonal, monthly, and even daily fluctuations, it is not possible to acquire power at a steady rate from such resources. Thus, it compels us to store the energy generated from renewable sources to compete with fossil fuels and ensure sustainability [5].

Energy storage technologies are classified according to converted energy, which is chemical, mechanical, electrochemical, cryogenic, or direct electrical energy storage [6]. Electrochemical energy storage (EES) provides a versatile, scalable, and efficient means of storing and delivering electricity. EES systems can be classified as (i) stationary–static devices (solid-state battery or supercapacitor) and (ii) flow-assisted devices (redox-flow batteries, suspension-based flow systems) (Figure 1.1) [7]. Stationary EES systems have played a significant role in developing portable consumer goods like laptops and mobile phones and in efforts to engineer electric vehicles [8]. Compared to stationary systems, flow-assisted electrochemical systems (FAES) provide greater scalability and flexibility in design. Thus, they have been intensely scrutinized for grid-scale energy storage. The most outstanding feature of FAES is the decoupling of energy and power units, giving flexible-independent construction opportunities [9].

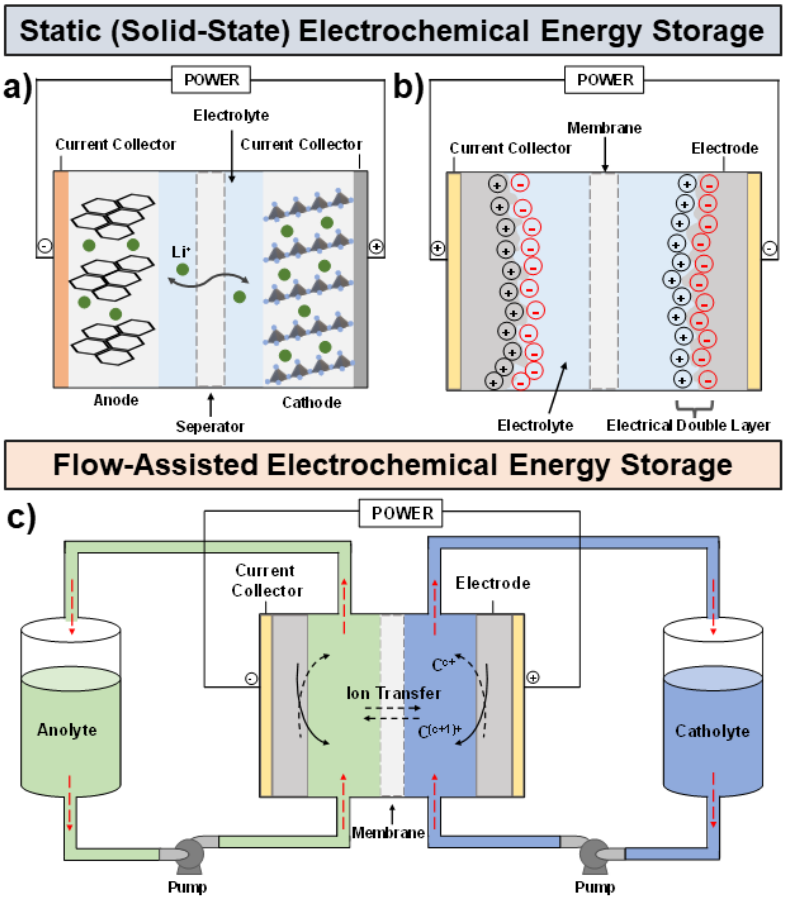

Figure 1.1 Schematic representation and basic working principles of stationary and flow-based electrochemical energy storage systems; (a) lithium-ion battery, (b) supercapacitor, and (c) redox flow battery.

A typical example of an FAES is a redox flow battery (RFB). An RFB is constructed via dissolving redox-active materials (vanadium, cerium, bromide, etc.) within the electrolyte referred to as anolyte and catholyte. The electrolytes in the external reservoirs are continuously circulated through the electrochemical cells for charge or discharge [10]. Although various materials have been studied, vanadium redox flow batteries (VRFBs) have become a hot topic due to the prominent characteristics of vanadium [11]. The vanadium-based systems are prevalent and have reached commercial fruition. However, the solubility limits of vanadium compounds are those systems' major problems. The low solubility of about 2 M remains the limiting

factor preventing intensive use as it results in relatively low energy density (~25 Wh/L) [12]. So many efforts were spent, and new strategies or approaches were proposed to overcome the solubility challenge of these systems. Suspension-based systems, where particles are dispersed (insoluble) rather than dissolved in the electrolyte, have attracted attention as one of the most promising ways to increase energy density [13,14].

1.1 Suspension-Based Flow-Assisted Systems

The fundamental challenge in RFBs is the solubility limit of the electroactive materials (EAMs) used. Therefore, efforts were generally directed toward increasing the solubility of the materials [15]. However, considering that most redox-active materials are insoluble in electrolytes, different strategies or approaches should be developed. Suspension-based flow-assisted systems (SFAS) represent one of the latest and most promising methods to fulfill large-scale energy storage demands. SFAS includes the implementation of insoluble EAMs in RFB configuration. Thus, it benefits from the high energy density of solid particles and the unique architecture of RFBs [16]. By using suspensions as electrodes, the primary concern related to the solubility limitations of RFBs would be passed over. Therefore, it enables the production of systems with increased energy-power density [17].

In an SFAS, an energy-storing suspension is created by dispersing a mixture of electroactive particles and conductive additives (CA) in a suitable electrolyte [18], as presented in Figure 1.2. Chiang's research group (Massachusetts Institute of Technology, MIT) introduced the first proof of concept of SFAS using different lithium-ion (Li) chemistries [19]. In the first demonstration, suspensions with a nominal molarity concentration of almost 12 M were obtained. The theoretical power density of suspension flow batteries was shown to be 300–500 Wh/L (with operational losses). This means nearly 20-fold higher energy-dense systems could be achieved compared to VRFBs. Such a significant leap in energy storage highlights the potential of SFAS to meet the future demand for large-scale energy storage.

Moreover, the concept of suspension electrodes also brought additional benefits to the FAESs. First, it is not restricted to one chemistry as in RFBs. Any EAM (Li [20–22], Na [23], polymers [24], carbon derivatives [25], etc.) can be utilized as long as it is dispersed in an electrolyte. Besides, SFAS is a more economical choice than RFBs because it does not require costly ion-selective membranes [19]. The variety of usable EAMs also allows for creating more economical alternatives.

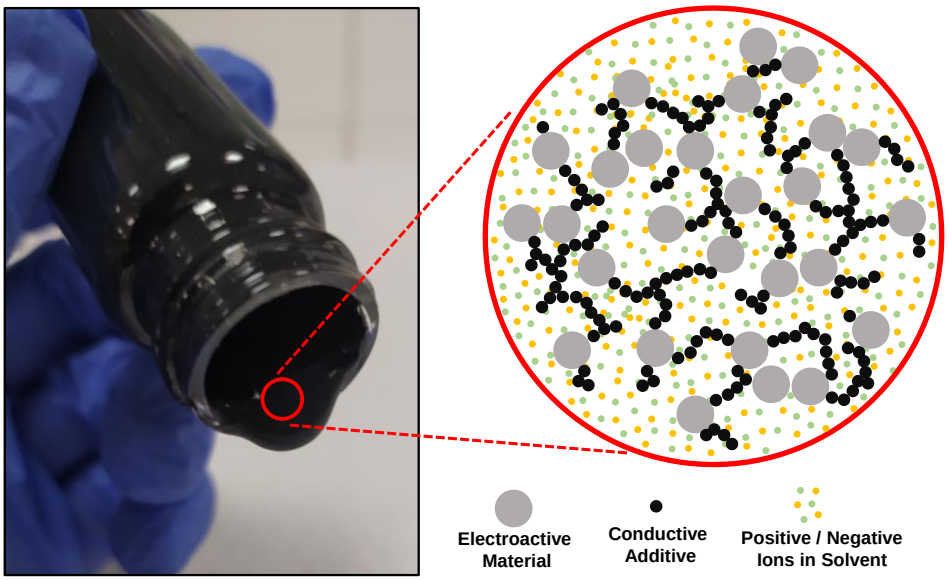

Figure 1.2 A typical suspension electrode specimen and illustration of its content.

The SFAS can be characterized or classified according to charge storage mechanisms as faradic, capacitive, and hybrid (a combination of faradic and capacitive). In grid-scale energy storage, suspension electrodes based on faradic storage mechanisms can be employed. On the other hand, capacitive storage-based suspension electrodes are convenient for use in wastewater treatment, capacitive deionization, and grid-scale energy storage. Flow batteries and capacitors equipped with suspension electrodes are two main systems under investigation for grid-scale energy storage. The working principle is similar to traditional solid-state systems, yet the electrodes are not dried and flowable dynamic systems. Intercalation/deintercalation occurs in the EAMs in

the flow-battery system, while accessible surface areas of active materials are covered with ions in the case of the flow capacitor [26].

Although the commercialization of RFBs has already come to fruition, SFAS technology is in its infancy stage and has a relatively short history - almost a decade. An MIT spinout, 24M Technologies, made progress in facilitating the manufacturing of lithium-ion batteries (LIBs) and developed a pouch cell that uses suspension electrodes. However, there is no large-scale installation of SFAS available. The critical bottleneck to commercialization and widespread use is the poor flow characteristics of prepared suspensions [16,18]. This scenario indeed influences both working and research conditions. For example, although the working principle is the same as in other conventional systems, it is impossible to see a well-established or default working system in research. Therefore, studies proceed by setting up a suitable cell arrangement in the laboratories and testing the electrodes. A noteworthy aspect is the variety of cell configurations used to measure the electrochemical performance of suspension electrodes [27]. The reported working cell types and operational modes are schematized in Figure 1.3. As depicted in Figure 1.3, three configurations are primarily utilized. The C1 configuration can be arranged as both a half-cell and a full-cell. The counter cell is organized with a stationary electrode (typically a lithium foil) without any flow in the half-cell configuration. In this configuration, the suspension electrodes in the external storage tanks are circulated through the electrochemical cells for charging or discharging processes [20]. The high viscosity of suspensions prompted the suggestion and adoption of various operating modes in SFAS. In a flow-through system (i.e., RFB), the anolyte or catholyte is continuously transported from the external tank to the electrochemical cell with a specific flow rate, and there is a circulation. The viscous nature of the suspension electrodes poses challenges to the feasibility of this mode of operation due to the high energy dissipation. For example, Duduta et al. showed that the energy required to circulate the suspension comprised 22 vol.% lithium cobalt oxide ($LiCoO_2$) – 0.6 vol.% CA accounts for almost 45% of the total energy drawn from the system [19].

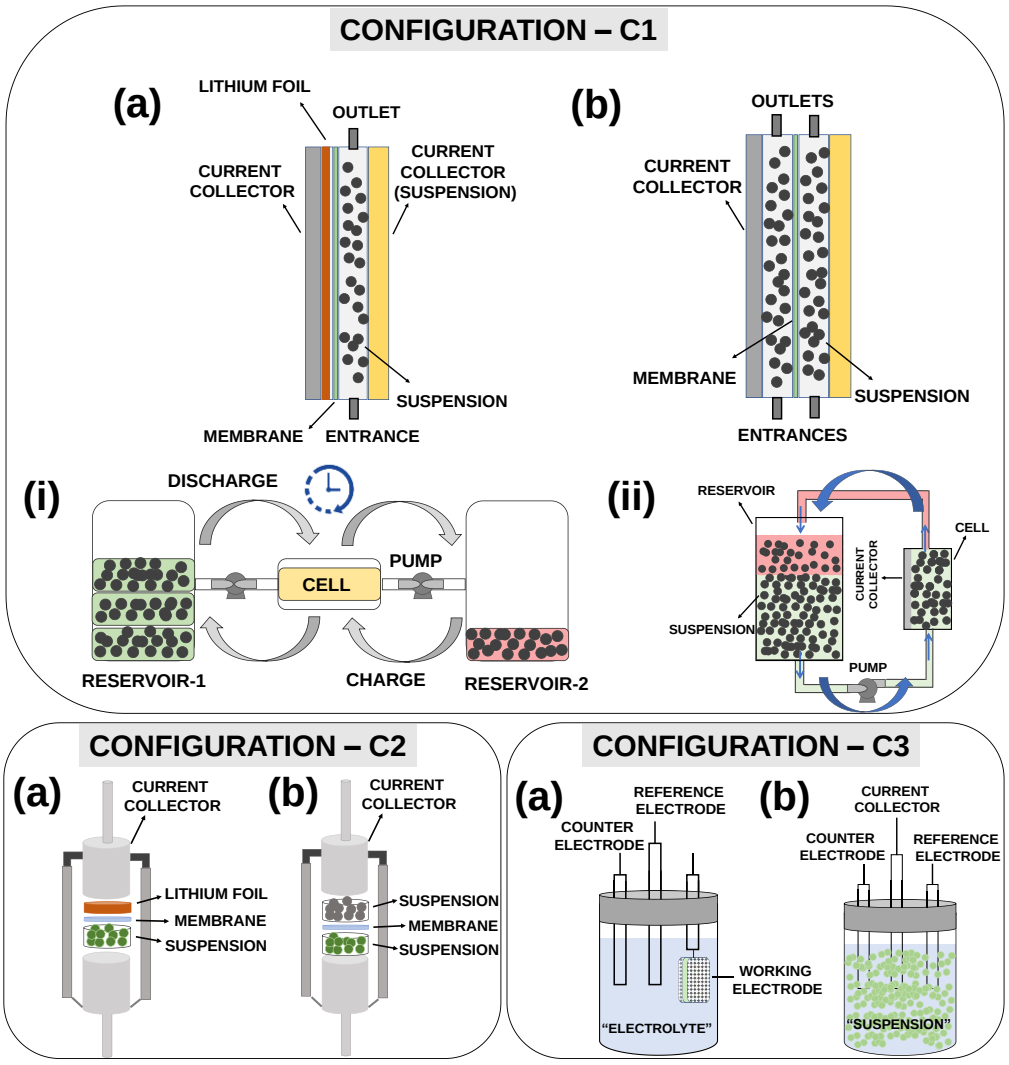

Figure 1.3 Proposed cell configurations and operational modes to evaluate the electrochemical performance of suspension electrodes; C1: flow-through system, C1-a: half cell, lithium counter electrode, C1-b: full cell, i: intermittent mode, ii: continuous flow mode (half cell presented), C2: modified Swagelok cell; C2-a: half cell, lithium counter electrode; C2-b: full cell, suspensions are present in both sides, C3: beaker-type cell, C3-a: vial system with working electrode as coin-type, C3-b: vial system with a suspension as working electrode.

High viscosity and the accompanying high energy loss are severe challenges for commercializing SFAS. Therefore, it encouraged the consideration of alternative operating modes (i.e., intermittent mode, as shown in Figure 1.3 (i)) to improve energy efficiency [28]. In the intermittent flow case, an aliquot of suspension electrode is conveyed into the electrochemical cell. After the complete charge/discharge cycle, a fresh aliquot is introduced to the cell, and the process repeats. However, it remains a fact that in numerous studies, suspension electrodes were characterized without flow. A modified Swagelok-type cell is used in the C2 configuration (Figure 1.3) [29]. In this configuration, a compartment is created where the suspension can be placed using spacers with a certain thickness. A half or full-cell setup can also be realized. In this configuration, which seems to be used in most investigations, the performance of the suspensions is studied under static (non-flowing) conditions [30,31]. Finally, the C3 configuration with beaker-type cells is also a preferred design for analyzing the performance of suspension electrodes. The suspension prepared as the working electrode is placed in a beaker-type cell. A current collector, counter electrode, and reference electrode are connected to this suspension [32]. Here, the electrochemical response of the suspension electrode can be analyzed in a static state or by stirring the suspension at a certain speed (Figure 1.3 (C3-b)). There are also investigations where the applicability of particles in suspension electrodes was explored, followed by transforming the electrode into a solid-state composite electrode and studying it in a typical 3-electrode setup (Figure 1.3 (C3-a) [33,34].

To enter the commercial market, suspension electrodes must possess a low viscosity. This ensures that the pump power to circulate the suspension remains minimized to the greatest extent possible. In vanadium-based systems, pump power loss is around 3-4%, and the viscosity of these systems is around 5 mPa·s [35]. Therefore, decreasing the viscosity of suspension electrodes to levels comparable to these values for commercialization is imperative. Considering that vanadium systems function as electrolytes with dissolved particles, the nature of these systems is notably inviscid. So, reaching these viscosity levels at suspension electrodes loaded

with large amounts of solid particles can be exceedingly challenging. Moreover, the suspension electrodes must exhibit high electrical conductivity to facilitate rapid and efficient charge transfer through the percolated network structure. Despite frequent emphasis on the importance of high conductivity in existing studies, no precise value is given. Notably, different values are recorded in many studies [20,36–40].

1.2 The Importance of Suspension Microstructure and Homogeneity

An energy-storing suspension employed in FAES serves as a dynamic system throughout the occupancy. In other words, the particle-particle and solvent-particle interactions in suspension are continuous [31]. Therefore, the flow characteristics and electrochemical behavior of suspension electrodes are closely linked to the suspension microstructure, which refers to the arrangement and distribution of particles in the liquid [41].

The suspension homogeneity refers to the uniformity and consistency of the microstructure. There is an increasing emphasis on the importance of the homogeneity of the suspension used in EES systems. This shift is attributed to its positive effects on enhancing electrochemical performance and improving the overall processability of the electrodes [42–45]. First, homogeneity is essential while establishing conductive and percolated networks by distributing a minimum amount of CAs between EAMs. Inhomogeneous distribution of EAMs and/or CAs, i.e., formation of CA or EAM clusters in electrode microstructure, breaks down or destroys the conductive pathways. This limits, if not wholly prevents, the charge transfer within the electrode and worsens the electrochemical performance [46]. Second, homogeneity is critical in obtaining low suspension viscosities. It is well-known that homogeneous suspensions have lower viscosities than their inhomogeneous counterparts [47,48]. Agglomerated or clustered structures in inhomogeneous suspensions contain immobilized water in their structure. This situation increases the effective solids fraction, resulting in higher suspension viscosity [49,50]. Moreover, suspension homogeneity holds significant importance

in terms of operational procedures, which are paramount for the feasibility and commercialization of SFAS. The viscous nature of heterogeneous suspensions can lead to relatively high energy consumption for suspension circulation, blockage in transfer pipelines or channels, etc. [51–53]. Hence, developing optimal suspension microstructures, characterized by a uniform distribution of CAs and EAMs, is crucial for the feasibility of SFASs and their integration into energy storage systems. This achievement is integral to attaining the desired viscosity and electrical conductivity to create high-performance electrodes.

1.3 Literature Survey of Suspension-Based Flow-Assisted Systems

Suspension microstructure is essentially governed by suspension features such as particle concentration, particle size, shape and type, dispersion uniformity, stability, and solvent properties. Numerous studies were devoted to understanding microstructural evolution and improving suspension electrode dispersion quality and stability. Existing studies are broadly categorized and summarized under three sub-headings: i) effect of suspension composition, ii) effect of particle characteristics, and iii) improvement of suspension microstructure.

1.3.1 Effect of Suspension Composition

The composition of the suspension electrode components was evaluated for their mutual influence on the microstructure, electrochemical behavior, and the processability of the electrodes. The proposed working principle of suspension electrodes depends on forming a percolation network. A percolation network is established by CAs to facilitate electron transport in the electrode structure. CA is also essential to compensate for the low conductivity of EAMs [26]. As expected, the CA is the root cause of the electrical conductivity of the suspension. Hence, with increasing CA, more conducting systems are obtained. However, the suspension viscosity increased significantly when using CAs, even in small quantities. For

instance, Su et al. reported forming a percolated structure in suspensions containing 10 wt.% $LiMn_{0.7}Fe_{0.3}PO_4$ (LMFP) through the addition of 0.5 – 0.6 wt.% CA, namely Ketjen Black (KB) [37]. Adding this small amount, which resulted in nearly a 100-fold increase in suspension conductivity, also caused a 5-fold rise in suspension viscosity. The use of CA in suspension electrodes is critical for better conductivity. However, it reduces the loadable EAM to the structure (due to high viscosity), which limits the energy density. A suspension electrode can also be engineered without using CAs [54]. The pioneering study eliminating CA from suspension demonstrated that the suspension electrode approach could work based on particle-particle and particle-current collector interactions (Figure 1.4) [32]. Considering that most EAMs have very low electrical conductivities [55], such an approximation necessitates different developments/adjustments in the cell design. Yet, this brings another challenge to suspension electrode research. If we analyze the impact of CA on the microstructural variation of suspension electrodes within this context, it was shown that eliminating CA can reduce suspension viscosity [56]. Additionally, it was demonstrated that EAM content ($LiFePO_4$ (LFP)) that can be loaded per unit volume can be increased by up to 40%, showing an energy capacity of 68 Ah/L with 3D current collectors.

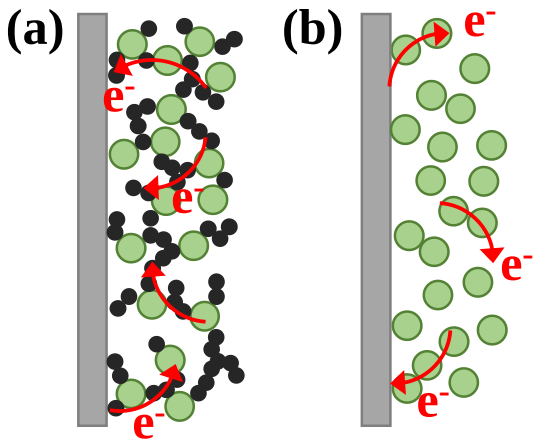

Figure 1.4 Charge transfer mechanisms in the suspension electrodes; (a) conductive additive-based percolation network and (b) particle-particle and particle-current collector collisions.

A significant advantage of the suspension electrode approach lies in the broad range of materials that can be utilized in these systems. It was observed that several materials that exhibit both faradic [57,58] and capacitive [59,60] properties were tested in different studies. Preparing suspensions with high EAM content is essential to obtaining a system with high energy density. However, it was demonstrated that the concentration of EAM has a notable impact on suspension microstructure. The EAM content significantly influences both the electrical conductivity and rheological behavior. A relatively higher suspension concentration (compared to the literature) was achieved by Li et al. in aqueous electrolytes [36]. In the study, 15-20 vol.% LFP and 27 vol.% $LiTi_2(PO_4)_3$ (LTP) (for 1 vol.% KB) were obtained. However, only 5 vol.% augmentations in LFP content (from 10 vol.% to 15 vol.%) for the suspension with 1 vol.% KB exhibited nearly 5 times higher viscosity at the shear rate of 10 s^{-1}. Comparable behavior was noted in suspensions containing LTP. However, it is essential to highlight that the viscosity values of suspensions prepared with LFP were significantly higher than those equipped with LTP. This implies that the types or properties of the employed EAM influence the microstructure, which will be discussed in detail in the following subheading. It was demonstrated that obtaining suspensions with high EAM content can increase energy density. However, it is noteworthy that electrochemical analyses of suspension electrodes were mainly conducted with significantly lower EAM content, which may stem from their paste-like structures [36,61].

The CA to EAM amounts ratio was also critical in obtaining the desired interconnected and highly conductive percolation networks. Li et al. showed that conductivity in suspensions prepared with 0 – 2.5 vol.% KB and 10 – 20 vol.% LFP can only be achieved after a certain amount of CA is reached [36]. Besides, the critical value was found to depend on the active particle loading amount (Figure 1.5). For instance, to achieve the electrical conductivity exhibited by a suspension containing 20 vol.% LFP and 1 vol.% KB, it was demonstrated that 2.5 vol.% KB must be added to a suspension with 10 vol.% LFP. Forming a percolated network structure in systems with high particle loading seems possible with much less carbon

addition. This may be attributed to increased crowdedness in the structure and the carbon-coated nature of EAMs. However, in both relatively higher or lower EAM content, the presence of the reticulated structure causes the viscosity values to increase to levels that prevent flow. The optimum ratio of CA to EAM was also emphasized by Youssry et al. [62]. In that study, the effect of EAM content on the rheo-electrical properties of $Li_4Ti_5O_{12}$ (LTO)/KB suspensions in organic media was investigated. They reported that too much increase in the EAM content (above 20 wt.% LTO for 2 wt.% KB) in suspension weakened the network strength. This resulted in a disjoint conducting network, inhibiting the transfer of electrons between KB islands in the electrode. Increasing the LTO content in the suspension also decreased the overall viscosity as it disrupted the CA continuity. The rupture of conductive networks with increasing electroactive particle loading has been reported in other studies [29,63]. The findings revealed that capacity decreases were due to the inability to use some electroactive particles effectively.

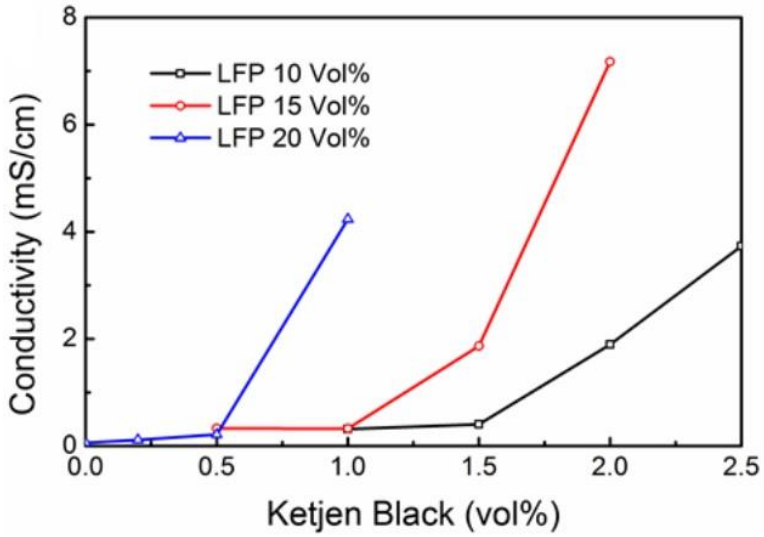

Figure 1.5 Variation of suspension electrical conductivity concerning the amount of electroactive material and conductive additive [36].

Considering all these aspects, it becomes evident that the suspension's composition influences the electrode's microstructure. Therefore, it is the decisive factor in suspensions' flow and electrochemical response.

1.3.2 Effect of Particle Characteristics

Particles dispersed in a suspension can exhibit different dispersion characteristics due to many properties such as particle size, dimension, morphology, and aspect ratio. This can lead to significant variation in the suspension microstructure and, hence, the corresponding flow and electrochemical behavior. The particle size of both CAs and EAMs was shown to be a critical parameter influencing the microstructure of the suspension. In one example, the percolation characteristics of two common CAs, KB (square and 300 nm) and Super C45 (spherical and 750 nm), were investigated by Youssry et al. [64]. The research revealed two significant rheological concentrations for both suspensions: the transition from liquid to weak gel structure and the transition from weak to strong gel structure. The critical rheological transition concentration ranges were lower in KB suspensions compared to C45 suspensions. Viscosity measurements further supported these values. The suspensions formed with larger CA particles had lower viscosity than their counterparts. The electrical percolation thresholds of the suspensions were also noted to vary based on the size of the CA. While the sample prepared with KB exhibited a conductive pattern at 0.003 vol.%, this value was determined to be 0.014 vol.% for the C45 suspension (Figure 1.6).

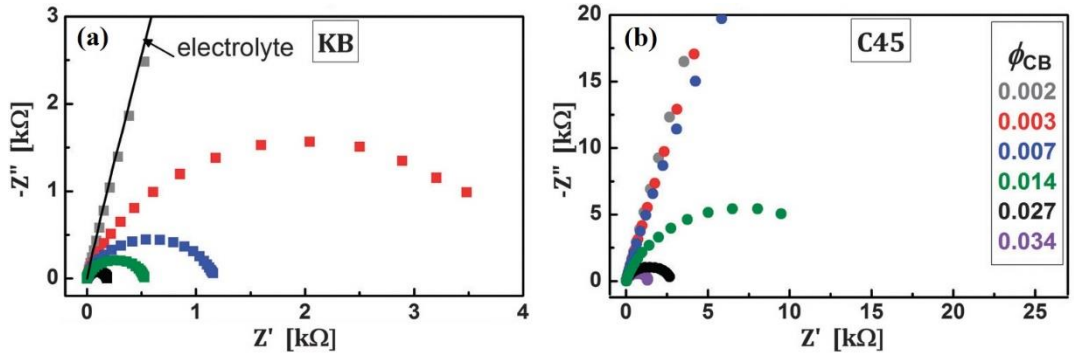

Figure 1.6 Dependence of the electrical percolation threshold of the suspension on the size and type of employed conductive additive; (a) Ketjen Black (KB, square and 300 nm) and (b) Super C45 (C45, spherical and 750 nm) (adapted from ref. [64]).

In another study with EAMs of similar aspect ratio, Campos et al. revealed that an increase in particle size resulted in a suspension with better flowability [65]. They also found that the aqueous suspensions, prepared with irregularly shaped activated carbon (AC), exhibited the highest viscosity compared to those with spherical carbon beads, as shown in Figure 1.7.

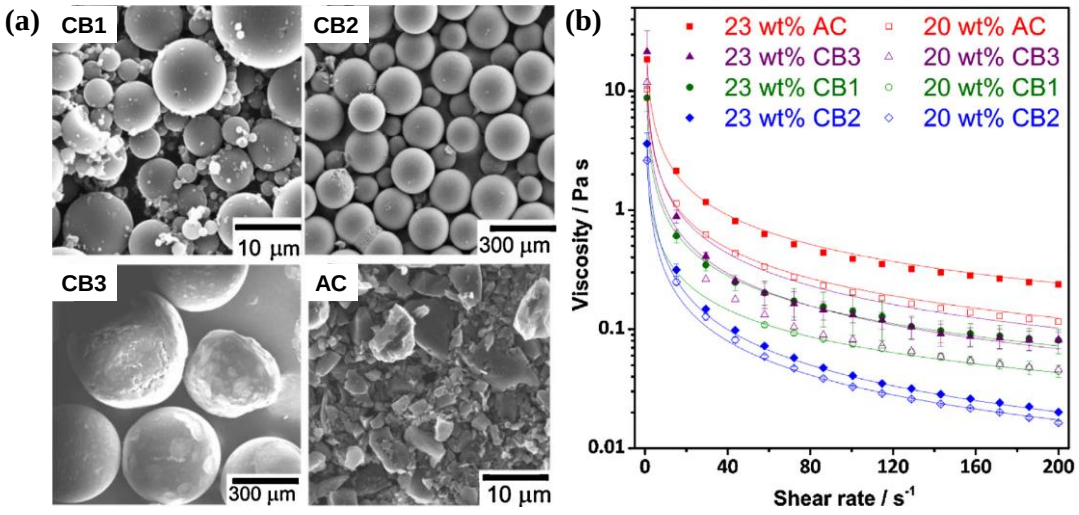

Figure 1.7 (a) Scanning electron micrographs informing about the size and shape of electroactive carbon beads (CB) and (b) Rheological behavior of suspensions regarding different solids content (adapted from ref. [65]).

The morphology and dimensions of the CA and/or EAM were other factors affecting suspensions' rheological and electrical conductivities. Percolation characteristics of CAs with different dimensions-morphologies (carbon black, carbon nanotubes, and graphene nanoplates) on suspension electrode behavior were examined by Akuzum et al. [66]. It was reported that agglomerate formation tendency influenced the packing efficiency of particles with various aspect ratios. The electrical conductivity increased with increasing CA concentration regardless of the particle morphology. However, the difference in resulting volumetric occupancy, which depends on the particle morphology, determined the resulting suspension's electrochemical and rheological response. The best compromise between electrochemical and rheological performance was provided by particle morphologies that enable the maximum material packing achieved before the rheological percolation threshold. In another study, Su et al. investigated the influence of EAM morphology (nanorod, nanosheet, nanoparticle) [40]. The suspension viscosity and electrical conductivity increased with EAM content up to 20 wt.% for each particle morphology at fixed CA concentration. At higher EAM contents, suspension viscosities continued to increase. However, conductivity values decreased as the percolated structure broke down due to the increased crowdedness of EAM. The flow characteristics of the suspensions were also found to depend on the particle morphology regardless of solids content. Suspensions prepared with EAM in the form of nanosheets consistently exhibited the highest viscosity.

Studies on the impact of EAM and/or CA particle characteristics in suspension electrodes revealed that the suspension microstructure, flow, and electrical properties were susceptible to the particle characteristics. This signifies that the characteristics of the employed particles must be taken very seriously for suspension electrodes to be commercialized and compete with current technologies.

1.3.3 Improvement of Suspension Microstructure

Reducing inter-particle forces through colloidal stabilization prevents the agglomeration of particles. Hence, it promotes a more uniform distribution of particles within the liquid medium. There are instances where this approach was also employed in studies related to suspension electrodes (in SFAS).

Employing surfactants or modifying the surface of particles is a common approach to attain a homogeneous suspension structure. Due to two distinct particles with potentially varying surface characteristics in the suspension electrodes, employing non-ionic surfactants becomes a promising approach. This is because non-ionic surfactants may hinder the flocculation settlement of particles and diminish the contact between particles [38]. This enhancement in stability is crucial for maintaining a homogeneous suspension, ensuring optimal performance in electrode applications. Madec et al. showed the inclusion of a non-ionic surfactant, Triton X-100 (TX), reduced attractive forces between KB clusters in the suspension electrode [67]. Such an impact led to a more homogeneous distribution of KB without disrupting the 3D conductive network in an LTO-KB suspension. The homogeneous dispersion of KB agglomerates allowed the wiring of all LTO particles and improved overall discharge capacity. It was also observed that surfactant improves the suspension viscosity by a factor of 10 at high shear rates. In another investigation by Wei et al., polyvinylpyrrolidone (PVP) allowed for the independent adjustment of particles' stability in the two-particle system [27]. Adding PVP created a biphasic structure, promoting a more homogeneous distribution of LFP and KB particles. This enabled the engineering of more concentrated suspension electrodes with comparable flow behavior. However, the electrical conductivity of the acquired biphasic structure decreased upon adding PVP. It contradicted the LTO-KB suspension examined by Madec et al., in which the suspension's electrical conductivity improved with TX-100. Similar flow and electrical response variation was also reported by Wu et al. [38]. Agglomeration of silicon nanoparticles is suppressed by the introduction of steric interactions due to the attachment of PVP

polymer to the surface of particles. Thus, the flowability of the suspension was enhanced with a certain amount of PVP use. However, it was not valid through the use of TX-100 in the same suspension as it reacted with salts in the suspension. These findings suggest that the impact of the non-ionic surfactants on the flow and electrical characteristics of suspension electrodes is somewhat contingent on the surfactant type and suspension composition.

Surface modification of EAMs is another choice to improve the colloidal stability of the systems. Steric stabilization of γ-Fe_2O_3 (maghemite) was realized by Timofeeva et al. by grafting 3-(trihydroxysilyl)-1-propane sulfonic acid on the nanopowders [34]. The grafting of maghemite nanoparticles' surface led to a nearly threefold reduction in the average particle size. It also improved the flowability of the suspension. The maximum amount of solid material loaded into the suspension could be increased from 15 vol.% to 40 vol.%. Although the viscosity was reduced, a significant decrease in the specific discharge capacity due to grafting was noted.

The reported studies proved the significant effect of stabilizing additives or dispersants in controlling the microstructure of the suspension electrodes.

1.4 Agglomeration State of Particles

When a particle system is characterized in terms of average size, it is assumed to be composed of individual particles. It refers to single and isolated entities with distinct boundaries. These particles are considered suspended in any liquid media and homogeneously dispersed. However, different forces, van der Waals, capillary forces, or even stronger chemical bonds cause primary or individual particles to adhere together and create agglomerates. Agglomerated particles may display varying properties compared to individual particles, with their behavior being determined by the collective characteristics of the clustered particles [68]. For example, individual particles and agglomerates behave differently when dispersed in a liquid. The variation in this behavior is illustrated in Figure 1.8.

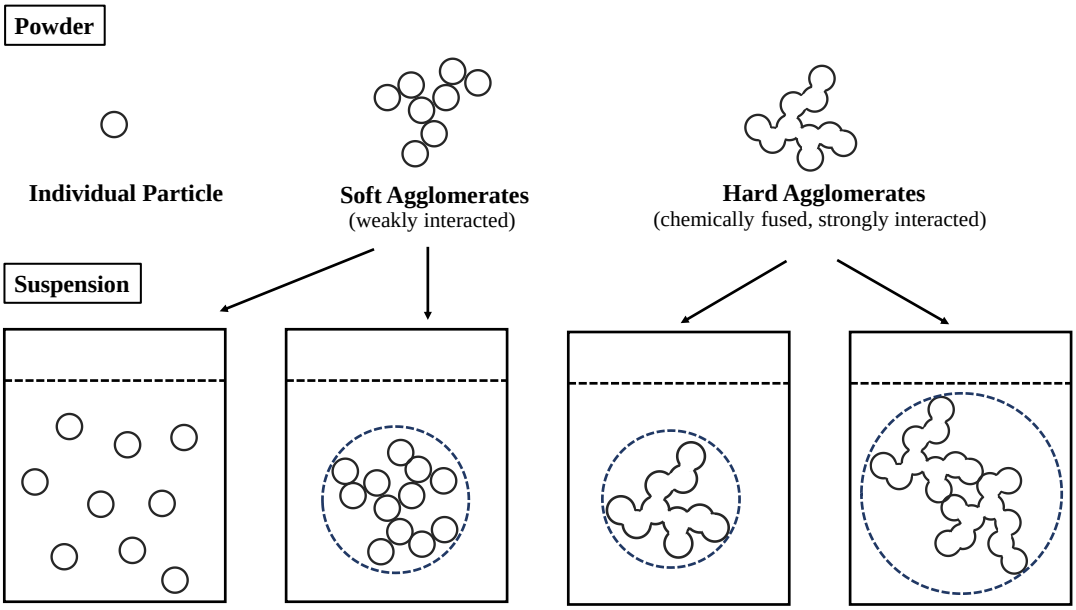

Figure 1.8 Possible state of the particles in dry form and a liquid media.

The soft agglomerates may either disintegrate into primary particles or persist as agglomerates when dry powders are dispersed in a liquid. In contrast, hard agglomerates cannot break apart; instead, they either retain their existing state or merge into larger clusters. This difference in behavior results in variations in dispersion stability since the agglomerates have a high settling rate in the liquid. Furthermore, this variation in particle distribution also impacts the maximum achievable solids content, a crucial factor influencing the energy capacity of the suspension. A suspension of agglomerated particles exhibits heterogeneous behavior. The heterogeneity increases the corresponding viscosity, which poses a significant challenge to processability. In addition, a detrimental effect on the electrochemical response would seen. Therefore, the agglomeration state of the particles is an effective parameter for the ultimate suspension microstructure, homogeneity of the suspension, and the corresponding electrochemical and rheological response. These instances highlight the importance of considering the agglomeration state of particles in a suspension formulation. This consideration is crucial for preparing suspension electrodes with reduced viscosity, enhanced

electrical conductivity, and increased EAM content and obtaining a feasible energy storage technology.

1.5 Thesis Objectives

A detailed review of studies aimed at understanding the microstructural changes and/or improving the microstructure of suspension electrodes was given in the previous part. The reported studies were primarily focused on altering the type (EAM and/or CA) and the amount of particles used and then determining an optimum ratio for suspension composition. However, when creating a homogeneous suspension formulation, one of the priorities is to use individual and non-agglomerated particles. Then, it should be followed by steps such as controlling/improving the distribution of particles in the resulting suspension, adjusting the composition of the suspension, etc. The agglomeration state of the particles significantly affects the maximum loadable EAM concentration in the suspension, suspension homogeneity, stability, and flowability. Nevertheless, the influence and importance of the particles' agglomeration state have been overlooked in suspension electrode formulations.

This thesis aimed to clarify the impact of the agglomeration state of particles on suspension electrodes' microstructure and resulting rheological and electrical-electrochemical properties. To the best of our knowledge, there is no comprehensive study to investigate this problem in depth, even in highly advanced suspension-based solid-state energy storage systems (i.e., LIBs, supercapacitors, etc.). Therefore, the findings of this research will play a pivotal role in advancing the development of improved electrochemical systems that involve suspension preparation.

In the current research, the olivine-structured carbon-coated LFP was chosen as the model EAM due to its wide use and superior characteristics for large-scale energy storage, such as non-toxicity, cheap, abundant resources, and electrochemical stability [69]. This approach or application was also assumed to be extended to different chemistries. Although utilizing organic electrolytes benefits higher power

densities, safety problems are a big concern for them [70]. Therefore, a safer and cheaper electrolyte is needed for large-scale storage. An aqueous electrolyte was employed as a dispersion medium due to benefits like safety, affordability, and higher ionic conductivity than organic electrolytes [71]. Moreover, it is known that obtaining homogeneous dispersions is more challenging in aqueous systems [72–74].

It was noticed that most of the commercially available powders (including LFP) are commonly in the form of hard agglomerates (or a mixture of soft and hard agglomerates). Since such particles almost chemically fused into each other, breaking/dispersing them, even using high-energy tools or dispersants, is difficult. Therefore, the synthesis of EAMs with submicron size, individual, and chemically non-fused structure was planned as the first stage in the present study. Then, the experimental protocol of suspension preparation was optimized to achieve a reproducible and homogeneous suspension structure in the aqueous electrolyte system. Subsequently, the influence of the particles' agglomeration state on the suspension electrode characteristics was examined. For comparison, a commercial powder (in the form of an agglomerated structure) and an as-synthesized powder (in the form of an individual-dispersible structure) were used. The prepared suspension electrodes were compared regarding their suspensions' microstructure, percolation characteristics, flow behavior, and electrical conductivity using oscillatory and rotational rheological tests and electrochemical impedance spectroscopy. Finally, the influence of fructose addition on the electrochemical performance of aqueous suspension electrodes was examined for the first time in the literature.

Taking into account all of these, the content of the present thesis was arranged as follows;

Chapter 2: Influence of Post-Synthesis Washing Process on Dispersibility of Lithium Iron Phosphate Particles

Chapter 3: Optimization of Aqueous Suspension Electrode Preparation Protocol

Chapter 4: The Influence of Agglomeration State of Lithium Iron Phosphate Particles on Aqueous Suspension Electrode Behavior

Chapter 5: Effect of Fructose Addition on Electrochemical Performance of Aqueous Suspension Electrodes

Chapter 6: Conclusions

CHAPTER 2

INFLUENCE OF POST-SYNTHESIS WASHING PROCESS ON DISPERSIBILITY OF LITHIUM IRON PHOSPHATE PARTICLES

2.1 Introduction

The particle characteristics employed in a suspension govern the microstructure of the system. The presence of agglomerated structures rather than individual and dispersible particles in a suspension has detrimental effects on homogeneity, stability, rheological behavior, and electrochemical response [46,48,75]. Therefore, controlling the agglomeration state of the particles is essential to obtain high-quality dispersions and meet specific requirements in SFAS.

It was realized that most commercially available powders, including LFP, exist in the form of hard agglomerates. Because these particles have chemically fused, it is challenging to break or disperse them. This renders the study of the impact of particles' agglomeration state on suspension behavior impossible. Therefore, in the initial phase of the current research, the synthesis of LFPs with individual and dispersible structures was intended.

The agglomeration states of the particles are directly associated with the synthesis method. For instance, while solid-state synthesis mainly forms larger particles with non-uniform and agglomerated structures, wet chemistries favor obtaining dispersible particles. Wu et al. found that agglomerated LFP particles, synthesized via solid-state reaction, showed a broader potential range for lithium-ion (de)intercalation than relatively non-agglomerated particles produced through hydrothermal methods [76]. The agglomerated particles also exhibited lower discharge capacity and a 20% reduction in capacity retention. In addition to the synthesis method, reaction parameters, i.e., temperature, duration [77], reagent

concentration [78], the stoichiometric ratio of reagents [79], reaction medium/solvent, and pH [80], were also reported to play a critical role in the agglomeration state of particles. The general approach in the literature is to optimize these parameters to obtain the best electrochemical performance (high discharge capacity, rate performance, low polarization, etc.) in LFP-containing electrodes. In addition to synthesis conditions, procedures applied after synthesis are also critical. The impact of washing and drying processes was extensively examined in general particle synthesis; however, it was neglected in LFP synthesis. For instance, the drying method-based agglomerate development in silica nanoparticles was investigated by Rahman et al. [81]. They showed an effective reduction in the agglomeration of particles with the drying technique in which conventional oven drying led to the formation of hard-agglomerated particles. In contrast, freeze drying yielded discrete and monodispersed particles, with soft agglomerates providing a higher surface area to the particles. The influence of washing on agglomeration was primarily documented for ceramic particles. Kaliszewski et al. observed the formation of hard agglomerates when washing zirconia powders with water, whereas ethanol (EtOH) washing resulted in relatively soft agglomerates [82]. This was found to impact particle crumbling and affected the homogeneity of sintering. In a recent study by Nyongombe et al., the impact of different washing solvents on the physical and electrochemical properties of an EAM (layered double hydroxide material, Nickel-Cobalt-Aluminium) was investigated [83]. Morphological variations were noted, resulting in a leaf-like structure after water treatment, while EtOH and acetone washing produced more closed structures with similar primary particles. Furthermore, samples washed with EtOH or acetone exhibited lower charge transfer resistances and higher capacitances than those washed with water.

The solubility of particles is a common phenomenon when a particle interacts with a solvent, and the degree of this solubility depends on the solvent properties. The solubility increases the dissolution-precipitation rate between contact points of particles, forming solid bridges and fused structures [84]. Besides, the discrepancy in the adhesion behavior of particles during separation from different solvents may

affect the ultimate structure of the synthesized particles. Therefore, both the solvents used in the washing step and the order of their application can influence the agglomeration state of the synthesized particles.

Despite the critical role of LFP as a commercial cathode material, the post-synthesis washing process's influence on the particles' physicochemical properties has been neglected. Various solvents have been used in the washing step without considering their impact on the particles' physicochemical properties [85–88]. Moreover, some studies did not mention the solvents used in the washing step. Herein, a two-step washing process was designed following the synthesis to clarify the effect of washing solvents on the agglomeration state of LFP particles. The LFP particles were synthesized via the solvothermal method and polyol method. We selected widely used washing solvents, deionized water (DIW), and EtOH and changed their application sequence in the washing step. Then, the obtained particles were thoroughly characterized by morphological, particle size, zeta potential, surface area, and hierarchical index (agglomeration state) analyses. Afterward, the impact of washing conditions on electrochemical performances was compared in both organic and aqueous electrolytes.

2.2 Experimental Procedure

2.2.1 Materials

Ethylene glycol (EG, ≥ 99.5%), lithium hydroxide (LiOH, 98%+), ortho-phosphoric acid (H_3PO_4, 85%), iron (II) sulfate heptahydrate ($FeSO_4 \cdot 7H_2O$, ACS Reagent) were used for LFP synthesis. Carbon black (CB, Alfa Aesar), battery-grade polyvinylidene fluoride (PVDF), and N-methyl-2-pyrrolidone (NMP, Merck) were used for composite electrode preparation. Lithium sulfate (Li_2SO_4, anhydrous, 99.7%) was purchased from Alfa Aesar and used for aqueous electrolyte preparation. Technical-grade EtOH (96%) and DIW with a resistivity of 18.2 MΩ were used in the washing procedures.

2.2.2 Particle Synthesis

Solvothermal Method

The LFP particles were synthesized through a solvothermal method in a 100 mL Teflon-lined stainless steel autoclave (Parr Instrument Company). The molar concentration of Fe^{2+} was fixed at 0.3 mol/L, and the reagent amounts were adjusted according to the chosen stoichiometric ratio of Li^{+}, PO_4^{3-}, and Fe^{2+} ions, which was set as 3:1.3:1, respectively. In the synthesis, 0.072 mol LiOH was first added to 80 mL of EG and magnetically stirred at 350 rpm for 30 minutes. To this mixture, 0.036 mol H_3PO_4 was added and stirred for 15 minutes, then 0.024 mol $FeSO_4 \cdot 7H_2O$ was added and stirred for another 15 minutes. The resultant dark green mixture was transferred into the autoclave. The sealed autoclave was then heated to 200 °C for 16 hours in an oven for the solvothermal reaction. The autoclave was rapidly cooled to room temperature after the process was completed.

Polyol Method

LFP particles were synthesized using the polyol method, as explained previously with the sample label LFP-NA [89].

2.2.3 Washing Procedure

Upon completion of reactions, particles were first separated from the mother liquor by centrifugation at 10,000 rpm for 30 minutes. Then, the precipitate was washed to remove the reaction residues. To understand the effect of the washing procedure/washing solvent sequence on particle characteristics, the acquired precipitate was washed with two different washing procedures:

i) In the first case, it was washed first with DIW and then with EtOH. The recovered precipitate from the mother liquor was mixed with DIW. Following the mixing of particles with washing medium, it was first magnetically stirred at 350 rpm for 15 minutes, then treated for 5 minutes with an ultrasonic homogenizer (Bandelin 2070,

operating at %75 power) equipped with MS 73 probe (φ = 3 mm) and magnetically stirred again for another 15 minutes. The supernatant and the particles were separated using centrifugation at 7,500 rpm for 10 minutes. The same procedure was then repeated using EtOH as the washing medium. This washing method was defined as **W1**.

ii) In the second case, the particles were washed, first with EtOH and then with DIW, using the same protocol in the first case. This washing method was defined as **W2**.

After washing, the synthesized LFP particles were dried overnight in an oven at 60 °C. The solvothermally synthesized LFP particles were labeled as **S1** and **S2**, indicating that the W1 and W2 methods were used to wash them. Similarly, LFP particles synthesized by the polyol method were labeled as **P1** and **P2**.

2.2.4 Characterization

The crystal structure of as-synthesized particles was analyzed by X-ray diffraction (XRD, Bruker D8, Cu-K_α radiation) working between 10° and 80° at a scan rate of 2°/minutes. Scanning electron microscopy (SEM) (Nova, NanoSEM 430) operating at 20 kV was used to analyze the morphology and size of the particles. Before microscopy examination, samples were coated with gold. Using the JEOL JEM2100F, the high-resolution transmission electron microscope (HRTEM) analysis was carried out. HRTEM samples were prepared by dispersing LFP particles in EtOH for 45 minutes in an ultrasonic bath (Bandelin RK-210H). Then, sufficient dispersion was placed on a carbon film grid and allowed to dry.

Particle size distribution was examined via dynamic light scattering (DLS) (Zetasizer Ultra, Malvern) at 25 °C. The zeta potential of the particles was also measured using the same appliance. Aqueous LFP dispersions with a solid concentration of 100 ppm were used for these analyses. To obtain homogeneous dispersions, each suspension was treated in an ultrasonic bath for 5 minutes and then 2 minutes with an ultrasonic homogenizer (Bandelin 2070, operating at %75 power) equipped with an MS 73

probe (φ = 3 mm) before the measurements. To evaluate larger particles (agglomerated ones) more clearly, particle size analysis using the laser diffraction (LD) method (Malvern Panalytical Zetasizer 2000S) was also conducted. Zeta potential and particle size analyses were repeated three times with different samples.

The specific surface area (SSA) analysis was carried out with a Quantachrome Autosorb 1C-MS analyzer under a nitrogen atmosphere using the Brunauer-Emmett-Teller (BET) method. Equation 2.1 [87], established with the assumption that any particle system is in spherical or close to spherical geometry, was used to calculate the particle size correlated with the BET analysis. The theoretical LFP density was taken as the basis for the density value in the equation. The hierarchical index of particles, the quantitative expression of the agglomeration state, was calculated by dividing the value obtained from particle size analysis by the particle size obtained from BET analysis. Here, the value of "1" indicates that the primary particle size of the system and the resulting ultimate particle size are equivalent. In contrast, the values above represent how many primary particles combined to form secondary structures/particles.

$$Particle\ Size_{BET}\ (nm) = \frac{6000}{SSA\ (m^2/g)\ x\ Density\ (g/cm^3)} \qquad \text{(Equation 2.1)}$$

The absorption bands at the surface of LFP particles were investigated using a Frontier IR (Perkin Elmer) instrument equipped with an attenuated total reflectance attachment. The Fourier Transform Infrared Spectra (FTIR) was collected between 4000 and 400 cm^{-1} in the wavenumber region. Analyses were conducted using dried powders.

For electrochemical characterization in organic electrolyte, electrodes were prepared by mixing LFP particles, CB, and PVDF in NMP solvent (5 wt.% PVDF – NMP solution) in a mixer mill (Retsch MM400) with a ratio of 60:30:10 by weight. The

electrode suspensions were spread on an aluminum foil with a thickness of 200 μm using the doctor blade method. To remove the NMP solvent thoroughly, the electrodes were pre-dried at 120 °C for 2 hours on a hot plate in a fume hood. Then, the coatings were cut into 18 mm circular discs and dried under vacuum at 120 °C for 12 hours before cell assembling. Lithium foil was used as the anode/reference electrode, and a glass microfiber sheet separated the electrodes. 1 M $LiPF_6$ dissolved in a mixture of ethylene carbonate (EC) and dimethyl carbonate (DMC) (1:1 by weight) was used as an electrolyte. The half-cell assembling was carried out in an argon-filled glove box. Cyclic voltammetry (CV) and galvanostatic charge-discharge measurements were performed in the 2.5 – 4.2 V operating potential range with MPG-200 electrochemical station (Bio-Logic Science Instruments).

The electrochemical behavior of LFP particles was examined in the 1 M Li_2SO_4 aqueous electrolyte using a three-electrode assembly. The cell was equipped with platinum wire as the reference electrode and Ag/AgCl (3M) as the counter electrode, as shown in Figure 2.1 (a). Nickel (Ni) foam attached to a nickel wire (Nickel 202, 0.8 mm in diameter) served as the current collector for the working electrode. For this purpose, two Ni foams with a diameter of 1.4 mm and one Ni foam with a diameter of 0.8 mm were used. Ni foams were washed with acetone and EtOH for 10 minutes in an ultrasonic bath and then dried at 90 °C for half an hour before use. To prepare the working electrode, the homogeneous electrode suspension was prepared in a mortar by gently mixing the LFP particles, CB, and PVDF in NMP solvent (5 wt.% PVDF – NMP solution) at a ratio of 60:30:10 by weight. The prepared suspension was thoroughly impregnated into small foam and then dried in an oven at 120 °C for 12 hours. A Ni wire was attached to suspension-coated small foam, and two sides were covered with more oversized foams as schematized in Figure 2.1 (b). The structure was pressed under 900 psi to obtain the working electrode. CV and galvanostatic charge-discharge measurements were performed in the -0.3 – 0.8 V operating potential range with the VersaSTAT 3 (Princeton Applied Research) instrument.

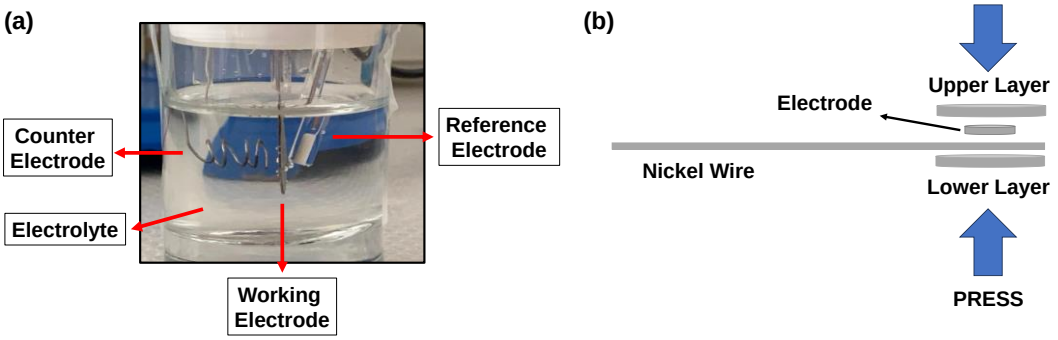

Figure 2.1 (a) A homemade three-electrode setup used for electrochemical characterizations in aqueous electrolytes and (b) a schematic representation of the working electrode designed to be employed in aqueous electrolyte measurements.

2.3 Results and Discussions

The crystallinity of LFP plays a crucial role in determining its electrochemical performance as it influences lithium-ion diffusion during charging and discharging cycles. Reaction residues or impurities in the structure can lead to diminished electrochemical performance, affecting the system's overall capacity, rate capability, and lifespan. Therefore, carefully choosing washing solvents is vital for removing possible reaction residues effectively. XRD analysis of LFP, following treatment with various washing solvents, offers valuable insights into the structural changes and purity of the material. The crystal structure analyses of the synthesized particles using two different washing procedures are presented in Figure 2.2. All distinctive peaks in the XRD pattern were assigned to orthorhombic LFP structure with Pnma space group, JCPDS card number 70-6684. No secondary phases were observed in any sample, while the sharp and narrow peaks indicated good crystallinity of the powders. Accordingly, pure LFP structures were synthesized via solvothermal and polyol methods, and regardless of application sequence, combinational use of DIW and EtOH effectively removed the reaction residues.

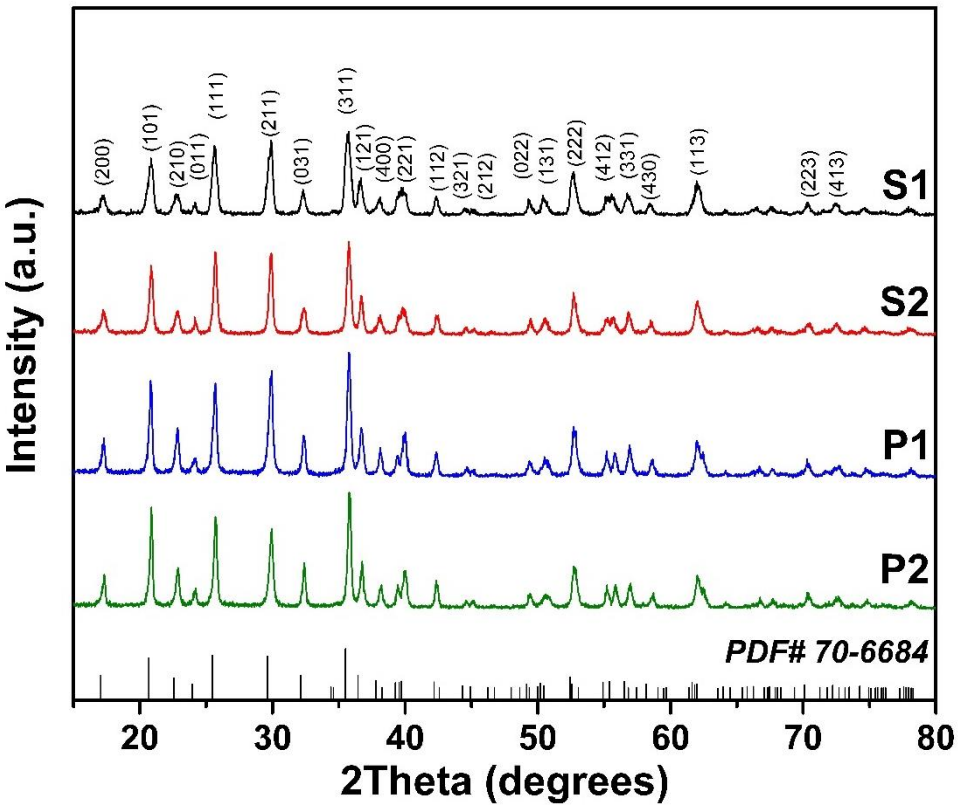

Figure 2.2 Crystallographic examination (XRD pattern) of LFP particles synthesized with the solvothermal and polyol methods and different washing procedures (W1 and W2). (W1 method: Particles were washed first with DIW and then with EtOH. W2 method: Particles were washed first with EtOH and then with DIW. S1 (solvothermal synthesized, W1 method), S2 (solvothermal synthesized, W2 method), P1 (polyol synthesized, W1 method), P2 (polyol synthesized, W2 method)).

The morphological and particle size variation due to the washing solvent sequence of the samples can be seen in the SEM images in Figure 2.3. The primary particles' properties depend on the chosen synthesis method, and different ways may enable the production of particles with distinct particle sizes and morphologies [90]. Upon scrutinizing the micrographs in Figures 2.3 (a) - (d), it is apparent that the characteristics of primary particles differed when employing solvothermal and

polyol methods. The solvothermal process resulted in nano-scale (a few hundred nanometers), square-like primary particles. The polyol method, on the other hand, yielded fusiform, submicron-sized, and discrete LFP particles. Even though the synthesis method predominantly influences the state of the primary particles, the post-synthesis washing process plays a crucial role in shaping the characteristics of the secondary particles. Comparing SEM images of solvothermally synthesized particles at high and low magnifications reveals noticeable variations in the secondary structures. The W1 procedure, in which the washing process was carried out in the order of DIW and EtOH, resulted in particles of a few hundred nanometers in size, discrete from each other, with clear particle boundaries (Figure 2.3 (e)). In contrast, in the W2 procedure, where the washing process was practiced in the order of EtOH and DIW, large clusters formed by gathering primary particles, reaching sizes of tens of micrometers, were observed (Figure 2.3 (f)). Sedimentation test samples (Figures 2.3 (i) and (j)), created through ultrasonic treatment of the particle suspensions, coupled with SEM results, provide comprehensive insights into the structure of these particles. Following a 6-hour sedimentation test, it was observed that the suspension prepared with S1 particles exhibited no changes. Therefore, S1 particles were able to form stable aqueous dispersions. However, a small portion of the S2 particles stayed suspended in the supernatant (presumed due to blurred vision), while the majority of particles accumulated at the bottom of the vial. Based on these observations, these structures can be considered chemically fused and hard agglomerates since they did not dissociate even after undergoing high-energy dispersion. For this reason, it can be inferred that the W1 procedure resulted in typically individual and dispersible particles. The W2 method, on the other hand, led to the formation of chemically fused and agglomerated particles.

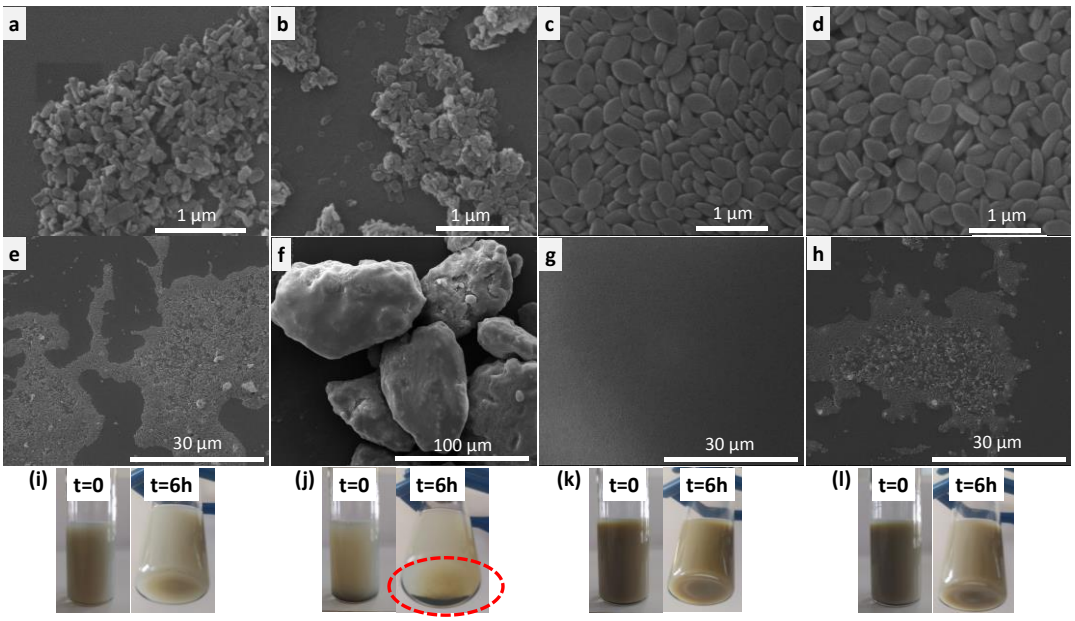

Figure 2.3 Morphological examination and stability analysis in aqueous media (initial and 6 hours later) of LFP particles synthesized with the solvothermal and polyol methods and different washing procedures (W1 and W2). High magnification SEM images of samples (a) S1, (b) S2, (c) P1, (d) P2; low magnification SEM images of samples (e) S1, (f) S2, (g) P1, (h) P2; sedimentation test of samples (i) S1, (j) S2, (k) P1, (l) P2. (W1 method: Particles were washed first with DIW and then with EtOH. W2 method: Particles were washed first with EtOH and then with DIW. S1 (solvothermal synthesized, W1 method), S2 (solvothermal synthesized, W2 method), P1 (polyol synthesized, W1 method), P2 (polyol synthesized, W2 method)).

Capillary pressure arises from the presence of liquid within the interparticle spaces of the powder. As the solvent evaporates, capillary forces come into play, affecting liquid distribution within the powder matrix. Since the surface tension of DIW is approximately three times greater than EtOH's, it results in a much higher capillary pressure. Therefore, higher pressure in the DIW-washed particle system should promote neck formation and bridging of neighboring particles that turn into hard

agglomerates. Additionally, surface ethoxide groups are possibly formed in the replacement of DIW in wet cake upon EtOH washing. The decomposition of those groups during drying may inhibit the formation of necks between neighboring particles [82,91,92].

Although the washing step severely impacted the particle structure obtained by the solvothermal method, it did not have the same effect on the particles synthesized by the polyol method. In both washing cases, particles with similar morphology and particle size were obtained (Figures 2.3 (c) and (d)). The dispersion characteristics of those particles also showed similarity, as seen from sedimentation analyses presented in Figures 2.3 (k) and (l). Since the particles are submicron and seem individual, highly stable dispersions were ensured in aqueous media without any sedimentation for a long time. Seemingly, the effect of the washing step on the particle structure depends on the synthesis method. Potential explanations for the various responses in polyol synthesis are explored with other analyses in the ensuing sections.

The physicochemical properties of EAMs play a crucial role in determining electrochemical performance. These properties of EAMs may differ according to the solvents used during washing and the order of their application. Therefore, understanding the interrelation between particles' physicochemical properties and washing procedure and optimizing these properties are essential for developing high-performance energy storage devices. The physicochemical properties of as-synthesized LFP particles are tabulated in Table 2.1. Zeta potential, the electrical potential values on the slip surfaces, provide crucial information on stability, coagulation probability, and dispersion quality [93]. Particles with higher absolute zeta potentials typically repel each other more strongly, increasing electrostatic repulsion and preventing particle agglomeration. Therefore, a high zeta potential value is desirable to obtain homogenous structures with those particles. When the zeta potential of the LFP particles was examined, all the particles were negatively charged, regardless of the synthesis conditions or the applied washing procedure. While a value of approximately -40 mV was recorded for the S1, P1, and P2 samples,

this value was measured as -31 mV for the S2 sample. As a rule of thumb, a zeta potential value higher than ± 30 mV ensures the formation of a sufficient repulsive force barrier between the particles [94]. Such a value provides the electrostatic balance that allows the particles to remain suspended in the media. Therefore, it can be said that all LFP particles have sufficient electrical potential to be considered stable in an aqueous environment. Even though each particle appears to have enough negative zeta potential to create a stable dispersion, the SEM and sedimentation test images presented in Figures 2.3 (f) and (j) conflict with these results for the S2 sample. Both particle agglomerates and deposits in the pictures show that the recorded zeta potential of sample S2 belongs to submicron-sized particles suspended in the supernatant, representing a meager fraction of the entire system. Hence, the stability from the elevated zeta potential value should be ascribed to a tiny fraction of the S2 sample rather than the whole system. On the contrary, the stability observed in the other three samples, as evidenced by the long-term sedimentation test, represents the entire system. Thus, it can be concluded that the applied washing step following the solvothermal synthesis controls the stability and dispersibility of the particles in aqueous media.

Table 2.1. Physicochemical properties of as-synthesized LFP particles.

Sample	Zeta Potential (mV)	D_{50} (DLS, nm)	D_{50} (LD, µm)	A_{BET} (m^2/g)	Particle Size (BET, nm)	Hierarchical Index
S1	- 38.6 ± 0.7	175 ± 0.4	-	33.8	50.7	3.5
S2	- 30.8 ± 0.4	136 ± 3.2	56.5 ± 4.7	32.9	52.1	1084
P1	- 40.9 ± 0.7	200 ± 1.5	-	25.1	68.2	2.9
P2	- 40.1 ± 1.2	206 ± 1.2	-	25.1	68.4	3.0

A_{BET}: specific surface area obtained from Brunauer-Emmett-Teller (BET) analysis, D_{50}: mean particle size measured with dynamic light scattering (DLS) or light diffraction (LD) (distribution based on intensity). (Particles washed through W1 and W2 methods in the washing step. W1 method: Particles were washed first with DIW and then with EtOH. W2 method: Particles were washed first with EtOH and then with DIW. S1 (solvothermal synthesized, W1 method), S2 (solvothermal synthesized, W2 method), P1 (polyol synthesized, W1 method), P2 (polyol synthesized, W2 method)).

Since the washing step is considered an influencing factor of secondary particles' structures, the average particle size of these powders may be affected. The comparison of the mean particle sizes of LFP samples measured with the DLS method can be seen in Table 2.1. P1 and P2 samples had average particle sizes of around 200 nm, respectively. The results were in line with the SEM analyses presented in Figure 1. Accordingly, there was no significant difference in the size/size distribution of the particles when the polyol synthesis was completed with different washing solvents. The average particle sizes of the S1 and S2 samples were 175 and 136 nm, respectively. When considered together with both SEM and sedimentation test findings, it is reasonable to conclude that the observed average particle size in sample S1 is consistent. This is because sample S1 comprises primary particles of several hundred nanometers with distinct boundaries, which can be dispersed in the liquid for a long time without settling. However, when a similar evaluation is examined for sample S2, the presence of immediately sedimented particles and massive clusters observed in SEM images (Figure 2.3 (f)) strongly suggests that the particle size in sample S2 cannot reasonably be at this level. The DLS measurement is limited to a scale of a few micrometers and is unsuitable for rapidly settling particles. Therefore, these results should represent the sizes of tiny particles that did not cluster somehow or could be separated from each other by ultrasonic homogenization. LD analysis was carried out for a detailed particle size examination of the S2 sample. The results showed that the volumetric population of the particles was around 56.5 micrometers overall, which correlates with and also explains the quick settlement and large agglomerates.

Another critical property of EAMs is their surface area. High surface area facilitates better contact between the EAM and the electrolyte, leading to enhanced electrochemical reactions. The measured SSA of the particles can be seen in Table 2.1. The results clearly show that the surface area of the particles mainly relies on the synthesis method. Accordingly, the solvotermally synthesized particles have a larger surface area than those synthesized with the polyol method. This may be attributed to the size of the particles in the SEM images in Figures 2.3 (a) – (d). It is

reasonable to expect that solvothermal synthesized particles will have a higher SSA since they are composed of nano-scale primary particles. If each method is examined within itself, having very close surface areas for P1 and P2 samples is reasonable since the other properties, such as morphology and particle size, are similar. In the case of solvothermally synthesized particles, since the primary particles' size and morphology shown in the SEM images in Figures 2.3 (a) and (b) are similar, it is meaningful to obtain close values. However, a slight variation in the SSA, i.e., the relatively lower surface area of sample S2 than sample S1, ascribed to the agglomerated structures that sample S2 comprised. As such, when individual particles chemically fuse or adhere together, they form larger entities with less external surface exposed to the surrounding environment. As a result, the total surface area per unit mass decreases.

Particle size values calculated based on BET measurements via Equation 2.1 are also compared in Table 2.1. The estimated particle sizes of the samples synthesized by the solvothermal and polyol methods were about 50 nm and 68 nm, respectively. This indicates that BET-based particle sizes were smaller than the measured with the DLS method. The comparison of hierarchical index values, i.e., an indicator of the agglomeration level of the particles, is given in Table 2.1. While this value was around 3-4 for the S1, P1, and P2 samples, it was around a thousand for the S2 sample. According to the applied approach, in samples S1, P1, and P2, a few primary particles combined or clustered to form secondary structures. However, in sample S2, secondary structures were formed by thousands of primary particles chemically fused.

When all physicochemical properties tabulated in Table 2.1 and presented in Figure 2.3 are examined, it is deduced that the washing step has different effects depending on the synthesis method. In solvothermal synthesis, it was noted that the agglomeration state and physicochemical properties of the particles were significantly impacted. However, in polyol synthesis, these effects were not as pronounced. The different responses of the as-synthesized particles encountered in this study may be related to their surface properties, which may vary depending on

the synthesis method used. FTIR analysis of the particles was carried out and presented in Figure 2.4 (a) to understand the changes on the sample surface. The peaks that appear at 1200 – 400 cm^{-1} generally belong to the fingerprint of LFP; that is, they are characteristic peaks of LFP [95]. While the region between 945 – 1139 cm^{-1} is attributed to the P – O stretching, the part between 400 – 647 cm^{-1} is due to lithium-ion vibration. On the other hand, the range between 1500 and 4000 cm^{-1} is the primary region to be considered. This is because information may be gathered regarding the ability of the various washing sequences to remove reaction residues that may remain on the LFP surface throughout the reaction. The flat peak at approximately 3450 cm^{-1} is common to all samples due to the -OH stretching. The presence of hydroxyl is likely to originate from the trapped solvent between the particles after washing with DIW or EtOH. On the other hand, the peaks at 2981 and 2889 cm^{-1} correspond to the C-C and C-H stretches, while those at 1382 and 1623 cm^{-1} refer to the C=C and C=C-C stretches. Despite all these bonds being observed in all samples, extra peaks at around 2300 cm^{-1} were noticed in the P1 and P2 samples. This peak corresponds to C≡C bonds, and the formation of such strong bonds after the washing procedure is not expected. Therefore, these bonds are assumed to result from the interaction of the reactants used with the solvent during polyol synthesis.

The difference in the surface structures of LFP particles is further supported by the TEM nanograph presented in Figure 2.4 (b). It shows that a different sheath quite densely surrounds the as-synthesized P1 particles. Combined with the findings from the FTIR analysis (C≡C scretching), this sheath may be a remnant of the organic solvent, EG, which is the mother liquor. Studies reported that some organic solvents remain in the structure after polyol synthesis of LFP particles are also available. The P1 and P2 samples showed similar morphology, particle size, zeta potential, and SSA. Therefore, the inability to efficiently remove the organic solvent from the structure may play a critical role in exhibiting similar physical-physicochemical properties for the particles synthesized via the polyol method, as our study showed. The organic solvent, which could not be properly eliminated from the structure by

washing, functions as a dispersing media for the particle system due to its dense and viscous structure. This situation enables a system with an individual and dispersible particle that exhibits the same physicochemical features. However, this was invalid in the solvothermal synthesis due to the possible reaction kinetics and atmosphere. The post-synthesis washing step adversely affected the agglomeration state of the particles in solvothermal synthesis. In light of these, a similar result or impact may be expected in the washing procedure if the residual organic solvent in the polyol-synthesized samples is successfully eliminated.

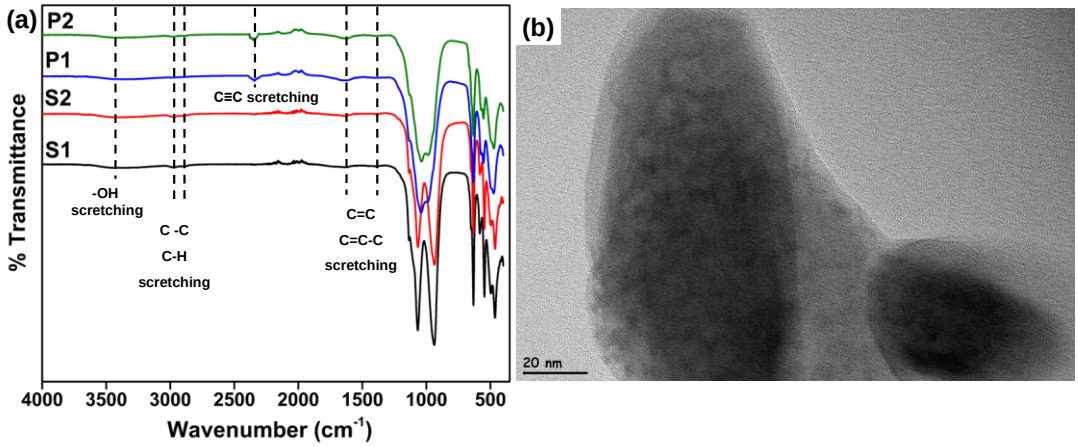

Figure 2.4 (a) Effect of washing procedure (W1 and W2 methods) on surface characteristics of LFP particles (FTIR analysis) and (b) HRTEM nanograph of sample P1. (W1 method: Particles were washed first with DIW and then with EtOH. W2 method: Particles were washed first with EtOH and then with DIW. S1 (solvothermal synthesized, W1 method), S2 (solvothermal synthesized, W2 method), P1 (polyol synthesized, W1 method), P2 (polyol synthesized, W2 method)).

All these analyses directly revealed that the post-synthesis washing step remarkably influences the physicochemical properties and agglomeration state of the solvothermally synthesized LFP particles. If the particles were cleansed from the

organic mother liquor, two-step washing in a different order, even if the same solvents were used in the washing step, was found to affect the agglomeration conditions of the particles. On the other hand, this washing solvent-based agglomeration was found to diminish the surface charge of the particles in the solvent, their stability in the dispersion, and specific surface area, yet increase the mean particle sizes. Therefore, since the particle characteristics varied, it is rational to assume that the electrochemical performance of such particle-prepared electrodes will be adversely affected. However, it was found that altering the washing sequence of the particles synthesized via the polyol method did not influence the physicochemical properties of the particles. This was ascribed to the inefficiency of removing organic residues between particles. Although the particles' dispersion characteristics remain unchanged, applying different washing solvent sequences may still impact the electrochemical properties.

2.3.1 Effect of Washing Procedure on Electrochemical Properties

The physicochemical properties of EAMs have a notable influence on electrochemical response. For this reason, the electrochemical performances of the as-synthesized particles were examined to understand the effect of the changes in the structure and the washing procedure.

LFP is known for its poor electronic and ionic conductivity, which remarkably affects the system's performance [96]. The as-synthesized LFP particles were not coated with carbon, and no additional treatment was applied. In this case, an effective way to enhance the electrode's specific gravimetric capacity is by adding CAs [97]. Since it is an inactive material in the electrode, its amount is required and desired to be low. Yet, it is better to use high amounts for very low electrically conductive EAMs. In the preliminary studies, we studied the effect of external carbon content in the composite electrode for as-synthesized bare LFP particles (sample S1) in the aqueous electrolyte. While the binder amount was kept constant (10 wt.%), the amount of CB was modified from 10 to 35 wt.%. The CV analyses of LFP-containing

electrodes are given in Figure 2.5. Figure 2.5 (a) shows that increasing carbon content resulted in more symmetrical redox peaks and increased the electrode's peak currents. The delivered specific discharge capacities of those electrodes with different carbon contents are given in Figure 2.5 (b). It is clear that the delivered specific discharge capacity increased with the increase in carbon amount to 30 wt.% of the total electrode structure. Besides that point, a decrease was seen in the electrode's specific discharge capacity. It can be said beyond a border, the carbon content may be detrimental to the electrochemical response of the electrodes. Also, sluggish kinetics of lithium-ion diffusion may be possible for low carbon contents and responsible for asymmetric redox peaks in the CVs. Since the highest specific discharge capacity was obtained with 30 wt.% CB, it was chosen as the optimum carbon content for further solid-state cell studies for both aqueous and organic electrolytes.

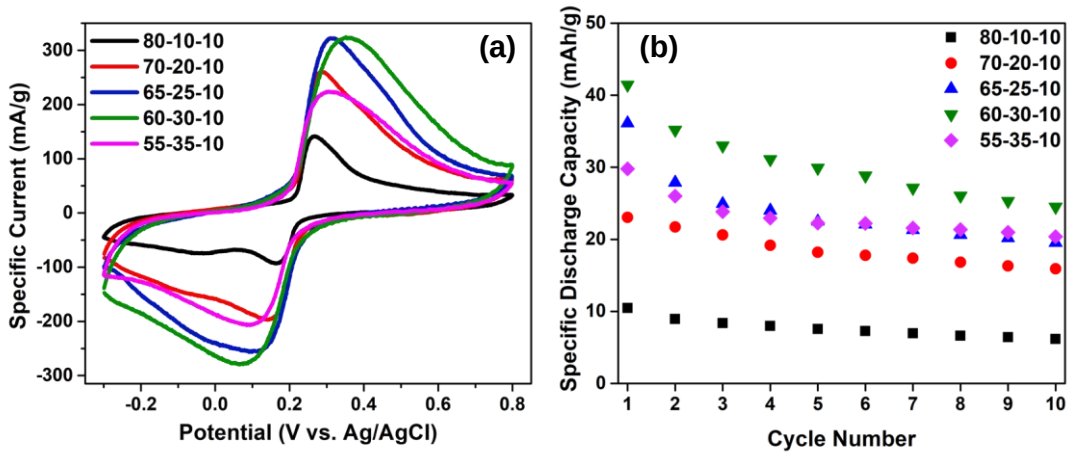

Figure 2.5 Effect of carbon content in the composite electrode on the electrochemical behavior of LFP particles in aqueous electrolyte (between -0.3 – 0.8 V operating potential); (a) electrochemical activity at a scan rate of 1 mV/s and (b) cycling discharge performance at 0.1 C rate.

Following the determination of CB concentration, the electrochemical performances of all LFP particles were investigated to comprehend the influence of the changes in the structure and the washing procedure. The corresponding electrochemical performances in organic electrolytes are presented in Figure 2.6. Considerable anodic and cathodic redox reactions, which correspond to almost 3.2 and 3.8 V (vs. Li^+/Li), can be seen in the CV analyses given in Figure 2.6 (a) and (c). Those values ascribed to the insertion/deinsertion of lithium ions into/from the electrode structure indicate that the synthesized particles are electrochemically active. The absence of other reaction peaks in the CV graph suggested that the particles contained no impurities, which agreed with the XRD results. However, the results show that both the synthesis method and washing procedure affected the electrochemical response of the samples. Although the potential distance between oxidation and reduction peaks that indicate electrochemical kinetics was similar, the peak currents (or area under the anodic/cathodic reaction parts) varied according to the applied washing procedure. Such that the maximum current drawn from particles washed through the W1 method was higher than their W2-washed counterparts. The maximum specific current densities corresponding to anodic and cathodic reactions were -380/580 mA/g and -290/410 mA/g for the S1 and S2 samples. This can be interpreted as a more favorable pathway for the insertion/deinsertion of lithium ions in the system of individual particles compared to the agglomerated structure. While the redox kinetics remained similar, the individual nature of the particles may attract a higher number of lithium ions from the surroundings. The anodic–cathodic current densities and the representative area under each reaction process differed. Hence, it can be deduced that the sample whose washing step was completed with EtOH instead of DIW may have a higher discharge capacity or better electrochemical performance – response.

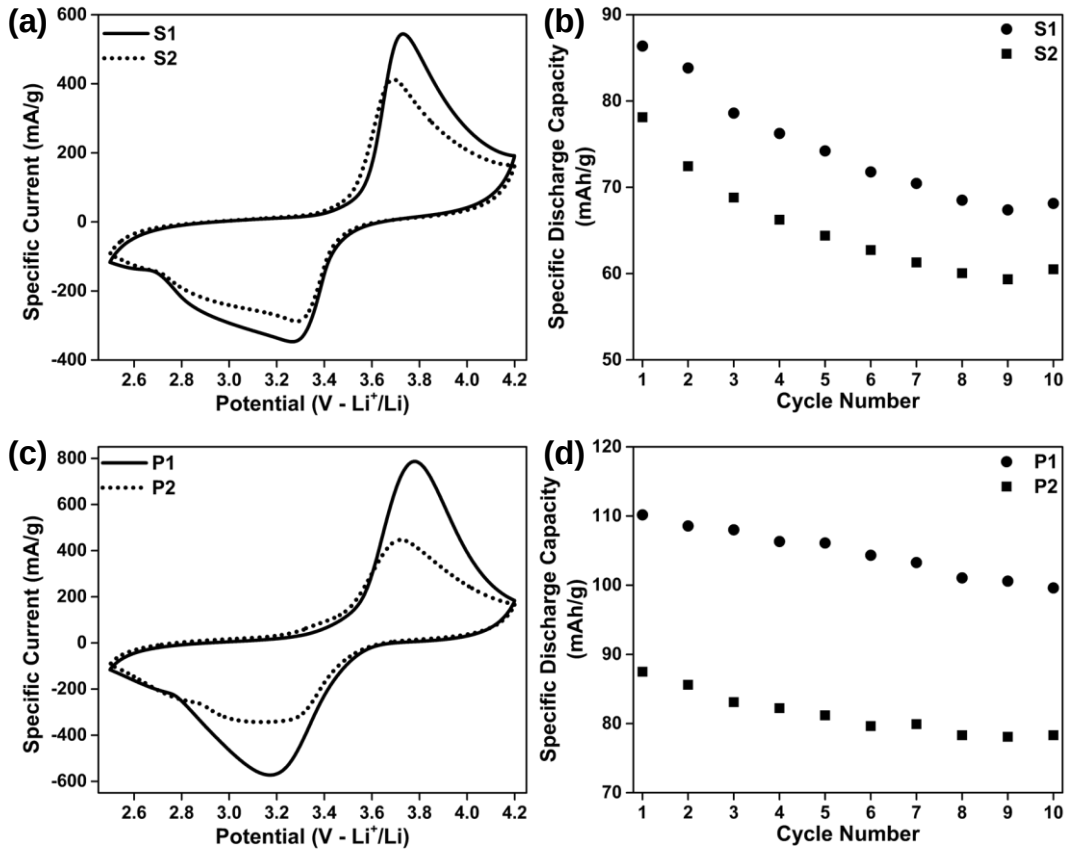

Figure 2.6 The impact of washing procedure (W1 and W2 methods) on the electrochemical performance of LFP particles in the organic electrolyte; (a) and (c) electrochemical activity analysis performed at 1 mV/s, (b) and (d) constant current discharge analysis performed at 0.1 C-rate. (W1 method: Particles were washed first with DIW and then with EtOH. W2 method: Particles were washed first with EtOH and then with DIW. S1 (solvothermal synthesized, W1 method), S2 (solvothermal synthesized, W2 method), P1 (polyol synthesized, W1 method), P2 (polyol synthesized, W2 method)).

Interestingly, it was observed that quite different current responses were recorded by samples P1 and P2 despite exhibiting the same physicochemical properties. This shows that even if other properties are unchanged, the washing procedure termination solvent may impact the electrochemical response of EAMs.

The specific discharge capacities of samples obtained at 0.1 C-rate are compared in Figure 2.6 (b) and (d). The discharge capacity measurements also supported the CV analyses, as the discharge capacities depended on the synthesis method and the applied washing procedure. The initial discharge capacity of the samples was measured to be 86 mAh/g and 78 mAh/g for S1 and S2, respectively. The S1 sample displayed a higher specific discharge capacity than the S2 particle during the entire measurement, carried out across ten cycles. When the SEM images were revisited (Figure 2.3), it was obvious that both S1 and S2 samples comprised indiscriminate and square-like primary particles. Therefore, the agglomerated and fused structure of the S2 sample stemming from the washing procedure should be the main reason for this capacity difference. The S1 sample consists of individual and dispersible particles that may have short pathways that facilitate the transfer of the lithium-ions to interior parts. The larger surface area of the S1 (revisit Table 2.1) resulting from the washing step also promoted the potential for lithium-ions to access the particles. However, the mobility and the concentration of lithium ions are restricted in the agglomerated structure and are not likely to reach the core of the EAM. Therefore, there is a worse corresponding electrochemical response compared to S1. The higher specific current of P1 and P2 samples in the CV measurements also manifested in the galvanostatic discharge analyses. Samples P1 and P2 were also seen to have comparable conditions, and their initial discharge capacities were found to be 110 mAh/g for P1 and 87 mAh/g for P2. This is interesting as all the physicochemical properties of samples P1 and P2 are similar. However, this scenario is the one that best demonstrates the significance of the washing process. It is confident that even if the other properties of the particles are similar, the solvent order in the washing step has the potential to positively or negatively affect these particles' electrochemical performance.

If we analyze the electrochemical performance based on the synthesis method, the specific discharge capacity of P1 and P2 samples was consistently higher than that of S1 and S2 samples throughout the cycle. Several factors typically influence the

discharge capacity that EAMs can provide. The variation in the morphology may be the major factor influencing the discharge capacities of the as-synthesized samples.

Another electrochemical performance metric, the discharge capacity retention, was determined to be 90% and 89% for P1 and P2 samples, respectively. S1 and S2 samples, on the other hand, only retained 79% and 77% at the end of the ten cycles, respectively. The washing procedure did not significantly affect the capacity retention of the samples since similar values were obtained. The capacity retention also shows better performance of polyol-synthesized particles in organic electrolytes. It can be concluded that P1 and P2 samples are advantageous compared to S1 and S2 samples for electrochemical applications due to high discharge capacities and higher capacity retentions. Accordingly, as-synthesized particles exhibited lower specific discharge capacities than the theoretical value (170 mAh/g) and rapid capacity decay. However, considering the overall structure of the particles, the delivered discharge capacities and capacity retentions are reasonable. It is suggested that the carbon coating of particles enhances the electrochemical performance (discharge capacity, cyclic stability, rate performance, etc.) [98]. Therefore, higher discharge capacities and better cyclic stability can be obtained with a controlled carbon coating of the samples. However, here, we only focused on the impact of the washing step on agglomeration states. So, such a surface modification and its favorable effect on electrochemical response are out of the concept.

Electrochemical examinations were also carried out in an aqueous electrolyte to compare the impact of electrolytes on the electrochemical performance of the samples, presented in Figure 2.7. The results show how the aqueous electrolyte measurements demonstrate a parallel response to that of the non-aqueous electrolyte. Like the organic electrolyte behavior, the samples' electrochemical response depended on the washing solvent sequence and synthesis method. In the aqueous electrolyte, on the other hand, it is explicit that the particles performed worse. Completing the washing step with DIW reduced the peak current by almost half, as shown in Figure 2.7 (a) and (c). It is noticeable that the peak currents of the particles

synthesized by the polyol method are nearly two times higher than those of the other particles.

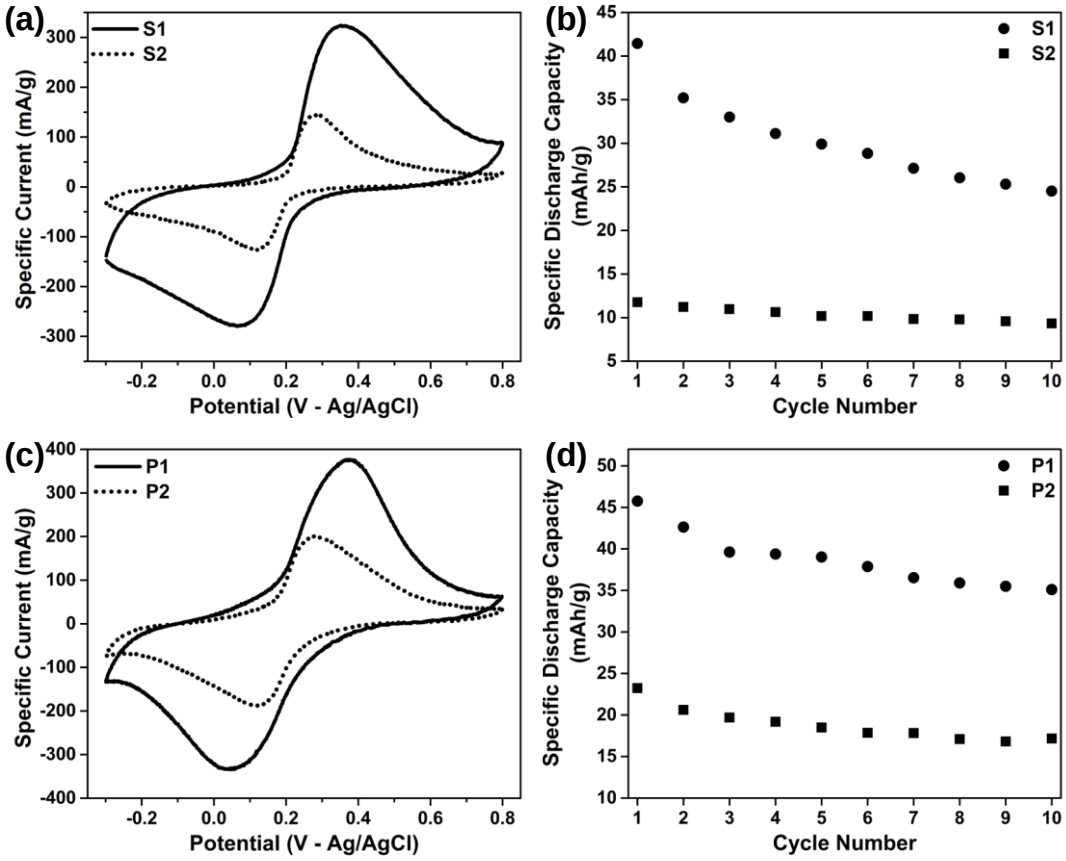

Figure 2.7 The impact of washing procedure (W1 and W2 methods) on the electrochemical performance of LFP particles in aqueous electrolyte; (a) and (c) CV analysis performed at 1 mV/s, (b) and (d) constant current discharge analysis performed at 0.1 C-rate. (W1 method: Particles were washed first with DIW and then with EtOH. W2 method: Particles were washed first with EtOH and then with DIW. S1 (solvothermal synthesized, W1 method), S2 (solvothermal synthesized, W2 method), P1 (polyol synthesized, W1 method), P2 (polyol synthesized, W2 method)).

Additionally, samples were susceptible to aqueous electrolytes and showed a lower discharge capacity than organic electrolytes, as shown in Figures 2.7 (b) and (d). Being non-covered with a protective sheath (carbon coating) makes the particles more vulnerable to the aqueous media than the organic electrolyte. Hence, the increased degradation of the samples in the aqueous electrolyte results in poorer electrochemical performance. In addition, optimization of pH, ionic concentration, dissolved oxygen amount, etc., of aqueous electrolytes is crucial and suggested to improve the electrochemical performance of LFP particles to be comparable with performance in the organic electrolytes [99]. Yet, we did not focus on that in this study.

All in all, examination of particles in both aqueous and non-aqueous electrolytes showed that different washing procedures significantly impact the corresponding electrochemical performance of the powders. The sensitivity of lithium-ion electrodes to moisture and its adverse effects on electrochemical performance have been reported in many studies [100,101]. Therefore, the possible remaining excess water in the structure due to the washing step ending with DIW may cause the particles to exhibit lower electrochemical performance. However, using EtOH in the last step, even if there is a trapped solvent inside, alcohol will be replaced by water, thus minimizing the adverse effect. The findings showed that the washing solvent sequence or the solvent used in the final step is determinative of the electrochemical performance of the EAMs.

This study revealed that the washing procedure used after solvothermal synthesis has a dual impact on electrochemical energy storage systems. First, individual and dispersible particles had better discharge capacity than agglomerated ones. As discussed earlier, the amount of solids loaded per unit volume in an electrode produced with individual particles would be higher than in those made with agglomerates. The synergistic effect of these two scenarios will enable the creation of an electrochemical energy storage system with higher energy density. The findings revealed that even if the polyol synthesis resulted in the same dispersion characteristic, a more energy-dense system can be established by controlling the

washing process since the discharge capacity differs. A synergistic effect, as in the case of solvothermally synthesized particles, may also be encountered in polyol synthesis if the trapped organic solvent within the particles is effectively removed.

Consequently, these results prove how the post-synthesis washing step critically impacts the fundamental characteristics (agglomeration, especially) of the as-synthesized particles and the energy capacity of a system established using these particles.

2.4 Conclusions

The agglomeration of electroactive particles that affects the microstructure, general characteristics, and electrochemical response of the electrode has to be avoided for enhanced performance in energy storage systems. In this part, we intended to obtain dispersible and individual LFP particles. We focused on the role of the post-synthesis washing process on the agglomeration state of the resulting electroactive particles, as well as other physicochemical properties and electrochemical behavior. A two-stage washing procedure was adopted to remove reaction residues. Completing the washing step with EtOH or DIW showed different impacts on the particle dispersion characteristic depending on the synthesis methods. While the washing stage in solvothermal synthesis impacted particles' agglomeration, the polyol method's particle dispersion/physicochemical characteristics were similar. The average particle sizes of the solvothermally synthesized dispersible and agglomerated particles were 175 nm and 56.5 micrometers, respectively. The polyol method also resulted in particles with an average size of almost 200 nm. Concluding the washing process with EtOH enabled the formation of stable aqueous suspensions, exhibiting zeta potential values around -40 mV. The hierarchical index value, indicating the agglomeration degree of particles, was 1084 for agglomerated particles, while it was only 3-4 for the other particles. Completing the washing step with DIW also adversely impacted the electrochemical response of particles regardless of the production method. An analysis specific to the particles discussed in this section

reveals that using DIW in the final washing step reduces the specific discharge capacity by 10-20% in organic electrolytes and by almost 50% in aqueous electrolytes. Additionally, it was seen that the particles perform worse in aqueous electrolytes compared to non-aqueous electrolytes.

This study showed that the post-synthesis washing procedure influences not only the agglomeration conditions but also the electrochemical performance of the particles. Therefore, it contributes to establishing improved electrochemical systems by explaining or introducing a facile method of avoiding agglomerated particles.

CHAPTER 3

OPTIMIZATION OF AQUEOUS SUSPENSION ELECTRODE PREPARATION PROTOCOL

3.1 Introduction

Establishing a percolated structure, crucial for effective charge transfer in suspension electrodes, relies on incorporating CAs. The homogeneous distribution of the CAs in suspension is essential for forming the reticulated structure with a minimum amount of CA. It also has a critical role in the overall processability, electrical conductivity, and wiring of all EAMs. Since suspension electrodes are intended for long-term use, achieving a homogeneous structure is not the only consideration. Simultaneously, preserving the homogeneity of the resulting suspensions, i.e., keeping them stable for a long time, is critical for the continuity of electrochemical performance.

In suspension electrode studies, carbon black (CB) derivatives are generally used as CA [102–105]. Different characteristics of these materials (type, size, morphology, and aspect ratio) were shown to affect the suspension electrode's microstructure/homogeneity and performance [66,105,106]. In addition to the inherent characteristics of particles and their interactions with each other, the interactions between particles and the solvent are also pivotal for the behavior and electrochemical performance of the suspension. Organic electrolytes are preferred to achieve high power density battery systems. Electrode preparations are also carried out in an organic solvent due to CBs' compatibility or wettability. Due to environmental and economic reasons, electrode formulation in aqueous media was underlined, and there is a notable trend in this direction [107]. However, CB particles commonly consist of 90–99% elemental carbon, leading to strong hydrophobicity

and a tendency to agglomerate when dispersed in water. Therefore, obtaining homogeneous carbon dispersions in aqueous systems is challenging [108,109].

Functional groups may remain on the surface of CB particles due to production methods, etc. The presence of these functional groups results in CB particles acquiring a surface charge through ionization or dissociation when immersed in water [106]. Depending on this surface charge and the properties of the aqueous medium (ionic strength, pH, etc.), the dispersibility and stability of the CB particles may vary. Diversity in manufacturers and production methods allows access to CBs with different surface properties. Therefore, even two carbon materials with the same label may have different surface properties and dispersibility. As a result, the microstructure may exhibit variations, potentially negatively impacting the prepared suspension's electrochemical performance. Hence, the distribution of carbon in systems employing aqueous electrolytes must be carefully controlled. To this end, numerous physical and chemical approaches were introduced to prepare homogeneous CB dispersions or enhance dispersibility, especially in aqueous processing studies. The general practice to improve water compatibility is surface functionalization, such as oxidation treatment, grafting process, and employment of dispersants that adsorb to the surface of CB particles [108,110].

In many studies, suspension electrodes were often prepared without a thorough investigation of the behavior of CB particles in the aqueous electrolyte. These studies generally reported mixing EAM and CA powders and combining them with an aqueous electrolyte [36,103]. Directly combining and mixing EAM, CA, and electrolytes to prepare suspensions were also reported [25,104,111,112]. In addition, even suspension electrodes prepared without details of any preparation procedure were reported [113,114]. Many research groups used different preparation methods, and no standard recipe exists. However, it's important to highlight that the suspensions were subjected to long-term treatment in high-energy dispersing systems (ball milling, shear mixing) to disperse and homogenize them [39,105,106,111,115]. This is usually due to the high viscosity of the prepared suspensions. Still, it indicates that high or extra mechanical force is applied to

disperse carbon structures in aqueous systems. The fact that particles can be mixed this way does not mean these dispersions are stable. It only means that the dispersion/homogenization process is possible. In addition, particle characteristics (size, morphology, etc.) can be altered during the preparation of suspensions in high-energy mixing systems. It can be particularly problematic for suspensions containing materials with high operating performance in a particular structure. Therefore, it is essential to investigate alternatives to these methods and develop the optimum formulation procedure for preparing carbon-containing suspension electrodes by considering the CB dispersibility in the suspension.

In the present part, we attempted to develop an optimal preparation guideline for aqueous suspension electrodes. To this end, the surface properties of particles were tested, and the experimental protocol for suspension preparation was simply adjusted. Thus, we engineered stable aqueous carbon dispersions that can endure for an extended period without requiring additives/surfactants or additional tools. The effect of the proposed formulation on the microstructure, stability, and electrical conductivity of the resulting carbon suspension was investigated. KB was used as a model CA because it is one of the most preferred highly conductive materials in suspension electrode studies [20,39,103].

3.2 Experimental Procedure

3.2.1 Materials

KB (EC600JD, Akzo Nobel) was used as a CA in aqueous suspensions. Li_2SO_4, (anhydrous, 99.7%) was purchased from Alfa Aesar to prepare an aqueous electrolyte. DIW with a resistivity of 18.2 MΩ was used to prepare aqueous suspensions. Commercially available LFP was used as received without any treatment.

3.2.2 Suspension Preparation

Two distinct approaches were employed to formulate aqueous KB suspensions and clarify the experimental protocol's impact on dispersion characteristics. For this purpose, the sequence of adding Li_2SO_4 salt to the suspension was altered to achieve an aqueous electrolyte with an adequate ionic concentration.

(*i*) An aqueous Li_2SO_4 electrolyte with the desired concentration was prepared in the first method by dissolving salt in DIW. Subsequently, KB particles were introduced into the aqueous electrolyte, gently shaken, and subjected to 20 minutes of ultrasonication in a bath for particle dispersion.

(*ii*) In the second method, KB was slowly added to the DIW, gently shaken, and then ultrasonicated in the bath for 10 minutes to disperse particles. Then, the required amount of Li_2SO_4 compound to reach the desired salt concentration was added in powder form. The suspension was ultrasonicated in the bath for another 10 min.

To homogenize the structure further, the suspension was stirred at 250 rpm in a magnetic stirrer for 24 hours following ultrasonication. The samples were labeled as "xKB" or "xKB – yLFP," where x and y denote the weight percentages of used materials. For instance, a 3 g suspension of 1KB – 10LFP contains 0.03 g KB, 0.3 g LFP, and 2.67 g DIW.

The suspension formulated following Method 1 was also subjected to ball milling to comprehend the microstructural alterations. For this purpose, the electrolyte and the required amount of KB powder were transferred to the agate jar and mixed at 250 rpm for 2 hours.

3.2.3 Characterization

Morphological investigation and size analysis of KB particles were realized with SEM (Nova, NanoSEM 430) operating at 20kV. At room temperature, particle size distribution was investigated via DLS (Zetasizer Ultra, Malvern). The zeta potential

of particles was also measured with the same instrument. For these analyses, aqueous suspensions with 0.001 wt.% solid particles were prepared and treated in an ultrasonic bath for 5 minutes and then for 2 minutes with an ultrasonic homogenizer (Bandelin 2070, operating at %75 power) equipped with an MS 73 probe (φ = 3 mm) to disperse each suspension homogeneously. Similar analyses were conducted at 0.01 wt.% solids content for LFP particles. Particle size and zeta potential measurements were repeated three times using distinct samples.

To study the effect of the applied suspension preparation approach on the dispersion kinetics of KB particles in aqueous electrolytes, suspensions containing 0.2 wt.% KB were prepared. The suspensions were prepared using only 20 minutes of ultrasonic treatment, as given in the suspension preparation step.

Potentiostatic electrochemical impedance spectroscopy (EIS) analyses of aqueous suspensions were performed using a homemade Swagelok-type cell with two stainless steel electrodes at two ends, as shown in Figure 3.1. The diameter of both electrodes was 10.4 mm, and the gap was adjusted to 0.5 mm. Potentiostatic EIS was acquired with a potentiostat/galvanostat/ZRA (Gamry Instruments, Reference 600) between 0.01 Hz and 200 kHz at a perturbation amplitude of 10 mV by collecting 6 points per decade at 0 V open circuit potential. To comprehend the stability and guarantee the reproducibility of the aqueous KB suspensions, we defined a specific procedure for testing. After the preparation of the suspensions, they were immediately transferred to the measurement cell, and it was sealed. The first measurement was performed instantly as the initial response, and continuous EIS measurements were performed with the same suspension without disassembling the cell for 24 hours. The results were represented with Nyquist plots. EIS analyses were repeated for at least three samples. In the 24-hour measurements, a single sample from the prepared batches was analyzed. Before EIS measurement, suspensions were subjected to 3 cycles of CV analysis at a scan rate of 1mV/s in the 0 – 0.1 V range.

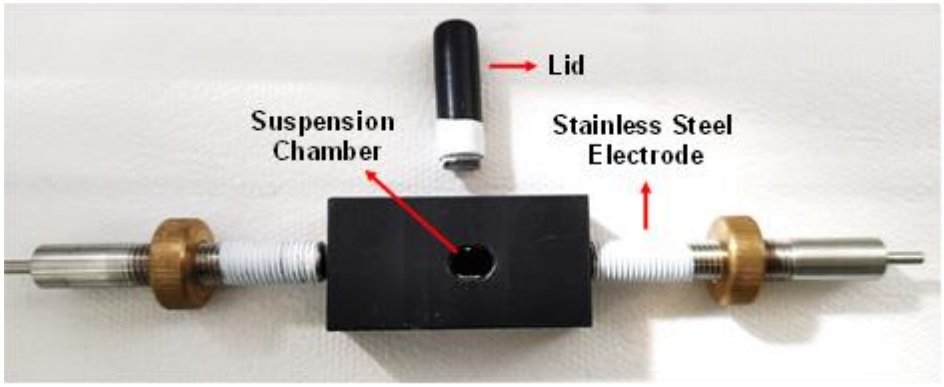

Figure 3.1 A homemade Swagelok-type cell used in electrochemical impedance analyses.

3.3 Results and Discussions

Preparing homogeneous suspensions to use as electrodes in flow-through energy storage systems is essential for better electrochemical performance and processability. Ensuring the reproducibility of the prepared suspensions is another critical consideration for their utilization in energy storage systems. Within the scope of this thesis, before examining the particles' agglomeration state on the microstructure and corresponding behavior of the suspension electrodes, it was focused on preparing suspensions reproducibly.

EIS analysis is a widely used technique to understand the microstructural changes in carbon-based slurries since it is a non-destructive method [116]. The microstructural evolution of a suspension can be comprehended by observing spectra change in the Nyquist plot consisting of both imaginary and real impedance parts. A current response related to the displacement of ions and electrical transmittance through the branched network is observed with the implementation of a potential difference between two metal blocks. Such a system is typically modeled with an electrical circuit consisting of three different circuit elements: ionic resistor, double layer capacitor, and electrical resistor. Additional components can also be integrated

according to variations in the response of the impedance spectra. Herein, an ionic resistor implies resistance of electrolytes related to the movement of ions. It is identified as the real part of impedance spectra at high frequencies. The double-layer capacitance is associated with the electrolyte-metal block interface and stems from the augmentation of ions at the metallic surface. The electrical resistance results from a sufficient CA within the structure and is parallel to an ionic resistor in the circuit. A transformation from a nearly straight line (seen in bare electrolytes) to a semicircle structure is observed in the Nyquist plot with increasing CA. Hence, the real impedance intercept at a low-frequency regime is ascribed as the electrical resistance of the dispersion [31,37,58].

The literature review indicated a prevalent use of high-energy mixing systems in the suspension electrode preparation. For this reason, high-energy tools (homogenizer and ball mill) were preferred to prepare suspension electrodes in preliminary studies. Using a homogenizer, EAM and CA particles were initially blended in an aqueous electrolyte. EIS measurements were conducted to analyze the electrical properties, specifically the percolation structure, and to control the suspensions' reproducibility.

The EIS results for three distinct 1KB – 10LFP suspensions prepared in this context are presented in Figure 3.2 (a). To ensure reproducibility, each suspension electrode is anticipated to yield a similar impedance result. However, upon examining the Nyquist plot (with the diameter of the formed semicircle as an indicator), it becomes apparent that suspensions prepared similarly exhibited distinct impedance responses. Similar variations encountered in 2KB suspensions prepared with ball milling are presented in Figure 3.2 (b). In addition, the time-dependent EIS analysis of a 2KB suspension (ball milled) sealed in the measurement cell is provided in Figure 3.2 (c). Time-dependent variation in the corresponding impedance spectra proved that suspension behavior was changed significantly. Although the initial resistance was approximately 4 kΩs, it increased to 9 kΩs after 24 hours. The alteration in response could suggest that the suspension has undergone structural modifications, potentially phase separation [31]. Due to the strong interactions between particles, particles may attract each other and form clusters over time. Hence, the established chain structure

could have been disrupted, and the percolated structure may have disintegrated. This may result in isolated KB islands and a more resistive structure.

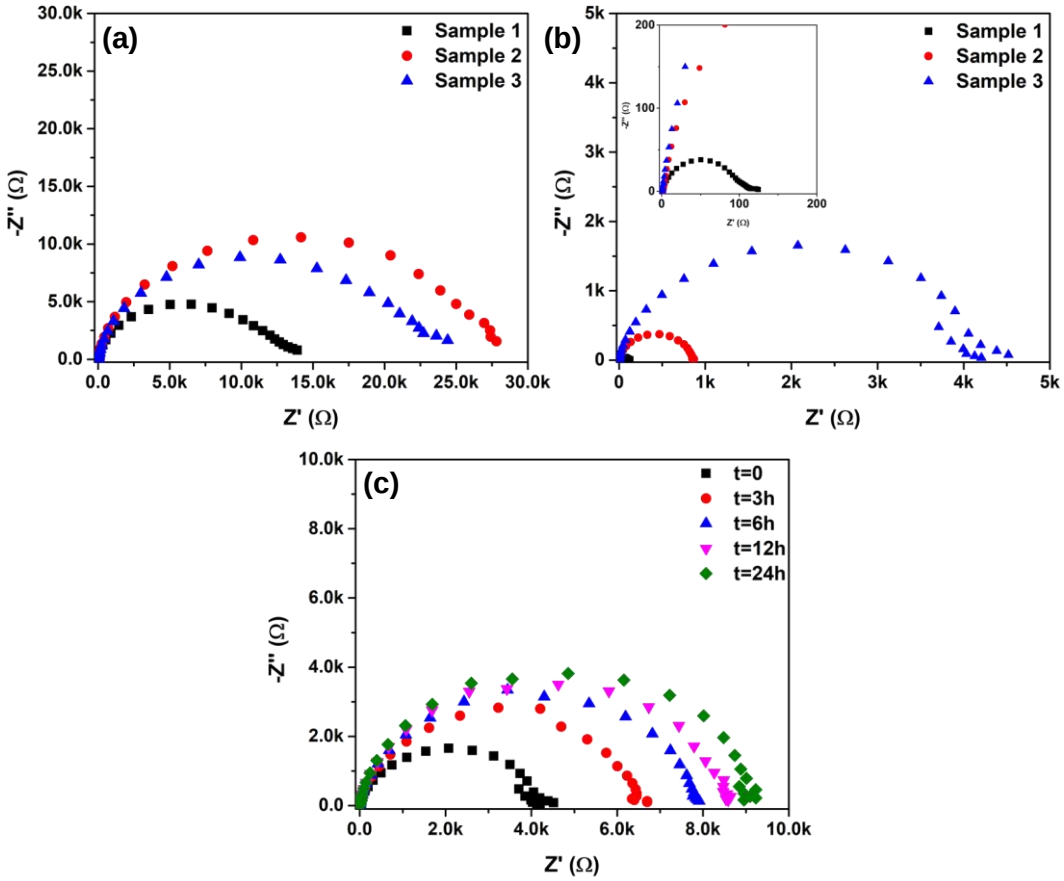

Figure 3.2 Electrochemical impedance spectra analyses of; (a) 1KB – 10LFP suspension electrodes prepared with a homogenizer, (b) 2KB suspensions prepared with ball milling, and (c) time-dependent variation of 2KB suspension prepared with ball milling.

The high-energy tools provide sufficient particle mixing. Thus, the primary reason leading to rapid structural changes could be the susceptibility of the particles to the attractive and repulsive forces within the suspension. Therefore, the problem could be the interaction of the particles with the electrolyte that results in microstructural

variations inside the electrode. To comprehend the potential source of this issue and achieve greater homogeneity/reproducibility in suspensions, it was proposed to optimize the suspension electrode formulation by controlling the surface properties of the particles. These processes are detailed in this chapter.

Dispersion of CAs in aqueous media is a challenge. Therefore, we first investigated the colloidal behavior of KB particles in Li_2SO_4 aqueous electrolytes. The stability, percolation, and the amount of CA that can be loaded into the suspension are directly related to the particle characteristics. The physical properties of the KB particles used in the present study can be seen in Figure 3.3. SEM analysis in Figure 3.3 (a) revealed the structural subunits of KB with sizes less than 50 nm. The hydrodynamic radius determined by DLS analysis (Figure 3.3 (b)), on the other hand, was 275 ± 9 nm, exhibiting subunit KB particles conglomerated and forming larger branches in aqueous media.

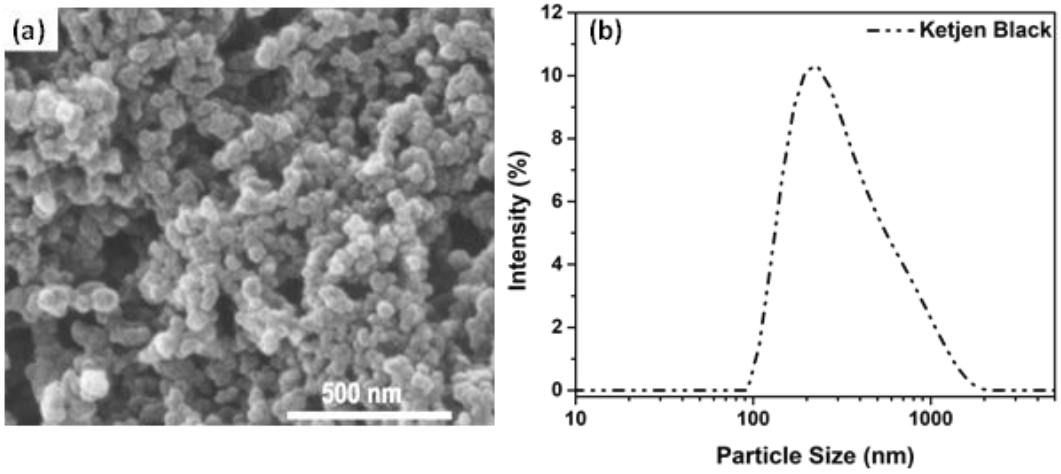

Figure 3.3 Physical properties of KB particles used in the study; (a) scanning electron micrograph and (b) particle size distribution.

Numerous studies showed that increasing ionic strength positively affected the electrode's electrochemical behavior (capacity, cyclic stability) [99,117,118].

However, it may have a detrimental influence on the stability of the suspension electrode as it may change the physical characteristics of the particles. The effect of the ionic strength of the electrolyte on the stability and particle size of KB particles is shown in Figure 3.4. It can be seen that the zeta potential value of the particles was around +30 mV when they were dispersed in DIW. Since the CB particles are inherently hydrophobic, the relatively high zeta potential recorded indicated the presence of bonded groups on their surfaces that dissociate in DIW. The surface charge on the particles leads to the formation of an electrical double layer (EDL) around the particles. The zeta potential value decreased with the increase in ionic strength, and the sign reversed around 0.3–0.4 M. As a rule of thumb, a zeta potential value higher than ± 30 mV is suggested to achieve electrostatic stabilization. Hence, stability is not anticipated at different ionic concentrations. The PSA analysis also showed that KB particles were around 300 nm in size in DIW, i.e., they consist of clusters of several primary KB particles (revisited Figure 3.3 (a)). An increase in the average particle size was also seen with rising electrolyte molarity.

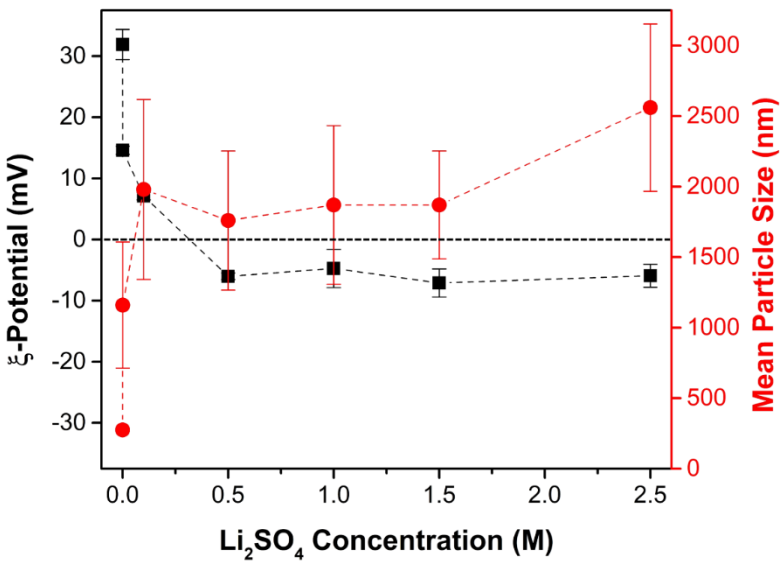

Figure 3.4 Effect of aqueous electrolyte's ionic concentration on zeta potential and average particle size of KB particles.

The properties of the electrolyte and the condition in which the electrolyte and particles interact (i.e., preparation protocol) can affect the dispersion of carbon particles. The dispersion kinetics of KB particles in aqueous electrolytes where KB particles were suspended through different suspension preparation procedures are compared in Figure 3.5. The KB particles' state after being directly mixed with DIW and gently agitated is presented in Figure 3.5 (a). Visual monitoring suggested that KB particles could be effectively dispersed in DIW and form a stable, – homogeneous structure. The stability in DIW was also proved by the recorded high zeta potential value (Figure 3.4).

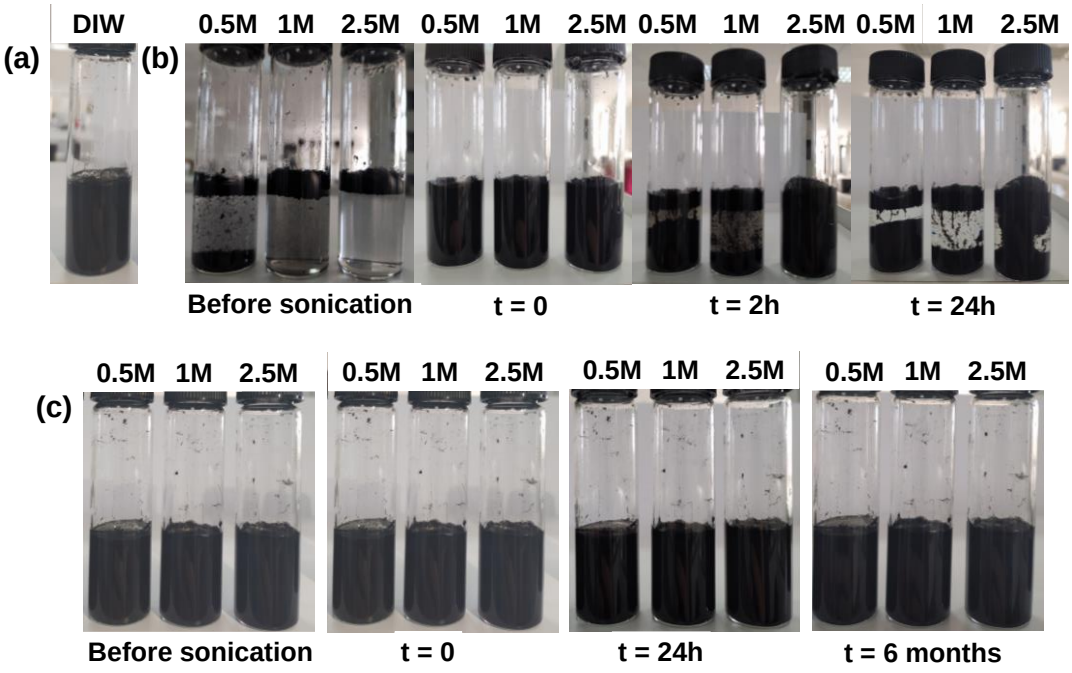

Figure 3.5 Dispersion behavior of KB particles in suspensions prepared with different salt addition sequences; (a) in DIW, (b) Method 1, i.e., direct mixing of KB particles with electrolyte, and (c) Method 2, i.e., the addition of salt as a powder after dispersing KB particles in DIW. (The numbers above the vials represent the molar concentration of the electrolyte)

Considering the benefits on electrochemical performance, it is crucial to prepare an electrolyte with high salt concentrations. However, the ionic strength of this electrolyte may alter the behavior of KB particles when mainly used as suspension electrodes. Figures 3.5 (b) and (c) illustrate the impact of suspension (or electrolyte) formulation and the ionic nature of the electrolyte on KB dispersion kinetics. When the aqueous KB suspensions formulated through Method 1, a direct mixing of particles and electrolytes, were examined, the mixture's agitation was insufficient to disperse the KB particles in the electrolyte presented as before ultrasonication in Figure 3.5 (b). This behavior, dependent on the electrolyte's ionic concentration, revealed that a few particles were present in the liquid media at relatively low ionic concentrations. The number of particles mixed with the electrolyte decreased with increasing salt concentration. Eventually, at a concentration of 2.5 M Li_2SO_4, almost no KB particles were observable in the electrolyte. The electrolyte concentration affected KB particles' wettability and dispersion in this liquid media, and at higher concentrations, all the particles floated on the electrolyte surface.

The ultrasonication process is an effective technique to disperse carbon particles or inhibit agglomeration [119]. When the mixtures were subjected to ultrasonication, it can be said that the dispersion characteristics of the particles changed (Figure 3.5 (b)). Although the ionic strength of the electrolyte prevented the dispersibility, ultrasonication allowed the electrolyte to penetrate between the particles. As a result of the liquid filling the inter-particle spaces, it can be seen that at t=0, the KB particles were mixed with electrolytes at all ionic concentrations. While ultrasonication enabled the inclusion of the particles into the liquid media, it was evident from the sedimentation analyses that these particles did not maintain this structure over time. An apparent phase separation was observed in the mixtures at the end of one-day settlement tests.

As shown in Figure 3.5 (c), KB dispersion characteristics were affected by suspension formulation. The particles could be dispersed in all electrolyte concentrations when the aqueous KB suspensions were prepared using Method 2, that is, by adjusting the ionic strength of the electrolyte following the dispersing of

the KB particles in DIW. Aqueous KB suspensions prepared using this method maintained stability for an extended period (more than six months). They did not exhibit precipitation or phase separation signs, as observed through time-dependent sedimentation monitoring.

To understand the effect of preparation protocol on suspension electrode characteristics, aqueous suspensions of 2 wt.% KB was prepared. While the particles mixed with direct electrolyte dispersed to some extent after ultrasonication, phase separation was observed in the structure over time. However, after 24 hours of magnetic stirring, it was seen that the suspension maintained its behavior for a long time. This indicates that the interaction between the particles may come to equilibrium after 24 hours of stirring and may also be due to the concentration effect. Time-dependent EIS analyses of 2 wt.% KB suspensions prepared with different methods (experimental protocols) are presented in Figure 3.6.

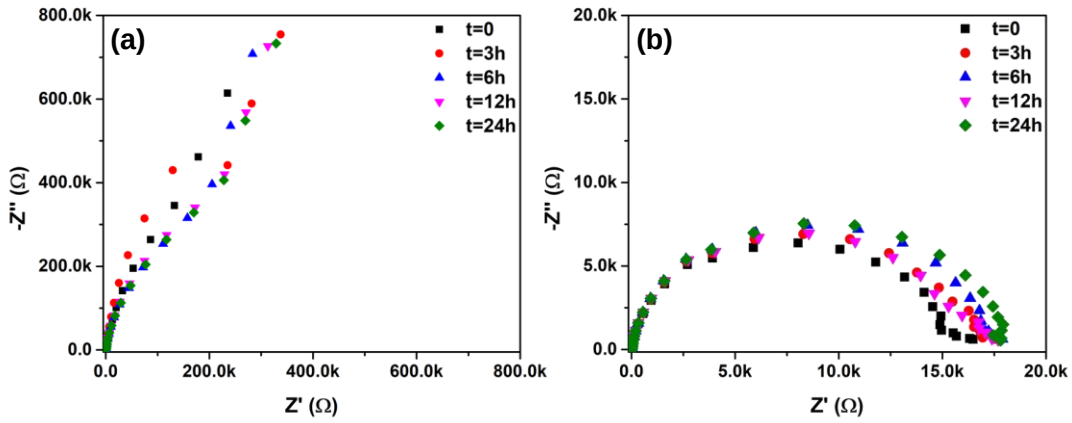

Figure 3.6 Time-dependent variation in the response of impedance spectra (Nyquist plot) of 2 wt.% KB aqueous suspensions; (a) suspension prepared with Method 1, i.e., direct mixing of KB particles with electrolyte and (b) suspension prepared with Method 2, i.e., the addition of salt as a powder after dispersing KB particles in DIW.

Comparing the impedance spectra proved that the preparation protocol had a significant impact on the electrical behavior and microstructure of the suspension electrode. While the suspension prepared following Method 1 exhibited a partially reticulated structure, it is evident that the resulting suspension had a high resistance (Figure 3.6 (a)). If we examine the response of the suspension prepared through Method 2, on the other hand, it is clear that a fully percolated structure responsible for charge transfer was formed (Figure 3.6 (b)). When the resistance values characterized by the diameter of the formed semicircle were compared, it can be easily said that the suspension prepared with Method 2 was significantly less resistive than the other sample. This can be attributed to the homogeneous distribution of KB particles with smaller particles in contact. The formation of large KB agglomerations or clusters in the suspension prepared with Method 1 or the particles' wettability should inhibit the formation of possible conductive pathways and percolated structure. This proves that the inhomogeneous suspension formulation requires much more KB to be loaded into the suspension to achieve a percolated structure with less resistivity values. This would increase both the viscosity of the suspension and the inactive material within it.

As seen in Figure 3.6, the control of the suspension preparation protocol allowed for creating homogeneous suspensions. This enabled the acquisition of consistent and similar EIS results. As discussed earlier, suspensions formed by directly combining particles with the electrolyte can be mixed and homogenized using a ball mill. However, it was observed that the microstructure may change due to possible phase separation in the resulting suspension, thus leading to varied impedance values over time. Compared to magnetic stirring, a ball mill is a method that can change the physical properties of the particles. Therefore, a different particle structure may be observed after ball milling in addition to microstructural change. SEM images of KB particles subjected to magnetic stirring and ball milling are presented in Figure 3.7. It can be said that the particles retain their initial particle size and shape (revisit Figure 3.3 (a)) after magnetic stirring. Similarly, there is not much difference in the morphology and structure of the KB particles after ball milling.

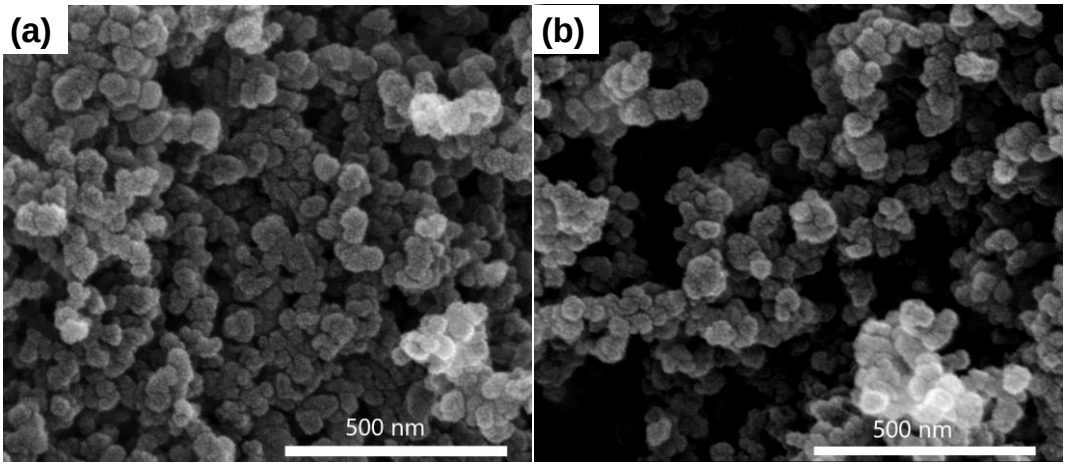

Figure 3.7 Scanning electron micrograph of KB particles; (a) magnetically stirred and (b) ball milled.

A suspension electrode is a multi-component system consisting of CA and EAM particles. In addition to the characteristics of CA, EAM's properties also contribute to the suspension microstructure and corresponding behavior. When the behavior of the LFP used to prepare the suspension electrode was examined concerning salt concentration, it was seen that the particles were negatively charged in DIW (Figure 3.8). It can be said that the particles have enough charge to remain relatively stable. While the zeta potential decreased with increasing lithium sulfate concentration, the surface charge screened with increasing ionic concentration as predicted by electrical double layer theory.

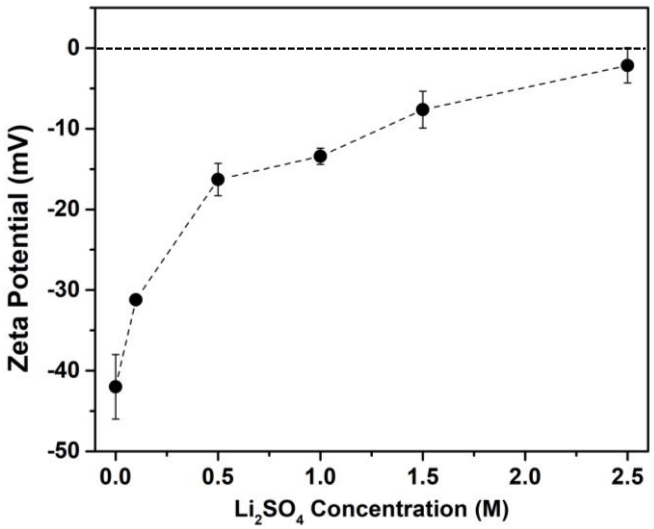

Figure 3.8 Effect of aqueous electrolyte's ionic concentration on zeta potential value of LFP particles.

Compared to the behavior of KB particles, the behavior of LFP particles once again underlined the necessity of preparing suspension electrodes by controlling the physicochemical properties of the particles. In DIW, the KB particles were positively charged, and the LFP particles were negatively charged. Therefore, it is expected that the clustering of those particles is due to the attraction of the opposite charges when both particles are mixed in a liquid with low ionic strength (less than 0.5 M). This uncontrolled clustering may also lead to different suspension formations and microstructures depending on the solids content of the particles and mixing conditions. However, dispersing KB in DIW and increasing the ionic concentration resulted in negatively charged particles. Hence, allowing the KB particles to acquire a negative charge first and adding LFP particles to the suspension would result in particle systems with more homogeneous distribution and structure.

3.4 Conclusions

Obtaining homogeneous and stable aqueous carbon dispersions poses a challenge, commonly intended to be overcome by high-energy mixing tools or additives. In this chapter, we showed that aqueous carbon dispersions with long-term stability can be obtained by simply controlling the surface properties of the particles and regulating the preparation protocol accordingly. The dispersion kinetics of KB particles were found to be significantly influenced by the electrolyte formulation. It was noticed that KB particles, readily dispersed in water, can only be dispersed in aqueous electrolytes with the help of ultrasonication. Yet, rapid, i.e., in a day, phase separation was observed. However, increasing the ionic strength of the medium after dispersing the KB particles in DIW led to a homogeneous and stable suspension. Such suspension electrode preparation procedure enabled the obtaining of stable and reproducible EIS results. Electrical potential, and thus the charge of the particles in aqueous media, changed according to the ionic concentration of electrolytes. This highlights the importance of considering EAMs' properties and the suspension formulation to establish a multicomponent suspension electrode. Such suspensions with different microstructures can be obtained according to the surface charge of the EAM and its response to the ionic nature of the electrolyte. The impedance analysis revealed that the suspension formulation also affects the electrical resistance of the suspension electrode. Suspensions formed by directly introducing KB particles into the electrolyte displayed elevated resistivity. However, the version with a homogeneous structure exhibited significantly lower resistivity values, signifying the development of a percolated structure. Furthermore, the impedance response value remained relatively constant throughout the extended measurement period, indicating the sustained homogeneity and stability of the obtained suspension. It was also shown by ball milling that the KB could be dispersed directly in the electrolyte, and the reticulated structure responsible for the conductivity was formed. However, even if such a dispersion was achieved, time-dependent impedance measurements showed that the resistance of the suspension increased from nearly 4 kΩs to 9 kΩs

at the end of 24 hours, indicating the structure's instability. This study showcased the feasibility of acquiring homogeneous and stable aqueous carbon dispersions and suspension electrodes, delivering consistent and reproducible EIS results without relying on high-energy mixing systems or dispersant usage.

CHAPTER 4

THE INFLUENCE OF AGGLOMERATION STATE OF LITHIUM IRON PHOSPHATE PARTICLES ON AQUEOUS SUSPENSION ELECTRODE BEHAVIOR

4.1 Introduction

Utilizing suspensions as electrodes in flow-through systems offers great promise for achieving high-energy dense systems. However, their high viscosity is the most critical bottleneck for suspension electrodes to be integrated into flow energy storage systems and become a feasible technology [26]. This is a direct consequence of the suspension microstructure and underlines the importance of controlling the suspension microstructure. Suspension microstructure is of great importance not only in terms of processability but also in terms of electrical-electrochemical performance. Achieving a homogeneous suspension is critical for the suspension to perform the same over a long period and to exhibit a consistent result. Therefore, a suspension electrode characterized by a homogeneous structure is essential for better processability and electrochemical performance.

Numerous investigations have been done to comprehend the suspension microstructure, and considerable effort has been spent to ameliorate the microstructure. All these studies devoted to improving the suspension microstructure primarily focused on altering the suspension preparation protocols and/or the type and the amount of the EAMs and CAs used. In investigations of suspension microstructure, findings indicated that particle characteristics such as size, shape, morphology, dimension, etc., dictated the microstructure. Thus, particle properties were found to influence flow and electrochemical behavior substantially [37,40,62,66,106].

In addition to these generally described particle properties, particles' agglomeration state is an important characteristic. The agglomeration state of particles has a pronounced impact on EAM concentration, suspension homogeneity, stability, and flowability. However, the significance of this agglomeration state has been overlooked in suspension electrode formulations. Although a few studies demonstrated the use of dispersible particles (especially in flow-through systems) [39,61], the agglomeration state of the particles was not the primary concern in these studies.

Here, it was intended to elucidate the influence of particle agglomeration on the microstructure of suspension electrodes and its subsequent effects on rheological and electrical properties. In this study, we selected two different LFP particles in agglomerated and dispersible forms. We systematically studied the influence of using individual particles in the suspension electrode's microstructure and the resulting flow and electrical responses. Most commercially available powders are hard agglomerates, i.e., consisting of particles almost chemically fused into each other. Hence, individual and colloidal LFP particles were synthesized using a suitable method for comparison. To this end, first, EAM powders were thoroughly characterized. Second, only CA and EAM-containing aqueous suspensions were studied, and the influences of the agglomeration state of EAM were discussed. Thirdly, the suspension electrodes were prepared by mixing EAM and CA, and suspension characteristics were analyzed. Lastly, the dispersion characteristics of the suspension electrodes were compared in suspension and cast form, and their effect on the energy capacities of electrodes was discussed.

4.2 Experimental Procedure

4.2.1 Materials

Li_2SO_4 (anhydrous, 99.7%) was purchased from Alfa Aesar. KB (EC600JD, Akzo Nobel) was used as a CA in aqueous suspensions. DIW with a resistivity of 18.2 MΩ was used to prepare aqueous suspensions. Two types of LFP particles were used in this study. One type was purchased and utilized without further treatment. The other was synthesized via the polyol method, as reported previously by our group, with the sample label of "LFP_B/C – 600" in that study [120]. These synthesized LFP particles were labeled 'dispersible' (LFP-D), while the as-received ones were labeled 'agglomerated' (LFP-A).

4.2.2 Suspension Preparation

Aqueous suspensions of bare KB, bare LFP, and the mixture of KB and LFP with different solid loadings were prepared. For KB suspension preparation, the required amount of KB was slowly added to the DIW, gently shaken, and then ultrasonicated in the bath for 10 minutes to disperse particles. The mixture was stirred with a magnetic stirrer at 250 rpm at room temperature for 24 hours. For KB-LFP suspension preparation, LFP particles were added in the last 3 hours of mixing to obtain a homogeneous suspension. The bare LFP suspensions were prepared by slowly adding LFP particles to the DIW and stirring them at 250 rpm for 2 hours. To ensure enough ionic concentration, the required amount of Li_2SO_4 to reach 1 M electrolyte concentration was added in powder form in pursuit of dispersion of KB or LFP particles in DIW. Then, the resulting suspension was ultrasonicated for 10 minutes before the stirring process. The samples were labeled as "**xKB - yLFP-(A or D),**" where x and y denote the weight percentages of KB and LFP, respectively. For instance, a 3 g suspension of 2KB – 30LFP contains 0.06 g KB, 0.9 g LFP, and 2.04 g DIW.

4.2.3 Characterization

The crystal structure of EAMs was characterized by XRD (Bruker D8, Cu-K_α radiation) operating between 10° and 80° at a scan rate of 2°/min. Morphological investigation and size analyses of particles were realized with SEM (Nova, NanoSEM 430) operating at 20kV. The dispersion characteristics of LFP and KB particles were analyzed over the tape-cast films via SEM and energy-dispersive X-ray spectroscopy (EDS). For this purpose, suspensions were prepared using an electrolyte concentration of 0.3 M to eliminate excess salt crystallization on the dried surface. They were spread on cover glass with a cast thickness of 150 μm using an applicator. SEM and EDS samples were coated with gold before examination. At room temperature, particle size distribution was investigated via DLS (Zetasizer Ultra, Malvern). The zeta potential of particles was also measured with the same instrument. For these analyses, aqueous suspensions with 0.01 wt.% solid particles were prepared. Suspensions were treated in an ultrasonic bath for 5 minutes and then for 2 minutes with an ultrasonic homogenizer (Bandelin 2070, operating at %75 power) equipped with an MS 73 probe (φ = 3 mm) to disperse each suspension homogeneously. The carbon content of the particles was measured by ELTRA CS 800, Carbon Sulfur Analyzer. Particle size, zeta potential, and carbon content measurements were repeated for three distinct samples.

The rheological behavior of aqueous suspensions was characterized by a rheometer (Anton Parr, MCR 102) with a parallel plate geometry (plate diameter 50 mm, gap 0.5 mm). A solvent trap was utilized to prevent electrolyte evaporation during the measurements. The rheological measurements were performed according to the following procedure: (i) The flow behavior of samples was measured between 0.01 – 100 s^{-1}. Three sequential runs were carried out, each comprising two half loops (upward and downward). Here, the shear rate ramps from 0.01 to 100 s^{-1} (first half loop) and down to 0.01 s^{-1} (second half loop). For each half-loop, 41 points were recorded. Reproducible data was obtained after the completion of the initial cycle, and the last loop was reported. For bare aqueous LFP suspensions, tests were carried

out between 0.01 – 500 s^{-1}, and 47 data points were collected for each run. (ii) following rheological behavior measurements, samples were left for 10 minutes for relaxation, and then strain sweep tests were done between 0.001 – 100% strain at an angular frequency of 1 rad/s to determine the linear viscoelastic region (LVER) for each sample, (iii) at the end of the strain sweep tests, samples were left 5 minutes for relaxation. Then, the frequency sweep tests were performed at a defined strain rate obtained from strain sweep measurements.

Potentiostatic EIS analyses of aqueous suspensions were performed using a homemade Swagelok-type cell with two stainless steel electrodes at two ends, as shown in Figure 3.1. The diameter of both electrodes was 10.4 mm, and the gap was adjusted to 0.5 mm. Potentiostatic EIS was acquired with a potentiostat/galvanostat/ZRA (Gamry Instruments, Reference 600) between 0.01 Hz and 200 kHz at a perturbation amplitude of 10 mV by collecting 6 points per decade at 0 V open circuit potential. The results were represented with Nyquist and Bode plots, and equivalent circuit fitting was done using EC-Lab software (Biologic). Electrical conductivity (σ) calculations were done by fitting the acquired Nyquist plots and using Equation 4.1 [37], considering the geometrical factor of the measurement cell.

$$\sigma = \frac{d}{A \; x \; R_{pn}} \qquad \text{(Equation 4.1)}$$

, where *d*, *A*, and R_{pn} represent the cell thickness, surface area of metal blocks, and electrical resistance of suspensions, respectively.

EIS analyses of KB suspensions were repeated for three different batches. Before EIS measurement, all suspensions were subjected to 3 cycles of cyclic voltammetry analysis at a scan rate of 1mV/s in the 0 – 0.1 V range.

4.3 Results and Discussions

4.3.1 Characterization of LFP particles

The physicochemical properties of used LFP particles are tabulated in Table 4.1, and the crystal structure, morphological, and particle size distribution analyses are presented in Figure 4.1.

Table 4.1. The physicochemical properties of LFP particles used in this study.

Sample	Tap Density (g/cm^3)	A_{BET} (m^2/g)	Carbon Content (wt.%)	D_{50} (nm)	ζ-Potential (mV)
LFP-A	0.84 ± 0.09	8.70	3.90 ± 0.05	747 ± 29	- 42 ± 4
LFP-D	1.16 ± 0.08	14	1.38 ± 0.04	392 ± 14	- 46 ± 2

** A_{BET}: specific surface area obtained from Brunauer-Emmett-Teller (BET) analysis, D_{50}: mean particle size measured with dynamic light scattering (distribution based on volume intensity). LFP-A represents the agglomerated particles, whereas LFP-D represents the dispersible particles.*

All intense peaks in the X-ray diffraction pattern presented in Figure 4.1 (a) were indexed to orthorhombic LFP structure with Pnma space group, JCPDS card number 83-2092. While secondary phases were not observed in either material, the sharp, narrow diffraction peaks demonstrated good crystallinity. The particle size distribution analyses in Figure 4.1 (b) showed a monomodal size distribution comprised of submicron particles for synthesized LFP particles. In contrast, the as-received particles exhibited bimodal behavior consisting of submicron particles and a few micron-scale particles. As expected from its agglomerated structure, the dispersion or sedimentation behaviors of the as-received particles showed graded turbidity in the supernatant, indicating the smaller particles' size-dependent sedimentation. In contrast, most large, agglomerated clusters settled down (Figure 4.1 (c)). Synthesized particles, on the other hand, led to more homogeneous turbid suspension without significant sedimentation. In line with this, SEM images of the

synthesized and as-received particles revealed substantial differences in particle shape and size. While the as-synthesized specimen consisted of individual and submicron particles with homogeneous distribution, the as-received sample comprised irregularly shaped, agglomerated particles with varying dimensions.

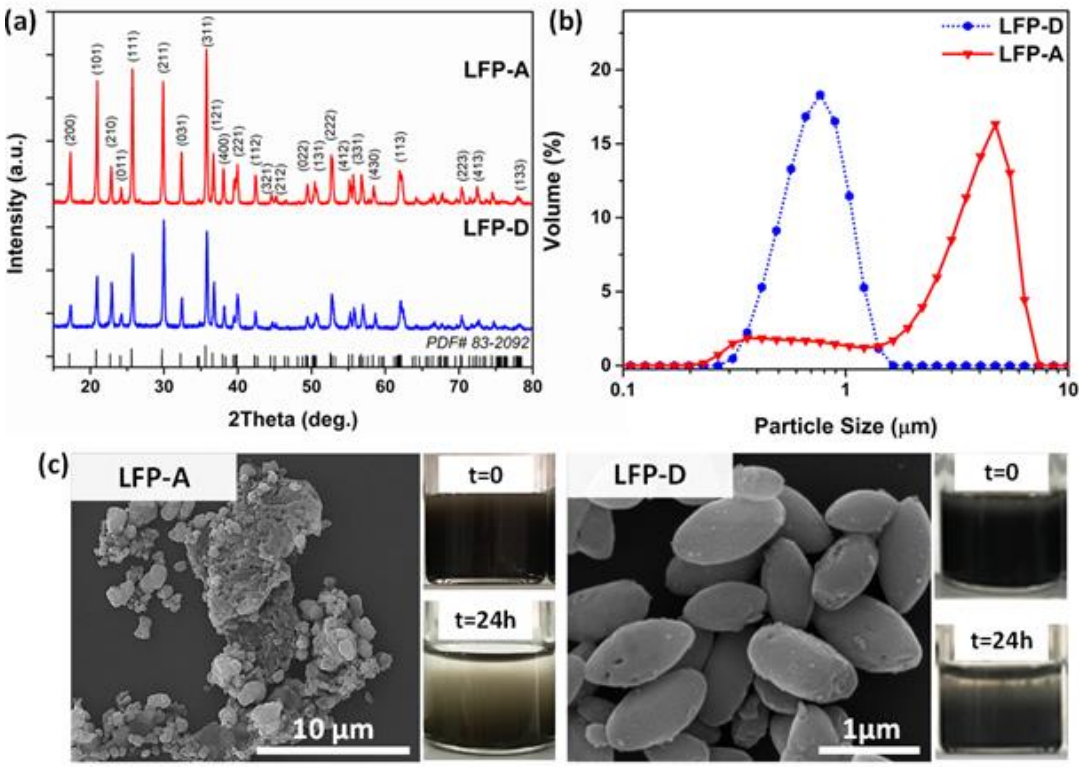

Figure 4.1. The crystal structure, morphological, and particle size analyses of utilized electroactive materials; (a) X-ray diffractogram, (b) particle size distribution by volume intensity (semi-log scale), and (c) scanning electron micrograph and sedimentation behavior of LFP particles.

4.3.2 Effect of KB Content on Percolation Network Formation in Aqueous Suspension

To obtain a conductive electrode, it is crucial to determine the amount of CA required to achieve the percolation network threshold. KB suspensions were prepared at varied weight percentages from 0.3% to 3% and characterized by EIS, as presented in Figure 4.2.

1 M Li_2SO_4 electrolyte and all the KB suspensions exhibited similar resistance (~1 Ω) values at high-frequency regions, showing independence of the response from the KB concentration of suspensions. At lower frequencies, the suspension prepared with 0.3 wt.% of KB exhibited a virtually linear Nyquist plot (Figure 4.2 (a)). It slightly deviated from that of the electrolyte, indicating that ionic conduction predominated in the system with no obvious conduction path between the KB particles. Increasing KB content from 0.3 wt.% to 0.5 wt.% resulted in a sharp transition from linear to almost perfect semicircle, indicating that an electrically conductive network started to form between the KB particles in the 1 M Li_2SO_4 aqueous electrolyte. As is apparent, further increasing KB concentration in the suspension led the semicircle structure to turn into a narrower and more depressed version, indicating the formation of an electrically less resistive structure.

The capacitance values of each KB suspension were similar, as shown in the Bode plot in Figure 4.2 (b). This signified that the values were independent of KB concentration and due to double-layer formation on the steel electrode surfaces.

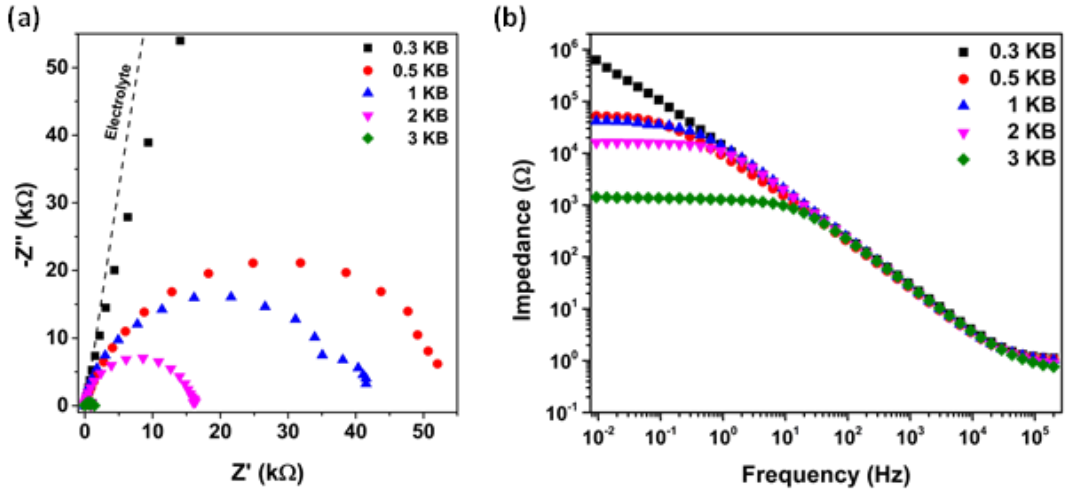

Figure 4.2. Electrochemical analyses of aqueous (1 M Li_2SO_4) KB suspensions with different solids loading; (a) impedance spectra (Nyquist plots) and (b) impedance spectra (Bode plots).

As the capacitive behavior of all samples was similar at the moderate frequency region in the Bode plot (Figure 4.2 (b)), the intercept at the low-frequency region gives the bulk resistance of the suspensions. Hence, it can be used to determine the electrical conductivity of the aqueous KB suspensions. The electrical conductivity values were calculated considering the cell factor and presented in Figure 4.3. Although the conductivity change seemed to show a nearly linear behavior at low concentrations of KB, a closer look at the data revealed a continuous scaling. Here, there was an almost 4-fold increase in conductivity between the KB concentrations of 0.3 wt.% and 1 wt.% (inset of Figure 4.3). In this relatively low concentration range, KB particles were probably insufficient to ensure a fully percolated network formed by interparticle connections to convey the electrical current. Conversely, a sharp increase of nearly 13 times in electrical conductivity was noted during the transition from 2 wt.% to 3 wt.% of KB. This signifies the attainment of the percolation threshold within this range. Increasing the electrical conductivity of the suspension with increasing KB content may indicate the formation of a denser

structure. Therefore, increasing the number of particles might cause the formation of more contact points, which results in the creation of conductive pathways for electrons. In this situation, electron transfer could be made more readily, resulting in a less resistant structure. The electrical conductivity of compressed KB particles is approximately 10^5 mS/cm [121], whereas the conductivity levels of KB suspensions are notably lower, as seen in Figure 4.3. It is noteworthy that when there is a substantial presence of KB chains in the suspension, accompanied by the formation of a percolated network structure, the electrical conductivity of the KB suspension reaches almost 0.05 mS/cm.

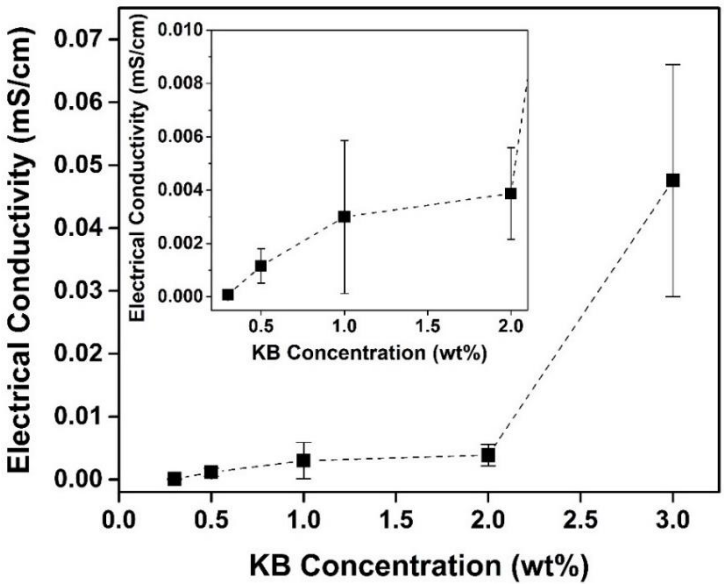

Figure 4.3 Calculated electrical conductivities of KB suspensions considering the geometrical factor of the measurement cell (the inset figure represents the data for KB concentration between 0.3 to 2 wt.%).

The rheological behavior of an electrode suspension is not only crucial to reveal its flow characteristics and, thus, for operation. It also gives insights into the

microstructure of the suspensions. Therefore, both rotational and oscillation rheology analyses of suspensions were conducted.

Dynamic oscillation tests were employed to investigate the viscoelastic characteristics of the aqueous KB suspensions. First, a strain amplitude sweep test was conducted to determine the LVER in a strain range from 0.001% to 100% at an angular frequency of 1 rad/s. Both the storage (elastic) modulus (G') and the loss (viscous) modulus (G'') are presented as a function of shear strain in Figure 4.4 (a). When the KB concentration increased from 0.3 wt.% to 3 wt.%, the storage modulus increased nearly a thousand times (from 0.4 Pa to approximately 318 Pa), indicating a significant increase in the rigidity of the structure and the more solid-like behavior of suspension. The LVER was determined to be almost 10% strain for 0.3 wt.% KB-containing suspensions while this range was narrowed to 1% when the KB concentration increased to 3 wt.%. In the LVER, the storage modulus was higher than the loss modulus. The KB suspensions behaved as a viscoelastic solid material, even at low concentrations, evidencing the presence of structured suspensions with strong interparticle interactions. As observed in Figure 4.4 (a), the loss modulus of suspensions got higher than the storage modulus at higher strains, meaning that the interparticle interactions might be overcome by applied shear stress. The particles got partially separated from each other, and thus, the suspension showed less resistance to flow and exhibited more liquid-like behavior. This shift in the structure is critical; therefore, this flow point (a.k.a. cross-over point) was determined for each suspension and plotted in Figure 4.4 (b). The critical shear strain/stress values in this plot are assigned as the intersection point of the storage and loss modulus values [105]. It showed a continuous decrease in strain amplitude and an increase in the corresponding shear stress with increasing KB amount in the suspension. The sharp changes in critical shear strain and stress values at KB concentrations higher than 1 wt.% indicate increasing rigidity and compactness of the suspension structure.

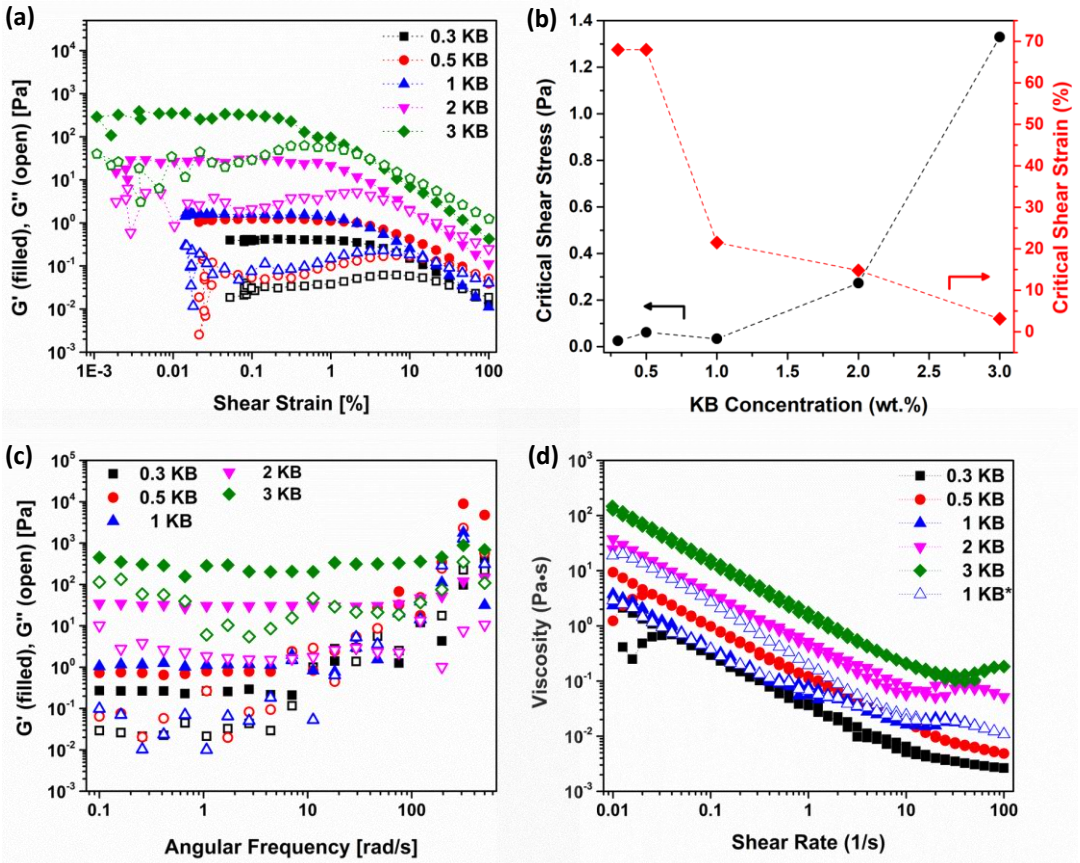

Figure 4.4 Rheological behavior analysis of aqueous (1 M Li_2SO_4) KB suspensions; (a) amplitude sweep test measurements recorded at constant angular frequency (1 rad/s), (b) concentration dependency of critical shear strain and stress values which were found from the intersection point of the storage modulus and loss modulus values, (c) frequency sweep tests investigated at a specific strain (0.01%), and (d) flow curves of aqueous KB suspensions (open and filled "up triangle symbol" (in blue color) shows the first cycle and last cycle of the flow for 1 wt.% KB, respectively).

Following the amplitude sweep tests, a shear strain level of 0.01% was chosen in LVER for all KB concentrations to conduct the frequency sweep analysis. As presented in Figure 4.4 (c), suspensions' time-dependent response at nearly static frequency sweep conditions changed dramatically when the KB concentration was

increased from 1 wt.% to 2 wt.%. At relatively low concentrations (up to 1 wt.%), the magnitudes of the moduli were constant at low angular frequencies with larger storage modulus than the viscous modulus. Still, they increased with increasing frequency, suggesting that the elastic structure had broken down. At higher KB concentrations, both moduli became frequency-independent, corresponding to strong, almost solid structures.

Rotational rheology test results are presented in Figure 4.4 (d). The viscosity of the suspension at a shear rate of 0.1 s^{-1} continuously increased from 0.3 Pa·s to 13 Pa·s when the KB amount was increased from 0.3 wt.% to 3 wt.% in aqueous suspension. As expected, increasing crowdedness in suspension led to more frequent particle interactions in suspensions and more resistance to flow. At all concentrations, suspensions exhibited shear thinning behavior (reduction in viscosity with increasing shear rate) over the significant portion of the applied shear rate range. The suspension with 1 wt.% KB seemed to be an exception in this increasing suspension viscosity trend. However, further analysis showed that this behavior could be related to the structural changes occurring in the suspension upon increasing the shear rate (Figure 4.4 (d)). As such, during the first flow cycle, the viscosity values of 1 wt.% KB suspension recorded at lower shear rates was higher than 0.5 wt.% KB. At 1 wt.% concentration, although the flow behavior was shear thinning at low shear rates, the flow characteristic was irreversibly changed after a shear rate of 10 s^{-1}. Similar flow behavior change was observed at all concentrations above 1 wt.%, yet at these high concentrations, the behavior was reversible. Therefore, this concentration was recorded as the concentration at which the suspension microstructure changed. If the hydro-clusters started to form at these concentrations, they might partially be fragmentized with an increasing shear rate. These fragments, particularly when aligned in the direction of applied shear, would resist less to the flow than the 3D clusters and lead to lower suspension viscosities. Depending on the cluster's strength, the behavior might be reversible or irreversible. Increasing KB concentration seemed to result in more robust clusters because of the reversibility of this rheological behavior change. Upon revisiting the EIS results depicted in Figure 4.2 (a) and

Figure 4.3, which were obtained under stationary conditions, it became evident that the slope of the electrical conductivity shift with rising KB concentration changed, occurring notably after reaching 1 wt.% and 2 wt.% of KB. Combining this observation with the rheological behavior change in these concentrations, more branched and stronger KB structure formation after 1 wt.% KB addition hypothesis seemed to be further supported.

The observed alterations in amplitude sweep and rotational tests were also reflected in the critical shear strain-stress behavior. Moreover, it is noticeable that the impedance and electrical conductivity results in Figure 4.2 and Figure 4.3 and the critical shear strain-stress plot agree with the change in suspension behavior. Therefore, the behavior change in the critical shear stress-strain graph can help determine the percolation network threshold. It can be identified as between 1 wt.% and 2 wt.% based on the changes in critical shear strain-stress behavior in our study.

When the oscillation measurement results were combined with the conductivity analyses, the change in suspension microstructure is visualized in Figure 4.5. The suspension displayed a solid-like structure at a KB concentration of 0.3 wt.%. So that particles were close enough to strongly interact with each other yet far enough not to convey electron flow. With increasing KB concentration to 0.5 wt.% and 1 wt.%, the particles started to get close enough to touch each other. Thus, conductive networks were formed for electron transfer, but resistance was high. At a concentration between 1 wt.% and 2 wt.%, the number and strength of interparticle interactions increased, and the percolation threshold was achieved. At even higher concentrations, the suspension displayed highly stiff, solid-like behavior with more pathways for electron transfer.

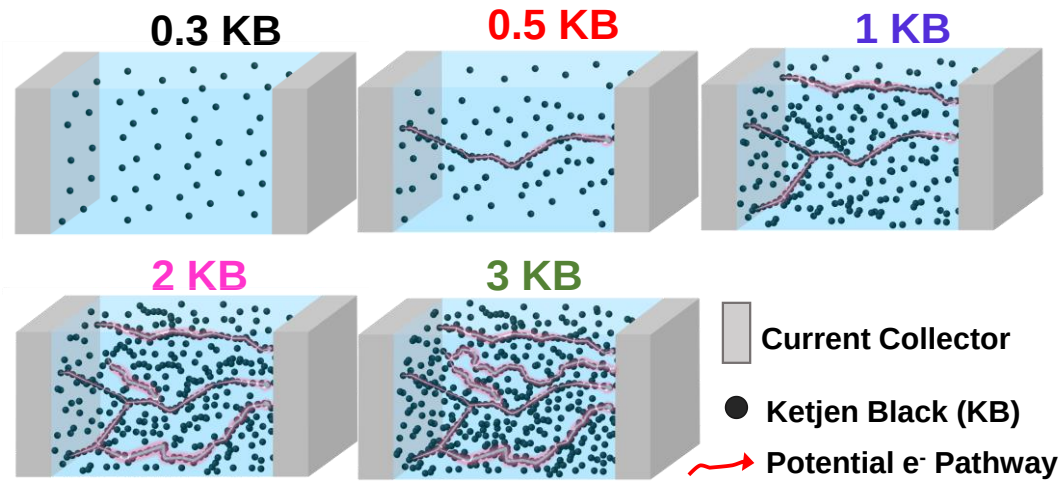

Figure 4.5 Representative illustration of changing suspension microstructures with KB concentration.

4.3.3 Rheological Behavior of Suspension Electrodes

After investigating the percolation network formation changes with KB amount in aqueous electrolyte and its flow response, KB suspension was combined with LFP to fabricate a suspension electrode. Concentration-dependent rheological analyses were first employed for only LFP-containing aqueous suspensions for each LFP type to reveal the influence of the agglomeration state of LFP particles on the rheological behavior of suspensions. Then, rheological analyses were repeated for suspension electrodes containing KB and LFP particles in 1 M Li_2SO_4 electrolyte.

As shown in Figures 4.6 (a) and **(**b), regardless of the active components' agglomeration state and solids content, all aqueous LFP suspensions showed shear-thinning flow characteristics. This behavior can be related to the rearrangement of the interacting particles in suspension with increasing flow rate, as in the case of KB suspensions. Besides, these flow rheology measurements realized a concentration-dependent reproducible hysteresis formation. Such behavior is commonly related to the variations in the rate of structural changes occurring while ramping up and ramping down the applied shear rate [122]. The shear rates at which hysteresis

formation occurred varied with concentration when agglomerated particles were used. In contrast, for dispersible particle suspensions, it happened at similar shear rates for all concentrations, indicating more consistent structure formation. As anticipated, both agglomerated and dispersible particle suspensions demonstrated a rise in viscosity with higher solids loading because of increasing crowdedness in suspension. On the other hand, when the magnitude of suspension viscosities was compared, the dispersible particles exhibited one order of magnitude lower viscosities almost over the entire shear range compared to agglomerated particles for all solids loading.

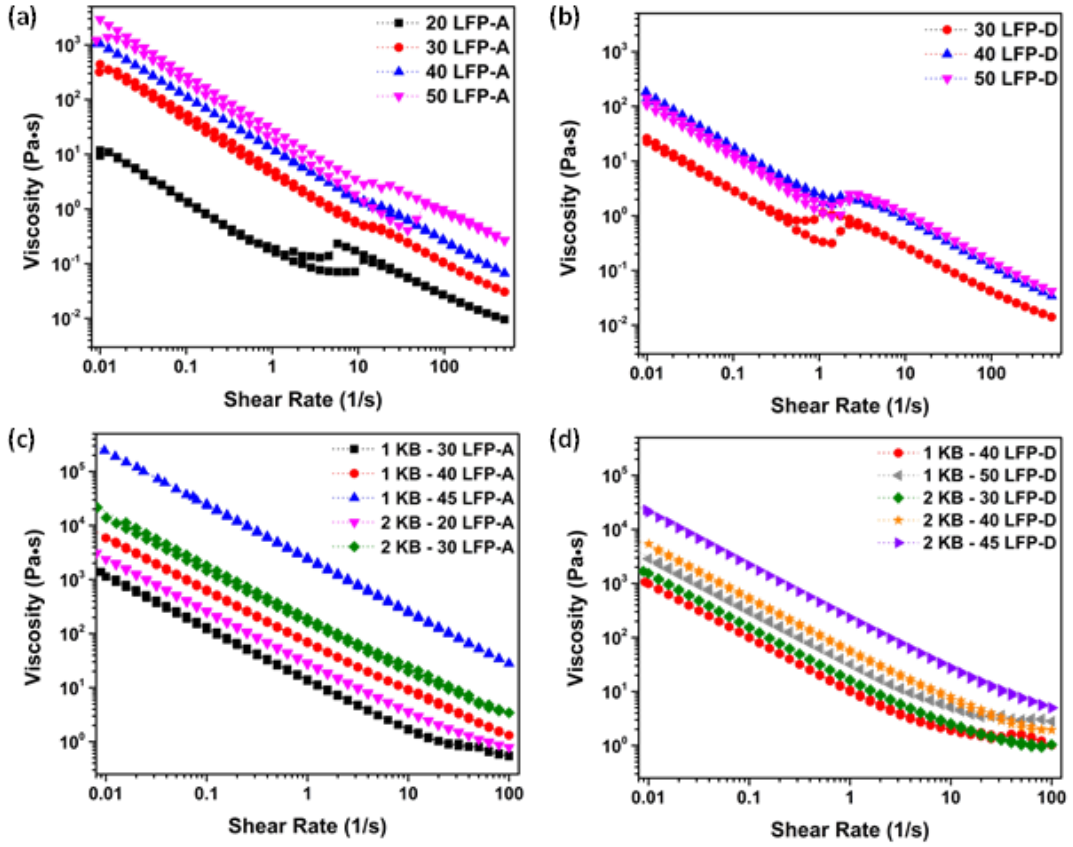

Figure 4.6. Rheological behavior analysis of aqueous (1 M Li_2SO_4) bare LFP and KB – LFP suspensions concerning solids content. Flow curves of aqueous LFP suspensions prepared with (a) agglomerated particles and (b) dispersible particles, flow curves of aqueous suspension electrodes prepared with (c) agglomerated particles and (d) dispersible particles.

In the next step, the rheological behaviors of aqueous suspension electrodes, i.e., KB – LFP aqueous suspensions, were investigated. From the previous analyses, the percolation network threshold for only KB-containing suspensions was determined to be achieved at KB concentrations between 1 and 2 wt.%. Based on this observation, the conductive electrode suspension was expected to be created at a concentration of 2 wt.% KB. The carbon shell around LFP particles may potentially contribute to the electrical conductivity. Besides, an increase in the number of contact points between particles is expected due to the increased crowdedness of suspensions. Therefore, in the presence of both KB and LFP, it was worth investigating the electrical conductivity and the rheological behavior of 1 wt.% KB-containing suspension electrodes. As in the previous flow measurements, suspension electrodes showed similar trends in flow behavior (Figures 4.6 (c) and (d)). The addition of KB to the suspension increased the suspension viscosities significantly. However, the beneficial effect of employing dispersible LFP particles instead of agglomerated ones on suspension viscosities remained consistent.

For a quantitative comparison of the flow behavior of suspensions, the changes in suspension viscosities with applied shear rate were fitted to the Power Law model. The results are presented in Table A1 and Figure 4.7, in which *K* is the consistency coefficient, and *n* is the power law index in the Power Law, $\eta = K \cdot \gamma^{n-1}$. In these results, in almost all cases, the power law index, *n*, was found to be very close to zero. This exemplifies a pronounced shear-thinning characteristic. The 1KB – 45LFP-A sample showed an *n* value of 0.002, almost the flow behavior limit. In other words, the limit of the maximum solids that can be loaded into the suspension was achieved. The similarity in the values for agglomerated and dispersible particle suspensions in all other cases showed that the mechanisms dominating the flow behavior were similar. The consistency index, *K*, shows the extent of viscosity. Its value significantly differed with LFP concentration, KB content, and the agglomeration state of the particles. As explained by the Krieger-Dougherty relation, a logarithmic increase in suspension viscosity with solids loading was expected in all suspensions [50,123].

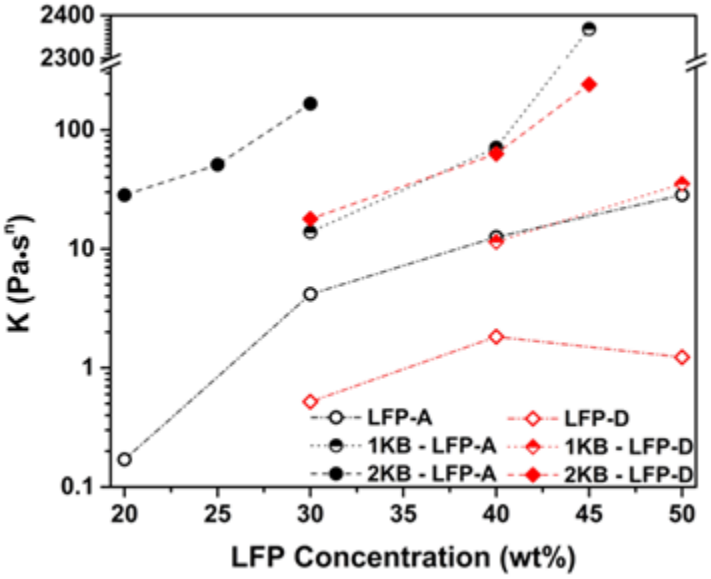

Figure 4.7. LFP concentration dependency of consistency index obtained from power law for bare LFP suspensions and suspension electrodes.

The influence of KB addition to the suspension viscosity, or on the consistency index, was significant (compare the values for 1 KB and 2 KB for 30 LFP-A or 40 LFP-D) regardless of particles being dispersible or agglomerated. Several groups reported the negative influence of CAs on suspension electrode viscosity [37,39,56,61,124]. Once the suspension viscosities were compared with respect to the agglomeration state of the particles, the difference was as dramatic as the influence of KB content. Almost one order of magnitude difference in *K* values was recorded for the samples of A and D for 1 KB – 40 LFP or 2 KB – 30 LFP. For 1 wt.% KB containing suspension electrode, 45 wt.% agglomerated particle addition exhibited a viscosity of 2368 $Pa{\cdot}s^n$. This value was only 35 $Pa{\cdot}s^n$ with 50 wt.% dispersible particle utilization. A similar flow behavior, in terms of suspension viscosity and the level of shear thinning behavior, can be achieved with suspensions of almost 50% more solids loading when using dispersible particles for the same KB content (either 1 or 2 wt.% KB). Utilizing the same approach, the maximum loading capacity of particles per unit solvent could be significantly increased using

dispersible particles. This limit was 30 wt.% and 45 wt.% for 2 wt.% KB and 1 wt.% KB containing agglomerated particle suspensions, respectively. However, it increased to 45 wt.% and 50 wt.% with dispersible particles. These accomplishments would translate to a volumetric energy capacity increase of over 50% for an electrode [16].

The strain amplitude sweep tests were carried out at an angular frequency of 1 rad/s (Figures 4.8 (a) and (b)) to reveal the changes in suspension microstructure.

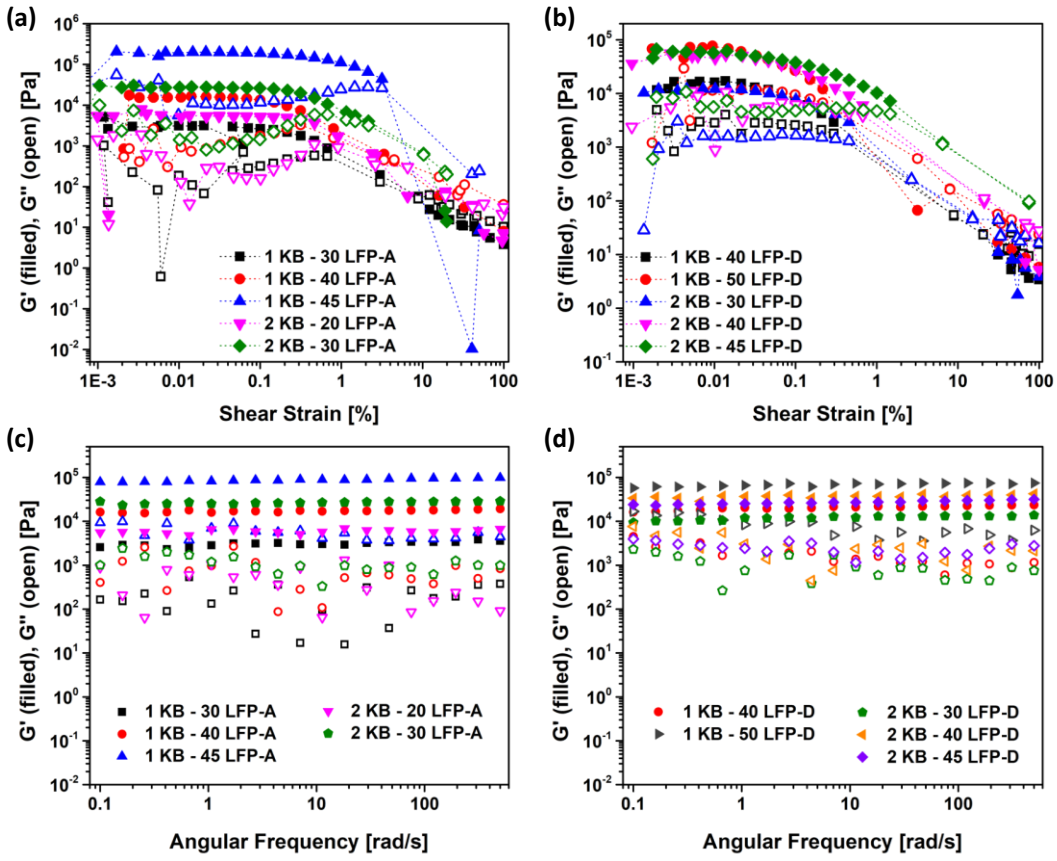

Figure 4.8 Rheological behavior analysis of aqueous (1 M Li_2SO_4) KB – LFP suspension electrodes. Amplitude sweep test measurements recorded at a constant angular frequency (1 rad/s) for (a) agglomerated particles and (b) dispersible particles; frequency sweep tests investigated at a specific strain (0.01%) for (c) agglomerated particles and (d) dispersible particles.

All suspensions showed almost one order of magnitude higher storage modulus (G') than their loss modulus (G'') over the studied frequency range (Figures 4.8 (c) and (d)). Therefore, regardless of whether the particles were dispersible or agglomerated, the suspension electrodes exhibited a solid-like structure, as in the case of KB suspensions. The mutual interactions of KB and LFP particles within the suspension consolidated a network structure and enhanced its strength.

Similarly, the storage modulus (G_0', *plateau value*) values increased with increased KB concentration and LFP loading for both agglomerated and dispersible particles (Figures 4.9 (a) and (b)). However, when the magnitude of storage modulus values was compared, relatively higher values of agglomerated particles were evident for the stronger interparticle interactions in the network formed by agglomerated particles. In line with this observation, critical strain values commonly decreased with increasing LFP concentration. It was expected that the suspension would get more solid-like with too much increase in the strength of interparticle interactions. At low solids loading, on the other hand, increasing interparticle interactions was helpful to retain the network structure. Thus, critical strain increased in this region.

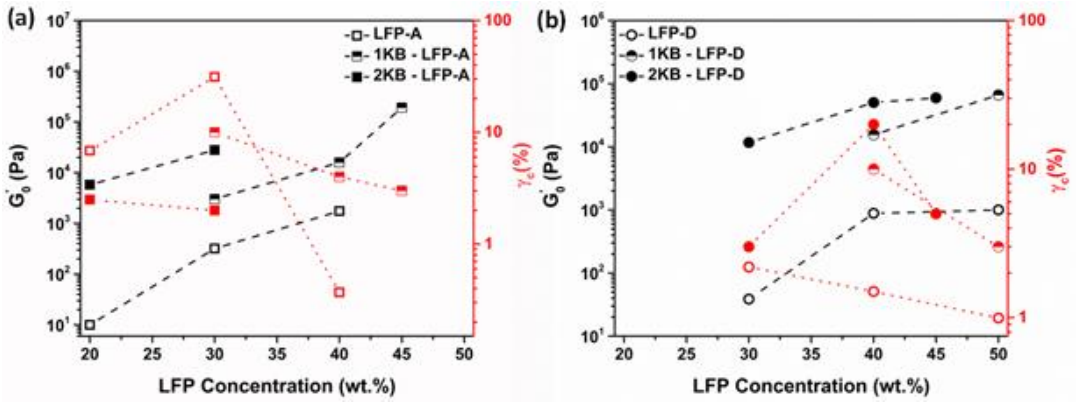

Figure 4.9. Concentration dependency of elastic modulus (plateau value from linear viscoelastic region) and critical strain for suspensions prepared with (a) agglomerated particles and (b) dispersible particles.

4.3.4 Electrical Conductivity of Suspension Electrodes

The EIS response of aqueous suspension electrodes was investigated for suspensions prepared with agglomerated and dispersible LFP particles. As presented in the Bode plot (Figure 4.10) and tabulated in Table A2, the capacitance values, and thus their effect on impedance results, were similar in both suspension electrodes of agglomerated and dispersible particles. Therefore, it can be anticipated that the impedance of the resulting suspensions indicates the bulk resistance of the suspensions.

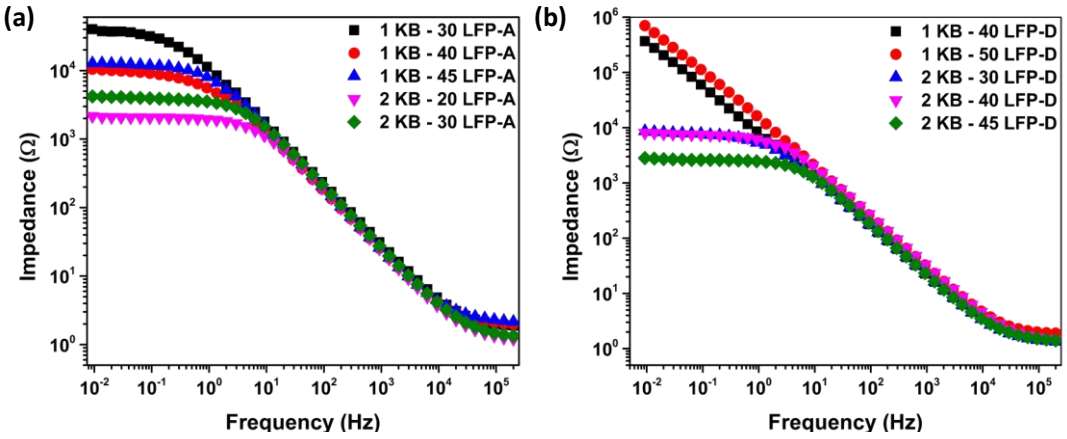

Figure 4.10 Electrochemical impedance spectra (Bode plot) of aqueous (1 M Li_2SO_4) suspension electrodes prepared with (a) agglomerated particles and (b) dispersible particles with varied solids loading.

For the suspensions of agglomerated particles (Figure 4.11 (a)), 1 wt.% KB (Figure 4.2 (a)) and 1 KB – 30 LFP-A exhibited similar behavior. The resistance of the suspension decreased with increasing EAM, as inferred from the decrease of the semicircle radius. This behavior can be associated with the positive influence of increased crowdedness of suspensions and the extra carbon content addition with the use of carbon-coated EAM. The movement of particles appeared to be restricted in

the highly loaded media, and the carbon content was forced to interact. Increasing the LFP loading to 40 wt.% significantly decreased the diameter of the semicircle (to about 10 kΩ). However, a further increase to 45 wt.% resulted in a slight increase in the impedance response of approximately 13 kΩ. Increasing the KB concentration to 2 wt.%, on the other hand, resulted in a considerable decrease in impedance response (in the range of 2 kΩ and 4 kΩ). Yet, the influence of increasing LFP concentration was similar and led to a slight increase in the diameter of the semicircle. The increase in impedance response with increasing LFP concentration may be explained by the domination of the structure with agglomerated LFP islands. It leaves only a few continuous electron paths over the more conductive KB particles trapped between these islands (Figure 4.11 (c)). Similar scenarios emphasizing the importance of the EAM to KB ratio on the conductivity and the electrochemical performance of electrodes have been thoroughly explored in existing literature [62,125].

When the impedance response of suspensions with dispersible particles was investigated (Figure 4.11 (b)), for 1 wt.% KB containing suspensions, it was interesting to observe that a conductive pattern could not be achieved with even 50 wt.% LFP addition. Compared to the behavior of KB aqueous suspensions presented in Figure 4.2 (a), the presence of LFP particles hindered the formation of a conductive percolation network. This behavior was expected because the individual particles would move more freely in the suspension than the bulky agglomerated ones, which, in turn, would break the conductive pathways (Figure 4.11 (c)). Increasing the KB concentration to 2 wt.% led to forming semicircles with significantly smaller diameters (in the range of 2.6 kΩ and 8 kΩ), i.e., much lower resistance. In contrast to agglomerated particles, the reduction in the semicircle diameter increased with increasing dispersible LFP concentration. The lowest resistance (nearly 2.6 kΩ) was obtained at an LFP concentration of 45 wt.% for dispersible particles. This level of conductivity was much lower than the one achieved using only KB in aqueous electrolyte. It indicates that the number of

electron pathways was increased in the presence of carbon-coated dispersible particles.

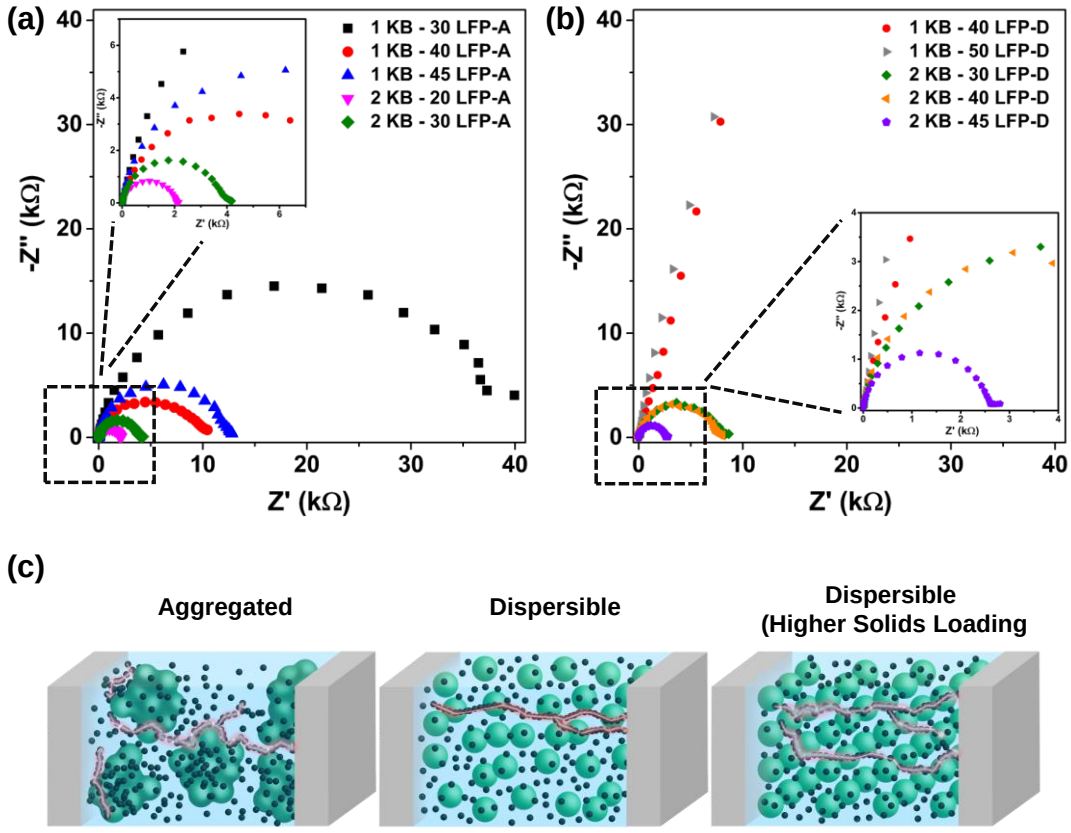

Figure 4.11 Electrochemical impedance spectra analysis (Nyquist plot) of aqueous (1 M Li_2SO_4) KB – LFP suspension electrodes with different electroactive material and additive loading, using (a) agglomerated particles, (b) dispersible particles, and (c) proposed microstructure and potential electron pathways for suspensions comprised of agglomerated and dispersible particles.

A suspension electrode's processability and electrical response are crucial for an efficient electrochemical system. Therefore, the consistency coefficient and the electrical conductivity are compared for 1 and 2 wt.% KB-containing suspension

electrodes in Figures 4.12 (a) and (b), respectively. When the EIS analysis results were converted to the electrical conductivities (fitting parameters used to obtain electrical conductivities were tabulated in Table A2), similar values (about 0.0015 mS/cm) were recorded for 1 KB and 1 KB – 30 LFP-A suspensions. However, an almost 4-fold increase to 0.0060 mS/cm was recorded when the EAM amount was increased to 40 wt.% (1 KB – 40 LFP-A). Adding more particles (1 KB – 45 LFP-A), on the other hand, decreased conductivity to 0.0047 mS/cm. When 1 wt.% KB was used instead of 2 wt.% KB, the suspensions had much lower viscosities. The literature does not provide a specific value for the electrical conductivity of suspension electrodes to ensure effective electrochemical performance. However, the low electrical conductivity of these suspensions (compared to 2 wt.% KB-containing electrodes) was expected to limit their use as a suspension electrode. This condition was even worse upon the use of dispersible particles, where an electrical conductivity as low as 0.00005 mS/cm was measured.

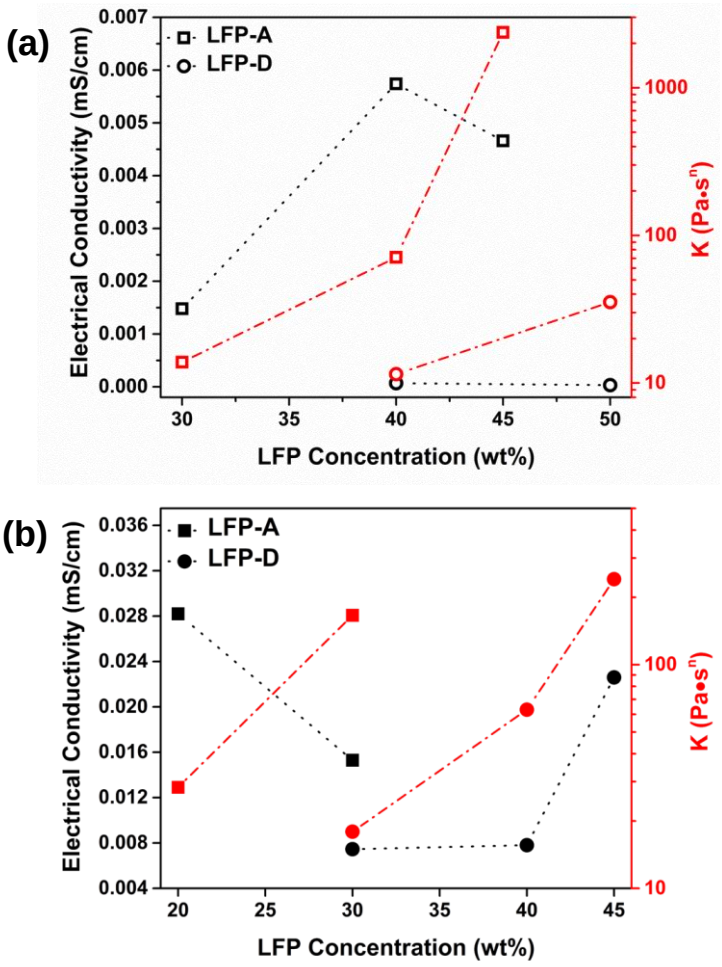

Figure 4.12 Comparison of electrical conductivity and consistency coefficient of aqueous suspension electrodes regarding LFP content; (a) suspensions including 1 wt.% KB and (b) suspensions including 2 wt.% KB.

More reasonable conductivities, along with the proper viscosity values allowing the processing of suspension electrodes, were achieved when the KB amount was increased to 2 wt.% regardless of the agglomeration state of particles. For the suspension electrodes of agglomerated particles, the electrical conductivity increased to 0.0150 mS/cm for 30 wt.% EAM-containing suspension. However, this value was even higher (0.0280 mS/cm) when the EAM loading was decreased to 20 wt.% as in the case of 1 wt.% KB-containing suspensions of agglomerated particles. Both

results showed the domination of agglomerated EAM in structure, as illustrated in Figure 4.11 (c). It resulted in the rupture of the percolated network of CAs, and the carbon coating around EAM particles was not enough to establish this network. When dispersible particles were used, the trend between electrical conductivity values and the EAM-loading differed. The increase in EAM-loading from 30 wt.% to 45 wt.% resulted in enhanced electrical conductivity, with values improving from 0.0075 mS/cm to 0.0230 mS/cm. Notably, the conductivity values reached comparable levels obtained when agglomerated particles were utilized despite the equivalent KB content.

To clarify the difference in the electrical response for EAMs for different KB concentrations in the suspension, the EIS was collected for bare LFP suspensions prepared with dispersible and agglomerated particles with varied solids loading (Figure 4.13). Dispersible LFP-containing suspensions were characterized by their viscous and compact structure with increasing solids content. However, the Nyquist plots in Figure 4.13 (a) revealed no significant variation in the impedance responses between 30 wt.% and 56 wt.%. On the contrary, distinct variations were observed in the impedance spectra of suspensions prepared with agglomerated LFP particles (Figure 4.13 (b)). The results showed that the agglomerated particle suspensions have higher conductivities than dispersible ones without KB particles. One possible explanation for this difference is the particles' carbon layer. Homogeneity, distribution, and thickness of the carbon layer were found effective on the electrical response of LFP particles [126]. Therefore, such a difference can be expected since the synthesis procedure and, hence, the amount and quality of the carbon layer of those particles were dissimilar. For example, the carbon content of the agglomerated particles was measured as 3.9%, whereas it was 1.38% in dispersible particles (Table 4.1). Since more carbon was present within the agglomerated particles' structure, it could introduce a more electrically conductive system.

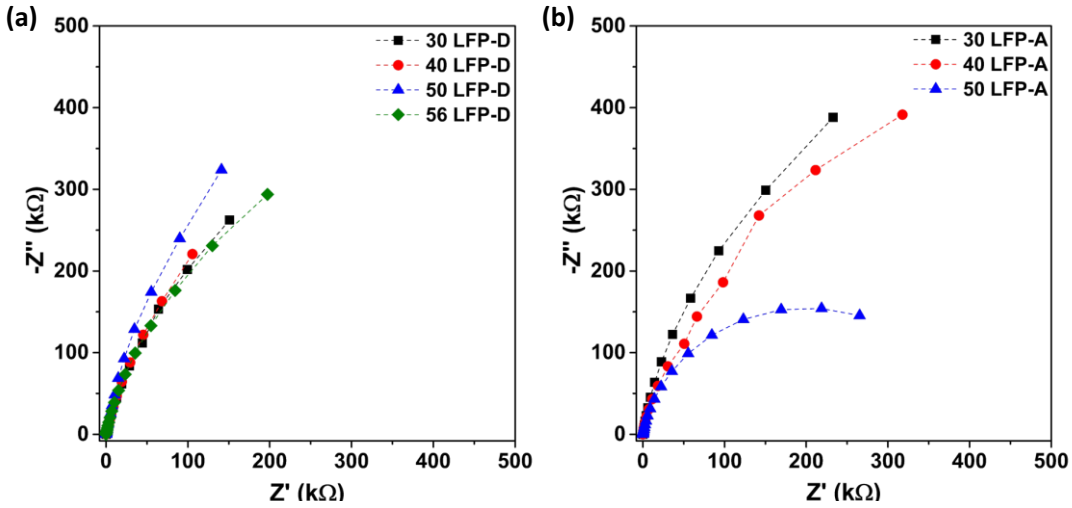

Figure 4.13 Solids content dependency of collected impedance spectra of aqueous (1 M Li_2SO_4) LFP suspensions comprised of (a) dispersible particles and (b) agglomerated particles.

Compared to the agglomerated counterparts, dispersible particles resulted in much lower suspension viscosities at any condition (Figure 4.12). This indicates that the particles could move more freely in the suspension even at high solids loadings. For example, for 2 KB – 30 LFP suspension electrodes, even though the suspensions were two times more electrically conductive when agglomerated particles were used, the consistency index was more than 9 times higher (166 $Pa.s^n$ vs. 18 $Pa.s^n$). Particles strongly interacted with each other at these concentrations, as supported by the oscillation rheology measurements. These particle interactions could be broken and re-made with the influence of shear. Thus, the increase in the viscosity values did not reach the levels that were observed in the case of agglomerated particles. As schematized in Figure 4.11 (c), an increase in crowdedness in the suspensions was possible with the use of dispersible particles. With this, a more homogeneous distribution of EAMs and CAs could be obtained. This would lead to a higher number of more uniform and strong percolation networks. In the case of agglomerated particles, the inter-particle interactions were too strong to be broken

by applied shear or simple mixing. These particle islands not only impacted suspension viscosities but also impeded the formation of the percolation network necessary for achieving electrically conductive electrodes. This is a significant conclusion, because obtaining similar conductivity and suspension viscosity values for more highly loaded suspension electrodes could enable us to formulize battery systems with much higher volumetric energy capacities. For instance, for a similar consistency index value (166 vs. 241 $Pa.s^n$), the conductivity value was much higher (0.015 vs. 0.023 mS/cm). Additionally, solids loading was 45 wt.% for the suspensions of dispersible particles, whereas it was only 30 wt.% upon the use of agglomerated particles. In other words, 50% more EAM could be loaded and processed in a suspension electrode. The EAM content and the corresponding volumetric energy capacities of suspension electrodes, including LFP particles in flow systems reported in the literature, are listed and compared in Table 4.2. As shown in the table, dispersible particles have the potential to provide considerably higher energy capacities compared to the others. Only one study, conducted by Wei et al., seemed to be competitive with the present study regarding volumetric energy capacity that can be achieved in suspension electrodes. It is worth noting that additives were employed to enhance particle dispersions within their suspensions, an approach that has not yet been applied to the suspensions in our study. Moreover, in their work, only 1.25 vol.% CA was used, while this value corresponded to 3.1 vol.% in our research. Therefore, our results suggested dispersible particles were pivotal in achieving better flow behavior and a competitive volumetric energy capacity. In addition, our results highlight that there is still plenty of room to improve the corresponding suspension performance further.

Table 4.2. Comparison of proposed energy capacities of LFP including suspension electrodes reported in the literature.

EAM Concentration (wt.%)	**Gravimetric Energy Capacity (Ah/kg)**	**EAM Concentration (vol.%)**	**Volumetric Energy Capacity (Ah/L)**	**CA Concentration (wt.% or vol.%)**	**Reference**
8.4	14.3	12.6	16.6	4.4 (vol.%)	64
-	-	6 – 10	25.4 – 48.6 *	1.5 – 2 (vol.%)	36
		20	93	1.25 (vol.%)	27
< 0.2 [+]	-	-	0.2	-	21
-	-	10 – 40	18.6 – 68	-	56
20	28.6 – 31.2	14.9 – 20.6	26.5 – 30.9	1 (wt.%)	61
35	50 – 54.6	26.4 – 34.7	44.7 – 54.8	1 (wt.%)	
< 13 [ǂ]	-	-	17.4	< 2 (wt.%)	22
30	39 – 51	11	50 – 65 *,#,A	2.6 (vol.%)	**This Study**
45	58.5 – 76.5	19.1	86 – 113 *,#,D	3.1 (vol.%)	

**Energy capacities were calculated based on the electroactive material's theoretical density (3.47 g/cm3).* [+]*In the study, the suspension was prepared with 1.4 g $LiFePO_4$ in 1 Liter of electrolyte.* [#]*In the energy capacity calculations, the delivered specific discharge capacity of the electrode is assumed to be between 130 – 170 mAh/g.* [A]*Suspension prepared with agglomerated particles and* [D]*suspension prepared with dispersible particles.* [ǂ]*In the calculations, the impact of electroactive material and other solid components' density was neglected (they were not provided in the study).*

To further support this conclusion, suspension electrodes were cast on a glass substrate, and particle distributions were investigated. As observed in the false-colored SEM images presented in Figure 4.14, the agglomeration state of LFP particles influenced the size and distribution of KB clusters. More homogeneous distributions of smaller KB clusters among the LFP particles were observed for dispersible LFP-containing suspension electrodes in the micrographs with lower magnifications. CAs tend to agglomerate in an aqueous environment, as also encountered in the case of agglomerated particles. Nevertheless, when dispersible

EAMs were used, a more homogeneous KB – LFP distribution could be obtained as opposed to this expectation. Additionally, the microstructure maintained continuity and exhibited a uniform distribution even with increasing LFP-D content. Therefore, the increase in the electrical conductivity with increasing dispersible LFP observed in EIS analyses was reasonable. This is because of the formation of compact and crowded structures with a uniform distribution of solid particles. Conversely, the utilization of agglomerated particles adversely affected the microstructure of the suspension electrode. The formation of bigger LFP-A chunks (see the inset of false-colored SEM images for LFP-A-containing electrodes) and KB clusters caused increased heterogeneity in the suspension microstructure. This would explain the decrease in electrical conductivity and flowability of the suspension electrodes as a result of the broken continuity in the conductive network, as discussed earlier.

To fully understand the KB distribution and network formation in the suspension electrode, dispersible LFP particles without any carbon coating were used to prepare the suspension electrode (2KB – 30LFP-D). The carbon distribution was investigated via EDS analysis, as presented in Figure 4.14. Regardless of the carbon coating, dispersible LFP particles showed a similar distribution in KB suspension as in carbon-coated samples shown in the figure insets. Carbon distribution was not limited to the clustered parts of those as visible in the SEM images. Carbon particles can be said to be spread over the entire area of the suspension electrode, indicating that dispersible LFPs are in contact with KBs present in almost every part of the electrode. Therefore, it can be concluded that KB was uniformly distributed over the entire suspension similarly, significantly increasing the number of contacts between the LFP particles and carbon particles. Consequently, this resulted in the forming of a conductive network with a compact KB – LFP-D structure that facilitated the electron transfer. It was not the microstructure that could be achieved with agglomerated particles.

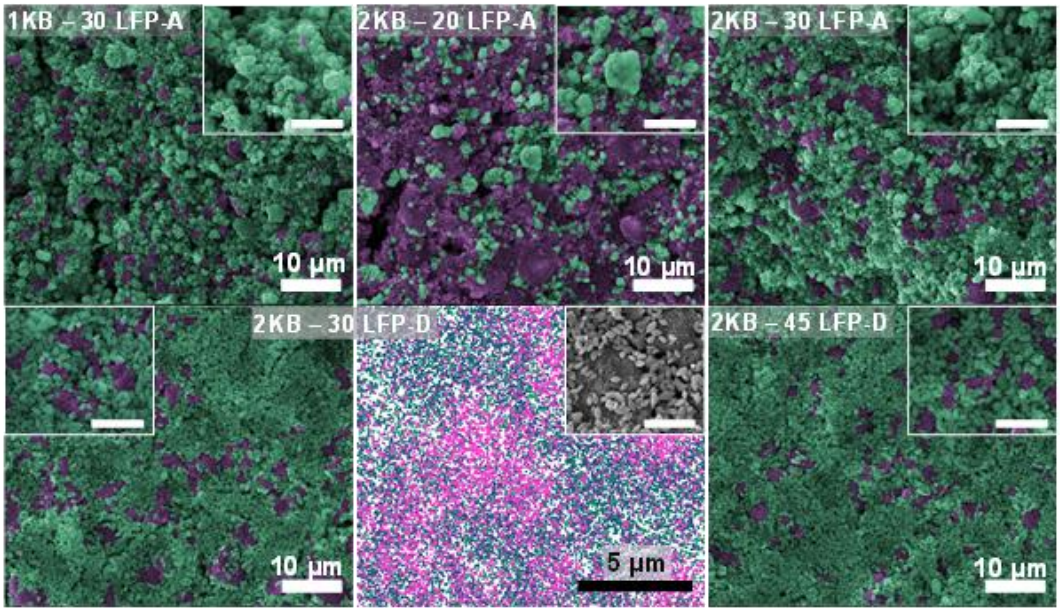

Figure 4.14. False colored scanning electron micrograph and elemental mapping analysis of aqueous (1 M Li_2SO_4) KB – LFP suspension electrodes with different electroactive material and additive solids loading (Green parts represent the LFP particles while purple parts represent the KB in the suspension electrode). Energy dispersive X-ray spectroscopy analysis of 2KB – 30LFP-D suspension prepared with non-carbon coated LFP (the colors in the figure were coded as magenta: carbon, green: iron, and blue: oxygen) (The scale bars given in the inset of the figures is 5 µm).

Even though the compositions were reported by weight in the literature, the KB to the LFP ratio must be different upon the use of volumetric occupancy. For example, KB occupied nearly one-fourth of the total solids loading in 2 KB – 20 LFP-A suspension. Such a high ratio explains the KB-LFP distribution in the false-colored SEM images where KB clusters covered almost the entire area and why this suspension had the highest electrical conductivity. As tabulated in Table 4.3, with increasing LFP amount, the KB additive used per EAM decreases for the same weight percentage of KB. This means that the amount of active material per unit volume of electrode increases in the cell. Therefore, we can conclude that when the

dispersible particles were used, not only was the amount of EAM that could be loaded per unit volume increased, but also the requirement of CAs decreased. Both would lead to an increase in the volumetric energy capacity of the electrodes. Considering the current state of the art, this approach, using dispersible EAM, can further improve the volumetric energy density of batteries.

Table 4.3. Electroactive material and conductive additive percentages of prepared aqueous suspension electrodes.

Suspension	Composition (wt.%)		KB/LFP (from wt.%)	Composition (vol.%)		KB/LFP (from vol. %)
	LFP	KB		LFP	KB	
2 KB – 20 LFP-A	20	2	10.0	6.7	2.4	35.8
2 KB – 30 LFP-A	30	2	6.6	11.0	2.6	24.0
2 KB – 30 LFP-D	30	2	6.6	11.0	2.6	24.0
2 KB – 45 LFP-D	45	2	4.4	19.1	3.1	16.2

4.4 Conclusions

The microstructure of a suspension electrode determines its processability and electrical behavior, which has to be controlled for improved performance in electrochemical energy storage systems. The present study elucidated the role of the agglomeration state of particles on suspension microstructure. In addition, it proved its remarkable influence on aqueous suspension flowability, percolation characteristics, and electrical behavior. Rheological analyses and the power law fitting parameters revealed that similar mechanisms dominated the flow response of the aqueous suspensions regardless of the agglomeration states of LFP particles. The consistency index values demonstrating the degree of viscosity considerably varied and increased with increasing LFP and KB concentration. More importantly, it exhibited almost one order of magnitude higher values when agglomerated particles were used compared to the dispersible ones at almost all solids loading.

It was found that the agglomeration state of LFP particles influenced KB distribution. The dispersible particles provided a more homogeneous distribution of KB particles, leading to a decrease in the requirement of KB amount per LFP. Moreover, it was shown that for a given KB content (2 wt.%), similar flow behavior and electrical conductivity values could be achieved. Yet nearly 50% more LFP could be loaded to the suspension when dispersible particles rather than agglomerated ones were used. Considering both the increase in the LFP amount in suspension and the decrease in inactive content per LFP, dispersible particles improved the microstructure of suspension electrodes. This conclusion has opened a window to enhance their processability and electrochemical performance, mainly increasing their volumetric energy capacity. The present study only focused on the influence of the agglomeration state of particles, but it is known that there are other approaches, such as using dispersants. Further improvement of the characteristics of suspension electrodes can be realized through these approaches, and therefore, the current limits of volumetric energy capacities can be further exceeded. This pioneering research, showing that the agglomeration state of particles affects the microstructure, flow, and electrochemical properties of suspension electrodes, contributes significantly to the establishment of improved electrochemical systems.

CHAPTER 5

EFFECT OF FRUCTOSE ADDITION ON ELECTROCHEMICAL PERFORMANCE OF AQUEOUS SUSPENSION ELECTRODES

5.1 Introduction

The impact of the agglomeration state of the particles on the microstructure of the suspension electrode and the resulting flow and electrical responses was investigated in Chapter 4. Following the comprehension of the impact of the agglomeration state on suspension properties, the objective was to explore the electrochemical behavior of aqueous suspensions.

As seen in Chapter 2, using aqueous electrolyte significantly diminishes the discharge capacity of the particles. Many research groups have reported such an issue, posing a substantial challenge to commercializing lithium-ion batteries incorporating aqueous electrolytes. Various approaches were developed to address this problem, which can be categorized as modification of the particles and the properties of the electrolyte. For instance, Tron et al. reported that coating the surface of LFP particles with a specific amount of AlF_3 diminished the formation of side reactions and detrimental surface passivation, improving the discharge capacity and capacity retention [127]. Properties of the aqueous electrolyte, including pH [99,128], salt concentration [117], type of salt employed [117,129], and O_2 content [130], were demonstrated as influential factors in the electrochemical performance of the particles. Optimizing these parameters was highlighted for the feasibility of aqueous lithium-ion battery technologies. Introducing organic additives into the electrolyte was also proposed as a beneficial approach to mitigate the rapid capacity decay in LFP electrodes [131,132]. For example, ethylene glycol addition to the aqueous electrolyte was reported to modify the LFP surface and, thus, the electrochemical response. The formation of a compact solid interface on the LFP

surface and reduction in the solubility of ferrous ions allowed faster lithium-ion transfer [132].

As an alternative to these approaches, our study introduces the use of fructose as an additive for the first time in the literature. In this context, we examined the impact of fructose addition and its content on the electrochemical performance of aqueous suspension electrodes.

5.2 Experimental Procedure

5.2.1 Materials

KB (EC600JD, Akzo Nobel) was used as a conductive additive in aqueous suspensions. Agglomerated $LiFePO_4$ (LFP-A) and dispersible $LiFePO_4$ (LFP-D), characterized in Chapter 4, were used as EAM to prepare suspension electrodes. D-(L)-fructose (99% purity; Sigma Aldrich) was used as an additive. Li_2SO_4 (anhydrous, 99.7%) was purchased from Alfa Aesar and used for aqueous electrolyte preparation. DIW with a resistivity of 18.2 MΩ was used to prepare aqueous suspensions.

CB (Alfa Aesar), battery-grade polyvinylidene fluoride (PVDF), and N-methyl-2-pyrrolidone (NMP, Merck) were used for composite electrode preparation to characterize it in organic electrolyte.

5.2.2 Suspension Preparation

The fraction of the fructose was calculated as a weight percentage of LFP powder in the suspension. The required amount of fructose was dissolved in DIW using an ultrasonic bath for 15 minutes. Then, the required amount of KB was slowly added to the solution, gently shaken, and then ultrasonicated in the bath for 10 minutes to disperse particles. Following this, to ensure a 2.5 M electrolyte concentration, the

required amount of Li_2SO_4 was added in powder form, and the suspension was ultrasonicated for another 10 minutes. The mixture was stirred with a magnetic stirrer at 250 rpm at room temperature for 21 hours. Then, LFP particles were added and mixed for 3 hours to obtain a homogeneous suspension. For comparison, suspension electrodes with the highest electrical conductivity prepared with dispersible (2KB – 45LFP-D) and agglomerated particles (2KB – 20LFP-A) in Chapter 4 were used.

5.2.3 Characterization

A homemade three-electrode cell configuration was used to evaluate the electrochemical behavior of aqueous suspensions, as shown in Figure 5.1. The proposed cell comprised two compartments, with the suspension electrode positioned on one side and the reference electrode and counter electrode on the other. A 0.5-mm-thick spacer (with a diameter of 20 mm) was used to place the suspension electrode. The counter compartment was filled with aqueous electrolytes. A helical platinum wire was employed as the reference electrode, and Ag/AgCl (3M) as the counter electrode. A graphite plate was used as the current collector for the suspension electrode. The cell compartments were separated from each other with a Celgard 3501 membrane. Galvanostatic charge-discharge measurements were performed at 0.1 C rate in the -0.6 – 0.8 V operating potential range with the VersaSTAT 3 (Princeton Applied Research) instrument. Galvanostatic charge-discharge measurements were repeated twice for suspension (2KB - 20LFP-A) containing 2% and 4% fructose.

For electrochemical characterization in the organic electrolyte (as solid-state electrodes), electrodes were prepared by mixing LFP particles, CB, and PVDF in NMP solvent (5 wt.% PVDF – NMP solution) in a mixer mill (Retsch MM400) with a ratio of 80:10:10 by weight. The electrode suspensions were spread on an aluminum foil with a thickness of 200 µm using the doctor blade method. To remove the NMP solvent thoroughly, the electrodes were pre-dried at 120 °C for 2 hours on a hot plate in a fume hood. Then, the coatings were cut into 18 mm circular discs and

dried under vacuum at 120 °C for 12 hours before cell assembling. Lithium foil was used as the anode/reference electrode, and a glass microfiber sheet separated the electrodes. 1 M $LiPF_6$ dissolved in a mixture of ethylene carbonate (EC) and dimethyl carbonate (DMC) (1:1 by weight) was used as an electrolyte. The half-cell assembling was carried out in an argon-filled glove box. Cyclic voltammetry (CV) and galvanostatic charge-discharge measurements were performed in the 2.5 – 4.2 V operating potential range with MPG-200 electrochemical station (Bio-Logic Science Instruments).

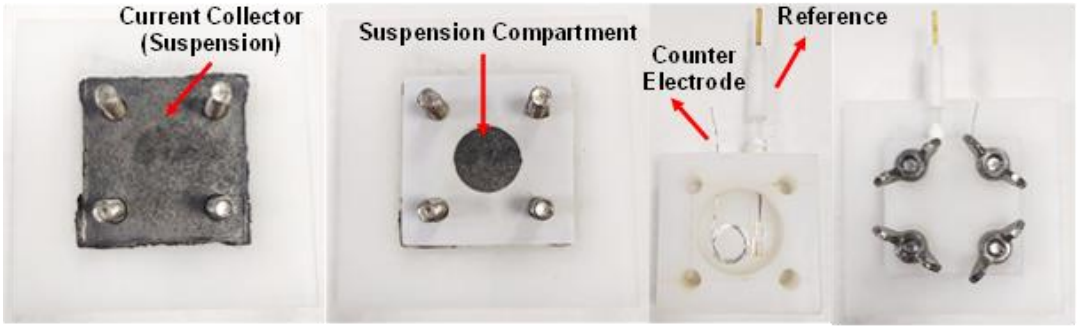

Figure 5.1 A home-made three-electrode cell configuration to analyze the electrochemical performance of aqueous suspension electrodes in non-flowing conditions.

5.3 Results and Discussions

5.3.1 Electrochemical Performance of Composite Electrodes in Organic Electrolyte

LFP particles generally exhibit a more stable behavior in organic electrolytes than aqueous electrolytes. Furthermore, given that research on organic electrolytes is more common than on aqueous electrolytes, conducting preliminary assessments in

organic electrolytes holds significance. Hence, the particles were initially examined in a solid-state form within an organic electrolyte to comprehend the alignment of the discharge capacity demonstrated by LFP with the theoretical capacity and the values documented in the literature.

The electrochemical behavior analysis of LFP-D and LFP-A particles in organic electrolyte is given in Figure 5.2. While the delivered specific discharge capacity from the agglomerated LFP was 153 mAh/g, the dispersible LFP particles exhibited an initial discharge capacity of 139 mAh/g. The initial discharge capacity of the particles closely approached the theoretical capacity of 170 mAh/g, aligning with values documented in the literature. When the cyclic stability of the prepared electrodes is examined, it is observed that the agglomerated LFP showed an almost constant discharge capacity over 10 cycles. On the other hand, the specific discharge capacity of the electrode prepared with dispersible LFP experienced a very rapid capacity decay. The electrode could only maintain 77% of its initial capacity at the end of 10 cycles. This may be due to the interaction of the particles with the organic solvent and may be caused by the quality of the carbon coating that acts as a protective shield around the LFP particles. A difference in the amount and quality of the carbon layer around those particles may expected since the synthesis procedures were dissimilar. Therefore, the coating process of dispersible LFP particles needs further optimization for better cyclic performance and higher discharge capacity [120]. Differences in the crystal structure and variations in the cell volume of the particles may also contribute to this fast capacity decay phenomenon.

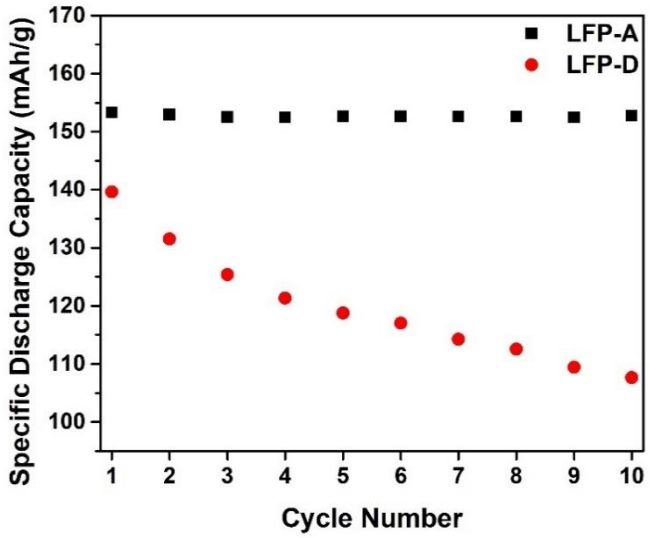

Figure 5.2 Specific discharge capacity and cyclic stability of agglomerated and dispersible LFP particles in organic electrolyte as solid state electrodes.

5.3.2 Electrochemical Performance of Aqueous Suspension Electrodes

Microstructural analysis of the suspension electrodes (Chapter 4) showed that the agglomeration state of the particles changed the suspension properties. The maximum amount of particles that could be loaded into the suspension was varied. 2KB – 20LFP-A and 2KB – 45LFP-D suspension electrodes showed the highest electrical conductivity. Besides, their flowability was similar. Therefore, these suspension electrodes were chosen and their electrochemical performance was studied. Additionally, an electrolyte with 2.5 M Li_2SO_4 concentration was used since the increasing ionic strength positively impacts the electrochemical performance.

The specific discharge measurement results of aqueous suspension electrodes are given in Figure 5.3. The results show that the behavior of not only dispersible particles but also agglomerated LFP particles with a denser carbon layer around them in an aqueous suspension electrode also changed significantly. While agglomerated LFP particles could maintain almost 100% of the initial discharge capacity in organic

electrolytes (in solid state), it was only 52% after 10 cycles in aqueous suspension electrode system. It indicates the adverse impact of aqueous electrolytes on the electrochemical performance of particles. Compared to the behavior in the organic electrolyte, the electrochemical response of the individual particles deteriorates in the aqueous suspension electrode. The discharge capacity started at 38 mAh/g and decreased to 16 mAh/g after 10 cycles.

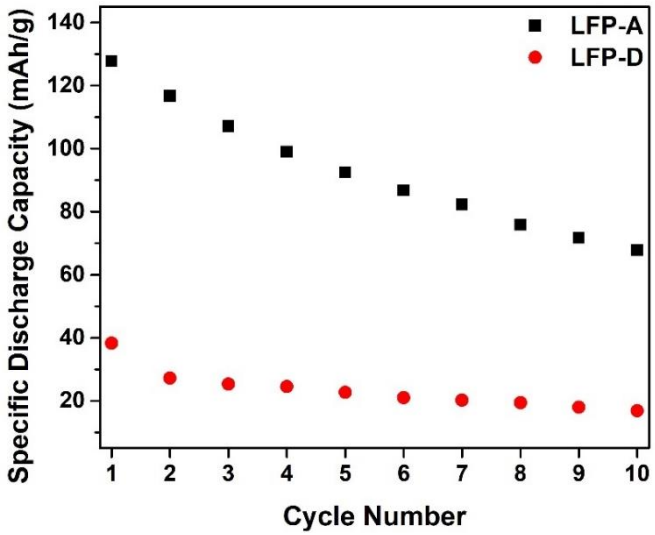

Figure 5.3 Specific discharge capacity and cyclic stability of aqueous suspension electrodes prepared with agglomerated and dispersible LFP particles (suspension electrodes; 2KB – 20LFP-A and 2KB – 45LFP-D).

The charge-discharge profiles of aqueous 2KB – 20LFP-A suspension electrode for ten cycles at 0.1 C rate within the voltage range of -0.6 to 0.8 V are presented in Figure 5.4. In the initial charge-discharge cycle, the suspension electrode exhibited a smooth plateau for an extended period between 0.2 and 0.26 V, corresponding to the transition of Fe^{3+}/Fe^{2+} due to lithium-ion de(insertion) in the electrode structure. Later, it showed an inclined trend, re-emerging as a relatively smaller plateau. It can be explained by the pseudo-capacitive effect, where lithium ions accumulate charge

through faradaic processes on the surface of EAMs. Furthermore, ions accumulated on the surface may gradually penetrate the electrode over time, potentially contributing to the appearance of the second small plateau. The relatively flat plateau that appeared in the first two cycles gradually lost its structure and acquired a more noticeable slope. A notable widening of the separation between charge-discharge potentials was observed with increasing cycles, indicating the deterioration of the lithium-ion transfer kinetics. Due to worsening kinetics, it was seen that the discharge capacity of the suspension electrode, which was initially 127 mAh/g, decreased to 67 mAh/g after 10 cycles.

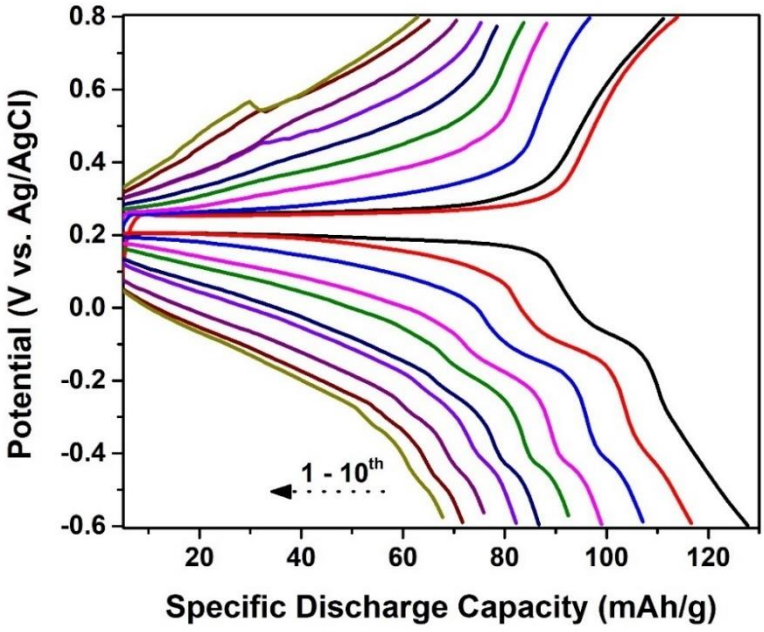

Figure 5.4 The charge-discharge potential profile of aqueous 2KB – 20LFP-A suspension electrode.

5.3.3 Effect of Fructose Concentration on Electrochemical Performance

As evident in the suspension electrode measurements, using aqueous electrolytes adversely impacts the electrochemical performance of the particles. To enhance the electrochemical performance of the aqueous suspension electrodes, we offered the utilization of fructose as an additive for the first time in the open literature. Therefore, in this part, we examined the influence of adding fructose and its concentration on the electrochemical performance of aqueous suspension electrodes. Due to the long-term electrochemical stability of suspension electrodes prepared with agglomerated particles, we first studied the impact of fructose content on these electrodes.

The 1st and 10th charge-discharge potential plots of the suspension electrodes (2KB – 20LFP-A) examined considering the fructose concentration are given in Figure 5.5. Upon reviewing the initial charge-discharge responses of the electrodes, it is evident that the reaction kinetics vary based on the fructose concentration. The bare suspension electrode exhibited a smooth discharge potential, whereas the dissolution of 2% fructose increased the insertion potential of lithium-ions into the electrode structure over time. Adding 4% fructose restored the redox potential to similar levels, but a higher fructose concentration (6%) worsened the reaction kinetics. Interestingly, suspension electrodes containing 2% and 4% fructose demonstrated similar discharge capacity despite the alterations in discharge potentials. When analyzing the behavior at the 10th cycle, a slight increase in polarization was observed in the suspension electrode with a 4% fructose addition. However, in all other suspensions, the potential gap widened significantly. This is critical for the power density of a suspension electrode, indicating that using 4% offers higher power density.

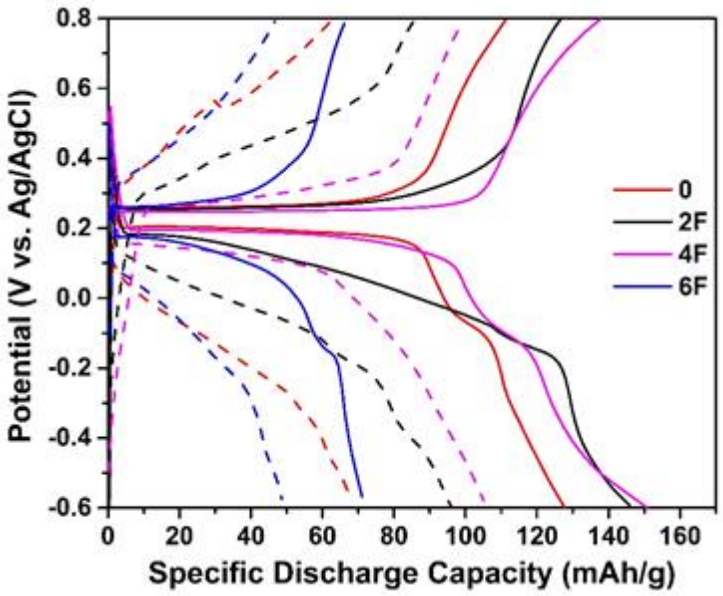

Figure 5.5 The charge and discharge profiles of aqueous 2KB – 20LFP-A suspension electrode prepared with different amounts of fructose (solid lines represent the 1st cycle while dashed lines represent the 10th cycle).

The cyclic stability of the suspension electrodes at 0.1 C regarding the fructose addition is given in Figure 5.6. Figure 5.6 (a) illustrates the impact of fructose content on the discharge capacity of the 2KB – 20LFP-A suspension electrode. While the delivered specific discharge capacity from the bare suspension electrode was 127 mAh/g, adding 2 and 4% fructose to the suspension increased the initial discharge capacity to 146 and 151 mAh/g, respectively. However, a further increase in the fructose content to 6% notably deteriorated the electrochemical performance of the suspension electrode, resulting in an initial discharge capacity of 71 mAh/g. Beyond increasing the discharge capacity, adding fructose also improved the cyclic stability of the suspension electrode. After 10 cycles, the bare suspension electrode retained 52% of its initial discharge capacity, while the suspension electrode with 4% fructose exhibited a higher capacity retention at 70%.

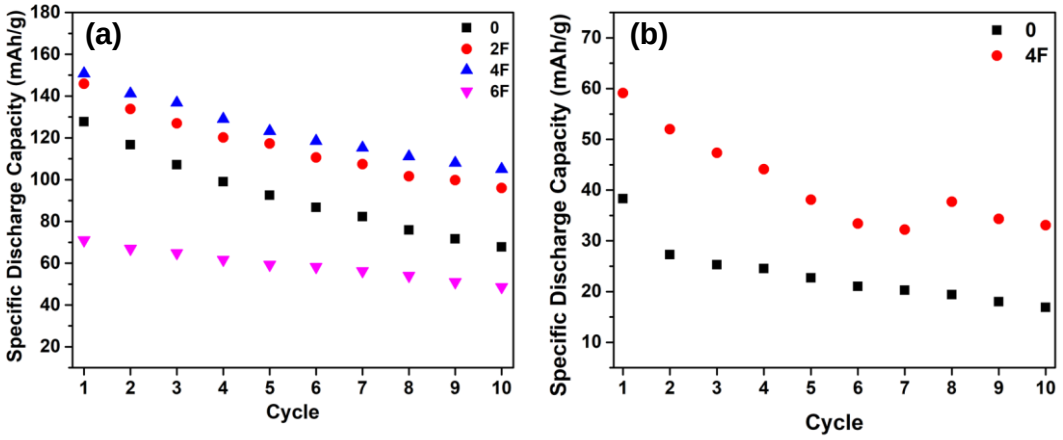

Figure 5.6 The impact of dissolved fructose content on the cyclic stability of aqueous suspension electrodes; (a) 2KB – 20LFP-A and (b) 2KB – 45LFP-D.

Reproducibility tests (Figure C1) showed that using fructose as an additive in aqueous suspension electrodes improves the electrochemical performance of the electrode (discharge capacity, polarization, and capacity retention). Analysis with 4% fructose showed that the suspension's initial discharge capacity was in the range of 131 - 151 mAh/g and was higher than that of the bare electrode throughout the whole cycle. In the sample prepared with 2% fructose, it was observed that although there was a significant decrease in the capacity values given by the electrode between the 5 – 8 cycles, the capacity increased again with the increasing number of cycles and reached similar levels. This may indicate changes in the percolated pattern in the microstructure over time and may suggest the utilization of intermittent flow mode for operation. This change may also attributed to the preparation of the suspensions and underline its importance. As a result, it was found that the impact varies with the concentration of fructose, and the optimal amount was determined to be 4% under the given conditions.

The optimum fructose amount of 4 wt.% was also tested in suspension electrodes containing dispersible particles. Its influence on the suspension’s discharge capacity is given in Figure 5.6 (b). Adding 4% fructose increased the initial discharge capacity

from 38 mAh/g to 59 mAh/g. Furthermore, the fructose-added suspension displayed a higher specific discharge capacity than the bare suspension electrode during the entire measurement, carried out across ten cycles. The capacity retention also increased from 44 to 56% by 4% fructose addition.

Introducing fructose into the electrolyte seems as a beneficial approach to increase the discharge capacity and mitigate the rapid capacity decay in LFP electrodes. Therefore, it is a promising way to significantly contribute to developing LIB technologies using aqueous electrolytes.

In reported studies, it was observed that incorporating fructose as an additive in aqueous suspensions containing oxide powders generally results in reduced viscosity [47,48,133]. A possible reason for viscosity reduction was shown by Akinc et al. [133–135]. A detailed examination involving alumina nanoparticles demonstrated the formation of bound water around particles dispersed in water, and the impact of fructose addition on bound water was revealed [136]. It was noted that fructose molecules and bound water were displaced, increasing the available water content in the suspension. Hence, exploring whether a comparable phenomenon occurs in suspension electrodes containing LFP and examining the mechanism through which it influences the electrochemical performance of the suspension might be intriguing to building higher energy-dense systems.

5.4 Conclusions

Despite its many advantages in energy storage systems, the commercialization of battery systems using aqueous electrolytes is limited due to the interaction of water molecules with EAM, adversely affecting the electrochemical performance of the electrode. In this part, we investigated the influence of fructose addition on the electrochemical performance of LFP-containing aqueous suspension electrodes. The impact of fructose addition on electrochemical response was concentration-

dependent. Using up to 4 wt% fructose significantly improved the discharge capacity and cyclic stability of the suspension electrode. The introduction of 4% fructose increased the initial discharge capacity of the electrode from 127 mAh/g to 151 mAh/g. Moreover, the capacity retention, initially at 52% for the bare electrode after 10 cycles, increased to 70% with the incorporation of 4% fructose. The fructose addition improved not only the capacity but also the charge-discharge potential, enabling more power-dense systems to be built.

CHAPTER 6

CONCLUSIONS

The present thesis aimed to reveal the influence of the agglomeration state of the electroactive material (EAM) on the microstructure, flow, and electrical-electrochemical performance of suspension electrodes. $LiFePO_4$ (LFP) cathode material was utilized as a model EAM.

In this context, first, it was intended to obtain individual and dispersible LFP particles. The significance of post-synthesis processes was realized in the study carried out for this purpose. The physicochemical and electrochemical characteristics of the particles were found to depend on the applied washing solvent sequence. Termination of the washing step with deionized water (DIW) or ethanol (EtOH) also showed different effects on particle characteristics depending on the synthesis methods. Nevertheless, completing the washing step with DIW adversely impacted the electrochemical response of particles regardless of the production method.

Then, it was focused on optimizing the suspension formulation to obtain homogeneous suspension electrodes capable of long-term stability. A suspension preparation protocol was investigated by changing the addition sequence of Li_2SO_4 salt into the suspension electrode. The adjustment of ionic strength of the aqueous medium after dispersing Ketjen Black (KB) particles in DIW allowed the formation of homogeneous and stable suspensions. Visual monitoring confirmed the stability of the dispersions for more than six months. This optimization enabled the acquisition of stable and reproducible electrochemical impedance spectroscopy results.

The role of the agglomeration state of particles on suspension microstructure and its remarkable influence on aqueous suspension flowability, percolation characteristics, and electrical behavior was elucidated. Rheological analyses indicated that

comparable mechanisms governed the flow response of aqueous suspensions, irrespective of the agglomeration state. However, the consistency index value, i.e., the mean viscosity value, significantly varied with the agglomeration state of the particles. More notably, when comparing agglomerated LFP particles to dispersible ones, the former exhibited almost one order of magnitude higher values across all solids loading. Another important finding of the current research is that the distribution of conductive additives in the suspension electrode was observed to be impacted by the agglomeration state of LFP particles. Individual-dispersible LFP particles in the suspension led to a more homogeneous KB distribution, resulting in a lower KB per unit of LFP to obtain a percolated structure. Moreover, it was shown that for a given KB content (2 wt.%), a suspension formulation with similar flow behavior and electrical conductivity can be loaded with approximately 50% more LFPs using dispersible particles instead of agglomerated particles. All these findings revealed the importance of the agglomeration state of the particles to obtain feasible suspension electrode-based energy storage systems. It was also deduced that using individual particles is one of the priorities for establishing high-energy-dense storage systems. The use of individual and dispersible particles significantly reduced the suspension viscosity. It also increased the maximum EAM amount that could be loaded into the suspension. This situation is essential because of the ever-increasing demand for energy and technological advancements. For instance, batteries that can be prepared using individual particles will enable electric vehicles to travel longer distances on a single charge, addressing range anxiety and encouraging widespread adoption. Additionally, individual particles would allow the creation of compact and lightweight devices with the same energy density in smaller sizes.

Finally, using fructose as an additive in the aqueous suspension electrodes was proposed to enhance electrochemical performance. In this study, improvements in discharge capacity were observed for the first time in aqueous lithium-ion batteries. The capacity retention was also improved with fructose addition. The results demonstrated that adding fructose is a promising approach to enhancing the

electrochemical performance of aqueous batteries. However, further investigation is required to fully comprehend the mechanism behind this effect.

REFERENCES

[1] Z. Zhu, T. Jiang, M. Ali, Y. Meng, Y. Jin, Y. Cui, W. Chen, Rechargeable Batteries for Grid Scale Energy Storage, Chem. Rev. 122 (2022) 16610–16751. https://doi.org/10.1021/acs.chemrev.2c00289.

[2] A.R. Dehghani-Sanij, E. Tharumalingam, M.B. Dusseault, R. Fraser, Study of energy storage systems and environmental challenges of batteries, Renew. Sustain. Energy Rev. 104 (2019) 192–208. https://doi.org/10.1016/j.rser.2019.01.023.

[3] M. Shahbaz, C. Raghutla, K.R. Chittedi, Z. Jiao, X.V. Vo, The effect of renewable energy consumption on economic growth: Evidence from the renewable energy country attractive index, Energy. 207 (2020) 118162. https://doi.org/10.1016/j.energy.2020.118162.

[4] J.Z. Thellufsen, H. Lund, P. Sorknæs, P.A. Østergaard, M. Chang, D. Drysdale, S. Nielsen, S.R. Djørup, K. Sperling, Smart energy cities in a 100% renewable energy context, Renew. Sustain. Energy Rev. 129 (2020). https://doi.org/10.1016/j.rser.2020.109922.

[5] A. Castillo, D.F. Gayme, Grid-scale energy storage applications in renewable energy integration: A survey, Energy Convers. Manag. 87 (2014) 885–894. https://doi.org/10.1016/j.enconman.2014.07.063.

[6] A.G. Olabi, C. Onumaegbu, T. Wilberforce, M. Ramadan, M.A. Abdelkareem, A.H. Al – Alami, Critical review of energy storage systems, Energy. 214 (2021) 118987. https://doi.org/10.1016/j.energy.2020.118987.

[7] S. Ould Amrouche, D. Rekioua, T. Rekioua, S. Bacha, Overview of energy storage in renewable energy systems, Int. J. Hydrogen Energy. 41 (2016) 20914–20927. https://doi.org/10.1016/j.ijhydene.2016.06.243.

[8] S. Chen, L. Qiu, H.M. Cheng, Carbon-Based Fibers for Advanced Electrochemical Energy Storage Devices, Chem. Rev. 120 (2020) 2811–2878. https://doi.org/10.1021/acs.chemrev.9b00466.

[9] C. Zhang, L. Zhang, Y. Ding, S. Peng, X. Guo, Y. Zhao, G. He, G. Yu, Progress and prospects of next-generation redox flow batteries, Energy Storage Mater. 15 (2018) 324–350. https://doi.org/10.1016/j.ensm.2018.06.008.

[10] E. Sánchez-Díez, E. Ventosa, M. Guarnieri, A. Trovò, C. Flox, R. Marcilla, F. Soavi, P. Mazur, E. Aranzabe, R. Ferret, Redox flow batteries: Status and perspective towards sustainable stationary energy storage, J. Power Sources. 481 (2021). https://doi.org/10.1016/j.jpowsour.2020.228804.

[11] R.K. Sankaralingam, S. Seshadri, J. Sunarso, A.I. Bhatt, A. Kapoor, Overview of the factors affecting the performance of vanadium redox flow batteries, J. Energy Storage. 41 (2021) 102857. https://doi.org/10.1016/j.est.2021.102857.

[12] C. Choi, S. Kim, R. Kim, Y. Choi, S. Kim, H. young Jung, J.H. Yang, H.T. Kim, A review of vanadium electrolytes for vanadium redox flow batteries, Renew. Sustain. Energy Rev. 69 (2017) 263–274. https://doi.org/10.1016/j.rser.2016.11.188.

[13] L. Zhang, R. Feng, W. Wang, G. Yu, Emerging chemistries and molecular designs for flow batteries, Nat. Rev. Chem. 6 (2022) 524–543. https://doi.org/10.1038/s41570-022-00394-6.

[14] J. Yuan, Y. Xue, L. Liu, J. Zhang, Y. Xia, Recent development of electrode materials in semi-solid lithium redox flow batteries, J. Energy Storage. 76 (2024) 109574. https://doi.org/10.1016/j.est.2023.109574.

[15] Z. Li, Y.C. Lu, Material Design of Aqueous Redox Flow Batteries: Fundamental Challenges and Mitigation Strategies, Adv. Mater. 32 (2020) 1–30. https://doi.org/10.1002/adma.202002132.

[16] Z. Qi, G.M. Koenig, Review Article: Flow battery systems with solid electroactive materials, J. Vac. Sci. Technol. B, Nanotechnol. Microelectron. Mater. Process. Meas. Phenom. 35 (2017) 040801. https://doi.org/10.1116/1.4983210.

[17] G. Shukla, A.A. Franco, Interphases in Electroactive Suspension Systems: Where Chemistry Meets Mesoscale Physics, Batter. Supercaps. 2 (2019) 579–590. https://doi.org/10.1002/batt.201800152.

[18] X. Wang, J. Chai, J. "Jimmy" Jiang, Redox flow batteries based on insoluble redox-active materials. A review, Nano Mater. Sci. 3 (2021) 17–24. https://doi.org/10.1016/j.nanoms.2020.06.003.

[19] M. Duduta, B. Ho, V.C. Wood, P. Limthongkul, V.E. Brunini, W.C. Carter, Y.M. Chiang, Semi-solid lithium rechargeable flow battery, Adv. Energy Mater. 1 (2011) 511–516. https://doi.org/10.1002/aenm.201100152.

[20] E. Ventosa, O. Amedu, W. Schuhmann, Aqueous Mixed-Cation Semi-solid Hybrid-Flow Batteries, ACS Appl. Energy Mater. 1 (2018) 5158–5162. https://doi.org/10.1021/acsaem.8b01418.

[21] D. Rueda-Garcia, Z. Cabán-Huertas, S. Sánchez-Ribot, C. Marchante, R. Benages, D.P. Dubal, O. Ayyad, P. Gómez-Romero, Battery and supercapacitor materials in flow cells. Electrochemical energy storage in a LiFePO4/reduced graphene oxide aqueous nanofluid, Electrochim. Acta. 281 (2018) 594–600. https://doi.org/10.1016/j.electacta.2018.05.151.

[22] T. Chen, B. Liu, M. Zheng, Y. Luo, Suspensions based on LiFePO4/carbon nanotubes composites with three-dimensional conductive network for lithium-ion semi-solid flow batteries, J. Energy Storage. 57 (2023) 106300. https://doi.org/10.1016/j.est.2022.106300.

[23] M. Zhou, Y. Chen, Q. Zhang, S. Xi, J. Yu, Y. Du, Y.S. Hu, Q. Wang, Na3V2(PO4)3 as the Sole Solid Energy Storage Material for Redox Flow Sodium-Ion Battery, Adv. Energy Mater. 9 (2019) 1–9. https://doi.org/10.1002/aenm.201901188.

[24] Y. Zhao, S. Si, L. Wang, P. Tang, H. Caoa, Electrochemical behavior of polyaniline microparticle suspension as flowing anode for rechargeable lead dioxide flow battery, J. Electrochem. Soc. 161 (2014) 330–335. https://doi.org/10.1149/2.048403jes.

[25] M. Tian, Y. Sun, C. (John) Zhang, J. Wang, W. Qiao, L. Ling, D. Long, Enabling high-rate electrochemical flow capacitors based on mesoporous carbon microspheres suspension electrodes, J. Power Sources. 364 (2017) 182–190. https://doi.org/10.1016/j.jpowsour.2017.08.001.

[26] K.B. Hatzell, M. Boota, Y. Gogotsi, Materials for suspension (semi-solid) electrodes for energy and water technologies, Chem. Soc. Rev. 44 (2015) 8664–8687. https://doi.org/10.1039/c5cs00279f.

[27] T.S. Wei, F.Y. Fan, A. Helal, K.C. Smith, G.H. McKinley, Y.M. Chiang, J.A. Lewis, Biphasic Electrode Suspensions for Li-Ion Semi-solid Flow Cells with High Energy Density, Fast Charge Transport, and Low-Dissipation Flow, Adv. Energy Mater. 5 (2015). https://doi.org/10.1002/aenm.201500535.

[28] F.Y. Fan, W.H. Woodford, Z. Li, N. Baram, K.C. Smith, A. Helal, G.H. McKinley, W.C. Carter, Y.M. Chiang, Polysulfide flow batteries enabled by percolating nanoscale conductor networks, Nano Lett. 14 (2014) 2210–2218. https://doi.org/10.1021/nl500740t.

[29] L. Madec, M. Youssry, M. Cerbelaud, P. Soudan, D. Guyomard, B. Lestriez, Electronic vs Ionic limitations to electrochemical performance in Li 4Ti5O12-based organic suspensions for lithium-redox flow batteries, J. Electrochem. Soc. 161 (2014). https://doi.org/10.1149/2.035405jes.

[30] C. Zhang, K.B. Hatzell, M. Boota, B. Dyatkin, M. Beidaghi, D. Long, W. Qiao, E.C. Kumbur, Y. Gogotsi, Highly porous carbon spheres for electrochemical capacitors and capacitive flowable suspension electrodes, Carbon N. Y. 77 (2014) 155–164. https://doi.org/10.1016/j.carbon.2014.05.017.

[31] A. Brilloni, F. Poli, G.E. Spina, D. Genovese, G. Pagnotta, F. Soavi, Improving the Electrical Percolating Network of Carbonaceous Slurries by Superconcentrated Electrolytes: An Electrochemical Impedance Spectroscopy Study, ACS Appl. Mater. Interfaces. 13 (2021) 13872–13882. https://doi.org/10.1021/acsami.1c02439.

[32] Z. Qi, G.M. Koenig, A carbon-free lithium-ion solid dispersion redox couple with low viscosity for redox flow batteries, J. Power Sources. 323 (2016) 97–106. https://doi.org/10.1016/j.jpowsour.2016.05.033.

[33] S. Sen, V. Govindarajan, C.J. Pelliccione, J. Wang, D.J. Miller, E. V. Timofeeva, Surface Modification Approach to TiO2 Nanofluids with High Particle Concentration, Low Viscosity, and Electrochemical Activity, ACS Appl. Mater. Interfaces. 7 (2015) 20538–20547. https://doi.org/10.1021/acsami.5b05864.

[34] S. Sen, E. Moazzen, S. Aryal, C.U. Segre, E. V. Timofeeva, Engineering nanofluid electrodes: controlling rheology and electrochemical activity of γ-Fe2O3 nanoparticles, J. Nanoparticle Res. 17 (2015) 1–10. https://doi.org/10.1007/s11051-015-3242-8.

[35] X. Li, J. Xiong, A. Tang, Y. Qin, J. Liu, C. Yan, Investigation of the use of electrolyte viscosity for online state-of-charge monitoring design in vanadium redox flow battery, Appl. Energy. 211 (2018) 1050–1059. https://doi.org/10.1016/j.apenergy.2017.12.009.

[36] Z. Li, K.C. Smith, Y. Dong, N. Baram, F.Y. Fan, J. Xie, P. Limthongkul, W.C. Carter, Y.M. Chiang, Aqueous semi-solid flow cell: Demonstration and analysis, Phys. Chem. Chem. Phys. 15 (2013) 15833–15839. https://doi.org/10.1039/c3cp53428f.

[37] P. Su, H. Zhang, L. Yang, C. Xing, S. Pan, W. Lu, S. Zhang, Effects of conductive additives on the percolation networks and rheological properties of LiMn0.7Fe0.3PO4 suspensions for lithium slurry battery, Chem. Eng. J. 433 (2022) 133203. https://doi.org/10.1016/j.cej.2021.133203.

[38] Y. Wu, D. Cao, X. Bai, H. Liu, H. Hao, J. Xing, J. Dong, L. Liao, Effects of Non-Ionic Surfactants on the Rheological, Electrical and Electrochemical Properties of Highly Loaded Silicon Suspension Electrodes for Semi-Solid Flow Batteries, ChemElectroChem. 7 (2020) 3623–3631. https://doi.org/10.1002/celc.202000873.

[39] M. Meslam, A.A. Elzatahry, M. Youssry, Promising aqueous dispersions of carbon black for semisolid flow battery application, Colloids Surfaces A Physicochem. Eng. Asp. 648 (2022) 129376. https://doi.org/10.1016/j.colsurfa.2022.129376.

[40] P. Su, D. Jiang, L. Yang, S. Pan, K. Yang, S. Xin, H. Zhang, Dimensional effects on the electronic conductivity and rheological behaviors of LiFePO4 catholytes for rechargeable lithium slurry flow battery, Electrochim. Acta. 428 (2022) 140956. https://doi.org/10.1016/J.ELECTACTA.2022.140956.

[41] H. Liu, X. Cheng, Y. Chong, H. Yuan, J.Q. Huang, Q. Zhang, Advanced electrode processing of lithium ion batteries: A review of powder technology in battery fabrication, Particuology. 57 (2021) 56–71. https://doi.org/10.1016/j.partic.2020.12.003.

[42] F.Y. Su, L.Q. Dai, X.Q. Guo, L.J. Xie, G.H. Sun, C.M. Chen, Micro-structure evolution and control of lithium-ion battery electrode laminate, J. Energy Storage. 14 (2017) 82–93. https://doi.org/10.1016/j.est.2017.09.016.

[43] S. Yari, H. Hamed, J. D'Haen, M.K. Van Bael, F.U. Renner, A. Hardy, M. Safari, Constructive versus Destructive Heterogeneity in Porous Electrodes of Lithium-Ion Batteries, ACS Appl. Energy Mater. 3 (2020) 11820–11829. https://doi.org/10.1021/acsaem.0c01966.

[44] F. Duffner, N. Kronemeyer, J. Tübke, J. Leker, M. Winter, R. Schmuch, Post-lithium-ion battery cell production and its compatibility with lithium-ion cell production infrastructure, Nat. Energy. 6 (2021) 123–134. https://doi.org/10.1038/s41560-020-00748-8.

[45] Y. He, L. Jing, Y. Ji, Z. Zhu, L. Feng, X. Fu, Y. Wang, Revisiting the electrode manufacturing: A look into electrode rheology and active material microenvironment, J. Energy Chem. 72 (2022) 41–55. https://doi.org/10.1016/j.jechem.2022.04.038.

[46] A. Kraytsberg, Y. Ein-Eli, Conveying Advanced Li-ion Battery Materials into Practice The Impact of Electrode Slurry Preparation Skills, Adv. Energy

Mater. 6 (2016). https://doi.org/10.1002/aenm.201600655.

[47] H.U. Kayacı, S. Çınar, Inter-particle spacing in aqueous suspensions of nanopowders and its effects on particle packing, green body formation and fabrication of alumina, Ceram. Int. 46 (2020) 20357–20368. https://doi.org/10.1016/j.ceramint.2020.05.126.

[48] S. Çinar, D.D. Anderson, M. Akinc, Combined effect of fructose and NaCl on the viscosity of alumina nanopowder suspensions, J. Eur. Ceram. Soc. 35 (2015) 377–382. https://doi.org/10.1016/j.jeurceramsoc.2014.08.018.

[49] K.B. Anoop, S. Kabelac, T. Sundararajan, S.K. Das, Rheological and flow characteristics of nanofluids: Influence of electroviscous effects and particle agglomeration, J. Appl. Phys. 106 (2009). https://doi.org/10.1063/1.3182807.

[50] S. Çinar, D.D. Anderson, M. Akinc, Influence of bound water layer on the viscosity of oxide nanopowder suspensions, J. Eur. Ceram. Soc. 35 (2015) 613–622. https://doi.org/10.1016/j.jeurceramsoc.2014.09.031.

[51] M. Mourshed, S.M.R. Niya, R. Ojha, G. Rosengarten, J. Andrews, B. Shabani, Carbon-based slurry electrodes for energy storage and power supply systems, Energy Storage Mater. 40 (2021) 461–489. https://doi.org/10.1016/j.ensm.2021.05.032.

[52] N.A.T. Tran, T.M. Khoi, N.M. Phuoc, H. Bin Jung, Y. Cho, A review of recent advances in electrode materials and applications for flow-electrode desalination systems, Desalination. 541 (2022) 116037. https://doi.org/10.1016/j.desal.2022.116037.

[53] W.B. Hawley, J. Li, Electrode manufacturing for lithium-ion batteries—Analysis of current and next generation processing, J. Energy Storage. 25 (2019) 100862. https://doi.org/10.1016/j.est.2019.100862.

[54] Z. Qi, A.L. Liu, G.M. Koenig, Carbon-free Solid Dispersion LiCoO2 Redox Couple Characterization and Electrochemical Evaluation for All Solid Dispersion Redox Flow Batteries, Electrochim. Acta. 228 (2017) 91–99.

https://doi.org/10.1016/j.electacta.2017.01.061.

[55] N. Mohamed, N.K. Allam, Recent advances in the design of cathode materials for Li-ion batteries, RSC Adv. 10 (2020) 21662–21685. https://doi.org/10.1039/d0ra03314f.

[56] H. Chen, Y. Liu, X. Zhang, Q. Lan, Y. Chu, Y. Li, Q. Wu, Single-component slurry based lithium-ion flow battery with 3D current collectors, J. Power Sources. 485 (2021) 229319. https://doi.org/10.1016/j.jpowsour.2020.229319.

[57] J.J. Biendicho, C. Flox, L. Sanz, J.R. Morante, Static and dynamic studies on LiNi1/3Co1/3Mn1/3O2-based suspensions for semi-solid flow batteries, ChemSusChem. 9 (2016) 1938–1944. https://doi.org/10.1002/cssc.201600285.

[58] M. Youssry, L. Madec, P. Soudan, M. Cerbelaud, D. Guyomard, B. Lestriez, Non-aqueous carbon black suspensions for lithium-based redox flow batteries: Rheology and simultaneous rheo-electrical behavior, Phys. Chem. Chem. Phys. 15 (2013) 14476–14486. https://doi.org/10.1039/c3cp51371h.

[59] P. Singh, K. Pal, Activated carbon-Polyaniline composite active material slurry electrode for high capacitance, improved rheological performance electrochemical flow capacitor, Electrochim. Acta. 354 (2020) 136719. https://doi.org/10.1016/j.electacta.2020.136719.

[60] M. Boota, K.B. Hatzell, M. Beidaghi, C.R. Dennison, E.C. Kumbur, Y. Gogotsi, Activated Carbon Spheres as a Flowable Electrode in Electrochemical Flow Capacitors, J. Electrochem. Soc. 161 (2014) A1078–A1083. https://doi.org/10.1149/2.072406jes.

[61] P. Su, D. Jiang, L. Yang, S. Pan, K. Yang, S. Xin, H. Zhang, Dimensional effects on the electronic conductivity and rheological behaviors of LiFePO4 catholytes for rechargeable lithium slurry flow battery, Electrochim. Acta. 428 (2022) 140956. https://doi.org/10.1016/j.electacta.2022.140956.

[62] M. Youssry, L. Madec, P. Soudan, M. Cerbelaud, D. Guyomard, B. Lestriez, Formulation of flowable anolyte for redox flow batteries: Rheo-electrical study, J. Power Sources. 274 (2015) 424–431. https://doi.org/10.1016/j.jpowsour.2014.10.076.

[63] B. Xue, X. Wu, Y. Ren, Y. Guo, C. Zhang, High-capacity semi – Solid cathodes slurry evaluation in pouch cell, J. Power Sources. 563 (2023) 232816. https://doi.org/10.1016/j.jpowsour.2023.232816.

[64] S. Hamelet, J.B. Leriche, D. Larcher, J.M. Tarascon, T. Tzedakis, S. Sailler, P.L. Taberna, P. Simon, P.L. Taberna, Non-Aqueous Li-Based Redox Flow Batteries, J. Electrochem. Soc. 159 (2012) A1360–A1367. https://doi.org/10.1149/2.071208jes.

[65] J.W. Campos, M. Beidaghi, K.B. Hatzell, C.R. Dennison, B. Musci, V. Presser, E.C. Kumbur, Y. Gogotsi, Investigation of carbon materials for use as a flowable electrode in electrochemical flow capacitors, Electrochim. Acta. 98 (2013) 123–130. https://doi.org/10.1016/j.electacta.2013.03.037.

[66] B. Akuzum, P. Singh, D.A. Eichfeld, L. Agartan, S. Uzun, Y. Gogotsi, E.C. Kumbur, Percolation Characteristics of Conductive Additives for Capacitive Flowable (Semi-Solid) Electrodes, ACS Appl. Mater. Interfaces. 12 (2020) 5866–5875. https://doi.org/10.1021/acsami.9b19739.

[67] L. Madec, M. Youssry, M. Cerbelaud, P. Soudan, D. Guyomard, B. Lestriez, Surfactant for enhanced rheological, electrical, and electrochemical performance of suspensions for semisolid redox flow batteries and supercapacitors, Chempluschem. 80 (2015) 396–401. https://doi.org/10.1002/cplu.201402042.

[68] J. Jiang, G. Oberdörster, P. Biswas, Characterization of size, surface charge, and agglomeration state of nanoparticle dispersions for toxicological studies, J. Nanoparticle Res. 11 (2009) 77–89. https://doi.org/10.1007/s11051-008-9446-4.

[69] S.P. Chen, D. Lv, J. Chen, Y.H. Zhang, F.N. Shi, Review on Defects and

Modification Methods of LiFePO4Cathode Material for Lithium-Ion Batteries, Energy and Fuels. 36 (2022) 1232–1251. https://doi.org/10.1021/acs.energyfuels.1c03757.

[70] J. Yue, L. Suo, Progress in Rechargeable Aqueous Alkali-Ion Batteries in China, Energy and Fuels. 35 (2021) 9228–9239. https://doi.org/10.1021/acs.energyfuels.1c00817.

[71] D. Chao, W. Zhou, F. Xie, C. Ye, H. Li, M. Jaroniec, S.Z. Qiao, Roadmap for advanced aqueous batteries: From design of materials to applications, Sci. Adv. 6 (2020). https://doi.org/10.1126/sciadv.aba4098.

[72] A. Kukay, R. Sahore, A. Parejiya, W. Blake Hawley, J. Li, D.L. Wood, Aqueous Ni-rich-cathode dispersions processed with phosphoric acid for lithium-ion batteries with ultra-thick electrodes, J. Colloid Interface Sci. 581 (2021) 635–643. https://doi.org/10.1016/j.jcis.2020.07.144.

[73] J. Li, B.L. Armstrong, C. Daniel, J. Kiggans, D.L. Wood, Optimization of multicomponent aqueous suspensions of lithium iron phosphate (LiFePO4) nanoparticles and carbon black for lithium-ion battery cathodes, J. Colloid Interface Sci. 405 (2013) 118–124. https://doi.org/10.1016/j.jcis.2013.05.030.

[74] J. Li, B.L. Armstrong, J. Kiggans, C. Daniel, D.L. Wood, Optimization of LiFePO 4 nanoparticle suspensions with polyethyleneimine for aqueous processing, Langmuir. 28 (2012) 3783–3790. https://doi.org/10.1021/la205157d.

[75] F. Wang, K. Yang, M. Ge, J. Wang, J. Wang, X. Xiao, W.K. Lee, L. Li, M. Tang, Reaction Heterogeneity in LiFePO4Agglomerates and the Role of Intercalation-Induced Stress, ACS Energy Lett. (2022) 1648–1656. https://doi.org/10.1021/acsenergylett.2c00226.

[76] G. Wu, N. Liu, X. Gao, X. Tian, Y. Zhu, Y. Zhou, Q. Zhu, A hydrothermally synthesized LiFePO 4 /C composite with superior low-temperature performance and cycle life, Appl. Surf. Sci. 435 (2018) 1329–1336. https://doi.org/10.1016/j.apsusc.2017.11.276.

[77] H. Gong, H. Xue, T. Wang, J. He, In-situ synthesis of monodisperse micro-nanospherical LiFePO4/carbon cathode composites for lithium-ion batteries, J. Power Sources. 318 (2016) 220–227. https://doi.org/10.1016/j.jpowsour.2016.03.100.

[78] X. Huang, Y. Yao, F. Liang, Y. Dai, Concentration-controlled morphology of LiFePO4 crystals with an exposed (100) facet and their enhanced performance for use in lithium-ion batteries, J. Alloys Compd. 743 (2018) 763–772. https://doi.org/10.1016/j.jallcom.2018.02.048.

[79] X. Huang, K. Zhang, F. Liang, Y. Dai, Y. Yao, Optimized solvothermal synthesis of LiFePO4 cathode material for enhanced high-rate and low temperature electrochemical performances, Electrochim. Acta. 258 (2017) 1149–1159. https://doi.org/10.1016/j.electacta.2017.11.167.

[80] W. Zhou, C. Liu, Z. Wen, J. Xu, T. Han, G. Li, D. Huang, X. Liang, Z. Lan, H. Ning, H. Huang, J. Guo, Effects of defect chemistry and kinetic behavior on electrochemical properties for hydrothermal synthesis of LiFePO 4 /C cathode materials, Mater. Chem. Phys. 227 (2019) 56–63. https://doi.org/10.1016/j.matchemphys.2019.01.050.

[81] I.A. Rahman, P. Vejayakumaran, C.S. Sipaut, J. Ismail, C.K. Chee, Effect of the drying techniques on the morphology of silica nanoparticles synthesized via sol-gel process, Ceram. Int. 34 (2008) 2059–2066. https://doi.org/10.1016/j.ceramint.2007.08.014.

[82] M.S. Kaliszewski, A.H. Heuer, n, (1990) 1504–1509.

[83] G. Nyongombe, G.L. Kabongo, L.L. Noto, M.S. Dhlamini, Investigating the Impact of the Washing Steps of Layered Double Hydroxides (LDH) on the Electrochemical Performance, Nanomaterials. 12 (2022). https://doi.org/10.3390/nano12030578.

[84] A. Seiphoori, X. guang Ma, P.E. Arratia, D.J. Jerolmack, Formation of stable aggregates by fluid-assembled solid bridges, Proc. Natl. Acad. Sci. U. S. A. 117 (2020) 3375–3381. https://doi.org/10.1073/pnas.1913855117.

[85] S. Bolloju, R. Rohan, S.T. Wu, H.X. Yen, G.D. Dwivedi, Y.A. Lin, J.T. Lee, A green and facile approach for hydrothermal synthesis of LiFePO4 using iron metal directly, Electrochim. Acta. 220 (2016) 164–168. https://doi.org/10.1016/j.electacta.2016.10.066.

[86] T. Wu, X. Ma, X. Liu, G. Zeng, W. Xiao, Effect of calcination temperature on electrochemical performances of LiFePO4/C cathode material, Mater. Technol. 30 (2015) A70–A74. https://doi.org/10.1179/17535557A15Y.000000011.

[87] R. Martins, R. Gonçalves, C.M. Costa, S. Ferdov, S. Lanceros-Méndez, Mild hydrothermal synthesis and crystal morphology control of LiFePO4 by lithium nitrate, Nano-Structures and Nano-Objects. 11 (2017) 82–87. https://doi.org/10.1016/j.nanoso.2017.07.001.

[88] Y. Liu, M. Zhang, Y. Li, Y. Hu, M. Zhu, H. Jin, W. Li, Nano-sized LiFePO4/C composite with core-shell structure as cathode material for lithium ion battery, Electrochim. Acta. 176 (2015) 689–693. https://doi.org/10.1016/j.electacta.2015.07.064.

[89] E. Coşkun, E. Kurşun, B. Yıldız, Y. Aşkar, D. Bahtiyar, M.K. Aydınol, B. Mavis, S. Çınar-Aygün, Size and morphology controlled polyol synthesis of LiFePO4 nanoparticles with addition of organic acid combinations, Ceram. Int. (2024). https://doi.org/10.1016/j.ceramint.2024.02.072.

[90] M.J. Uddin, P.K. Alaboina, S.J. Cho, Nanostructured cathode materials synthesis for lithium-ion batteries, Mater. Today Energy. 5 (2017) 138–157. https://doi.org/10.1016/j.mtener.2017.06.008.

[91] O. Vasylkiv, Y. Sakka, Synthesis and Colloidal Processing of Zirconia Nanopowder, J. Am. Ceram. Soc. 84 (2001) 2489–2494. https://doi.org/10.1111/j.1151-2916.2001.tb01041.x.

[92] M. J. Readey, R. R. Lee, J. W. Halloran, & A. H. Heuer, Processing and sintering of ultrafine MgO- ZrO2 and (MgO, Y2O3)- ZrO2 powders. Journal of the American Ceramic Society, 73(6) (1990), 1499-1503.

[93] A. Serrano-Lotina, R. Portela, P. Baeza, V. Alcolea-Rodriguez, M. Villarroel, P. Ávila, Zeta potential as a tool for functional materials development, Catal. Today. 423 (2023). https://doi.org/10.1016/j.cattod.2022.08.004.

[94] K. Cacua, F. Ordoñez, C. Zapata, B. Herrera, E. Pabón, R. Buitrago-Sierra, Surfactant concentration and pH effects on the zeta potential values of alumina nanofluids to inspect stability, Colloids Surfaces A Physicochem. Eng. Asp. 583 (2019). https://doi.org/10.1016/j.colsurfa.2019.123960.

[95] C. Berthomieu, R. Hienerwadel, Fourier transform infrared (FTIR) spectroscopy, Photosynth. Res. 101 (2009) 157–170. https://doi.org/10.1007/s11120-009-9439-x.

[96] Y. Zhang, Q.Y. Huo, P.P. Du, L.Z. Wang, A.Q. Zhang, Y.H. Song, Y. Lv, G.Y. Li, Advances in new cathode material LiFePO 4 for lithium-ion batteries, Synth. Met. 162 (2012) 1315–1326. https://doi.org/10.1016/j.synthmet.2012.04.025.

[97] J. Wang, X. Sun, Understanding and recent development of carbon coating on LiFePO 4 cathode materials for lithium-ion batteries, Energy Environ. Sci. 5 (2012) 5163–5185. https://doi.org/10.1039/c1ee01263k.

[98] L. Li, L. Wu, F. Wu, S. Song, X. Zhang, C. Fu, D. Yuan, Y. Xiang, Review—Recent Research Progress in Surface Modification of LiFePO 4 Cathode Materials , J. Electrochem. Soc. 164 (2017) A2138–A2150. https://doi.org/10.1149/2.1571709jes.

[99] W. Duan, M. Zhao, Y. Mizuta, Y. Li, T. Xu, F. Wang, T. Moriga, X. Song, Superior electrochemical performance of a novel LiFePO4/C/CNTs composite for aqueous rechargeable lithium-ion batteries, Phys. Chem. Chem. Phys. 22 (2020) 1953–1962. https://doi.org/10.1039/c9cp06042a.

[100] L. Geng, S.B. Foley, H. Dong, G.M. Koenig, LiFePO 4 -Accelerated Change in Surface and Electrochemical Properties in Aqueous Systems Induced by Mechanical Agitation, Energy Technol. 7 (2019) 1–10. https://doi.org/10.1002/ente.201801116.

[101] W. Porcher, P. Moreau, B. Lestriez, S. Jouanneau, F. Le Cras, D. Guyomard, Stability of LiFePO4 in water and consequence on the Li battery behaviour, Ionics (Kiel). 14 (2008) 583–587. https://doi.org/10.1007/s11581-008-0215-2.

[102] S. Hamelet, D. Larcher, L. Dupont, J.M. Tarascon, Silicon-based non aqueous anolyte for li redox-flow batteries, J. Electrochem. Soc. 160 (2013) 516–520. https://doi.org/10.1149/2.002304jes.

[103] D. Cao, X. Bai, J. Wang, H. Liu, L. Liao, High Performance Aqueous Li-Ion Flow Capacitor Realized Through Microstructure Design of Suspension Electrode, Front. Chem. 9 (2021) 1–8. https://doi.org/10.3389/fchem.2021.673179.

[104] J. Jacas Biendicho, A. Hemesh, V. Izquierdo, C. Flox, J.R. Morante, Contact resistance stability and cation mixing in a Vulcan-based LiNi1/3Co1/3Mn1/3O2slurry for semi-solid flow batteries, Dalt. Trans. 50 (2021) 6710–6717. https://doi.org/10.1039/d1dt00495f.

[105] M. Youssry, F.Z. Kamand, M.I. Magzoub, M.S. Nasser, Aqueous dispersions of carbon black and its hybrid with carbon nanofibers, RSC Adv. 8 (2018) 32119–32131. https://doi.org/10.1039/c8ra05446k.

[106] H. Parant, G. Muller, T. Le Mercier, J.M. Tarascon, P. Poulin, A. Colin, Flowing suspensions of carbon black with high electronic conductivity for flow applications: Comparison between carbons black and exhibition of specific aggregation of carbon particles, Carbon N. Y. 119 (2017) 10–20. https://doi.org/10.1016/j.carbon.2017.04.014.

[107] W. Bauer, F.A. Çetinel, M. Müller, U. Kaufmann, Effects of pH control by acid addition at the aqueous processing of cathodes for lithium ion batteries, Electrochim. Acta. 317 (2019) 112–119. https://doi.org/10.1016/j.electacta.2019.05.141.

[108] H.Y. Li, H.Z. Chen, W.J. Xu, F. Yuan, J.R. Wang, M. Wang, Polymer-encapsulated hydrophilic carbon black nanoparticles free from aggregation,

Colloids Surfaces A Physicochem. Eng. Asp. 254 (2005) 173–178. https://doi.org/10.1016/j.colsurfa.2004.12.002.

[109] Y. Hanada, S. Masuda, M. Iijima, H. Kamiya, Analysis of dispersion and aggregation behavior of carbon black particles in aqueous suspension by colloid probe AFM method, Adv. Powder Technol. 24 (2013) 844–851. https://doi.org/10.1016/j.apt.2013.02.010.

[110] A.O. Borode, N.A. Ahmed, P.A. Olubambi, Surfactant-aided dispersion of carbon nanomaterials in aqueous solution, Phys. Fluids. 31 (2019). https://doi.org/10.1063/1.5105380.

[111] H. Liu, K. Zhao, Asymmetric flow electrochemical capacitor with high energy densities based on birnessite-type manganese oxide nanosheets and activated carbon slurries, J. Mater. Sci. 51 (2016) 9306–9313. https://doi.org/10.1007/s10853-016-0177-0.

[112] H. Chen, N.C. Lai, Y.C. Lu, Silicon-Carbon Nanocomposite Semi-Solid Negolyte and Its Application in Redox Flow Batteries, Chem. Mater. 29 (2017) 7533–7542. https://doi.org/10.1021/acs.chemmater.7b02561.

[113] V. Presser, C.R. Dennison, J. Campos, K.W. Knehr, E.C. Kumbur, Y. Gogotsi, The electrochemical flow capacitor: A new concept for rapid energy storage and recovery, Adv. Energy Mater. 2 (2012) 895–902. https://doi.org/10.1002/aenm.201100768.

[114] H. Yoon, H.J. Kim, J.J. Yoo, C.Y. Yoo, J.H. Park, Y.A. Lee, W.K. Cho, Y.K. Han, D.H. Kim, Pseudocapacitive slurry electrodes using redox-active quinone for high-performance flow capacitors: An atomic-level understanding of pore texture and capacitance enhancement, J. Mater. Chem. A. 3 (2015) 23323–23332. https://doi.org/10.1039/c5ta05403f.

[115] B. Akuzum, L. Agartan, J. Locco, E.C. Kumbur, Effects of particle dispersion and slurry preparation protocol on electrochemical performance of capacitive flowable electrodes, J. Appl. Electrochem. 47 (2017) 369–380. https://doi.org/10.1007/s10800-017-1046-5.

[116] M. Youssry, D. Guyomard, B. Lestriez, Suspensions of carbon nanofibers in organic medium: Rheo-electrical properties, Phys. Chem. Chem. Phys. 17 (2015) 32316–32327. https://doi.org/10.1039/c5cp06303e.

[117] D. Gordon, M.Y. Wu, A. Ramanujapuram, J. Benson, J.T. Lee, A. Magasinski, N. Nitta, C. Huang, G. Yushin, Enhancing cycle stability of lithium iron phosphate in aqueous electrolytes by increasing electrolyte molarity, Adv. Energy Mater. 6 (2016) 1–11. https://doi.org/10.1002/aenm.201501805.

[118] S. Lee, J. Jang, D. Lee, J. Kim, J. Mun, Synergetic effect of aqueous electrolyte and ultra-thick millimeter-scale LiFePO4 cathode in aqueous lithium-ion batteries, Int. J. Energy Res. 46 (2022) 6480–6486. https://doi.org/10.1002/er.7584.

[119] H. Kato, A. Nakamura, M. Shimizu, Effect of surfactant micelle size on the dispersibility of aqueous carbon black particle suspensions prepared by ultrasonication, Powder Technol. 399 (2022) 117206. https://doi.org/10.1016/j.powtec.2022.117206.

[120] Y. Aşkar, Utilization of Colloidal Principles in Carbon Coating of Electroactive Materials, M.S. - Master of Science, Middle East Technical University (2022).

[121] M.D. Via, J.A. King, J.M. Keith, G.R. Bogucki, Electrical conductivity modeling of carbon black/polycarbonate, carbon nanotube/polycarbonate, and exfoliated graphite nanoplatelet/polycarbonate composites, J. Appl. Polym. Sci. 124 (2012) 182–189. https://doi.org/10.1002/APP.35096.

[122] S. Mortazavi-Manesh, J.M. Shaw, Thixotropic rheological behavior of maya crude oil, Energy and Fuels. 28 (2014) 972–979. https://doi.org/10.1021/ef4022637.

[123] I.M. Krieger, T.J. Dougherty, A Mechanism for Non- Newtonian Flow in Suspensions of Rigid Spheres, Trans. Soc. Rheol. 3 (1959) 137–152. https://doi.org/10.1122/1.548848.

[124] S. Pan, H. Zhang, C. Xing, L. Yang, P. Su, J. Bi, S. Zhang, Ultrahigh-capacity semi-solid SiOx anolytes enabled by robust nanotube conductive networks for Li-ion flow batteries, J. Power Sources. 508 (2021) 230341. https://doi.org/10.1016/j.jpowsour.2021.230341.

[125] J.K. Koo, H. Choi, J. kwon Seo, S.M. Hwang, J. Lee, Y.J. Kim, Microstructure engineering of nickel-rich oxide/carbon composite cathodes for fast charging of lithium-ion batteries, Ceram. Int. 48 (2022) 31859–31865. https://doi.org/10.1016/j.ceramint.2022.07.119.

[126] W.J. Zhang, Structure and performance of LiFePO4 cathode materials: A review, J. Power Sources. 196 (2011) 2962–2970. https://doi.org/10.1016/j.jpowsour.2010.11.113.

[127] A. Tron, Y.N. Jo, S.H. Oh, Y.D. Park, J. Mun, Surface Modification of the LiFePO4 Cathode for the Aqueous Rechargeable Lithium Ion Battery, ACS Appl. Mater. Interfaces. 9 (2017) 12391–12399. https://doi.org/10.1021/acsami.6b16675.

[128] X. Liu, W. Xiong, J. Zheng, J. Wu, B. Huang, Q. Zhu, Y. Li, S. Xiao, Q. Chen, J. Yang, Z. Yang, Electrochemical Performance and Behavior Mechanism for Zn/LiFePO4 Battery in a Slightly Acidic Aqueous Electrolyte, ChemSusChem. 15 (2022). https://doi.org/10.1002/cssc.202102631.

[129] Y. Yin, Y.H. Wen, Y.L. Lu, J. Cheng, G.P. Cao, Y.S. Yang, Electrochemical performance and capacity fading mechanism of LiFePO4 at different pH aqueous electrolyte solutions, Chinese J. Chem. Phys. 28 (2015) 315–322. https://doi.org/10.1063/1674-0068/28/cjcp1502020.

[130] J.Y. Luo, W.J. Cui, P. He, Y.Y. Xia, Raising the cycling stability of aqueous lithium-ion batteries by eliminating oxygen in the electrolyte, Nat. Chem. 2 (2010) 760–765. https://doi.org/10.1038/nchem.763.

[131] A. Tron, S. Jeong, Y.D. Park, J. Mun, Aqueous Lithium-Ion Battery of Nano-LiFePO4 with Antifreezing Agent of Ethyleneglycol for Low-Temperature Operation, ACS Sustain. Chem. Eng. 7 (2019) 14531–14538.

https://doi.org/10.1021/acssuschemeng.9b02042.

[132] A. Tron, Y.D. Park, J. Mun, Influence of organic additive on the electrochemical performance of LiFePO4 cathode in an aqueous electrolyte solution, Solid State Sci. 101 (2020) 106152. https://doi.org/10.1016/j.solidstatesciences.2020.106152.

[133] S. Çinar, L. Van Steenhuyse, M. Akinc, Elucidation of viscosity reduction mechanism of nano alumina suspensions with fructose addition by DSC, J. Am. Ceram. Soc. 96 (2013) 1077–1084. https://doi.org/10.1111/jace.12232.

[134] C. Li, M. Akinc, J. Wiench, M. Pruski, C.H. Schilling, Relationship between water mobility and viscosity of nanometric alumina suspensions, J. Am. Ceram. Soc. 88 (2005) 2762–2768. https://doi.org/10.1111/j.1551-2916.2005.00535.x.

[135] C. Li, M. Akinc, Role of bound water on the viscosity of nanometric alumina suspensions, J. Am. Ceram. Soc. 88 (2005) 1448–1454. https://doi.org/10.1111/j.1551-2916.2005.00339.x.

[136] E. Firlar, S. Çlnar, S. Kashyap, M. Akinc, T. Prozorov, Direct visualization of the hydration layer on alumina nanoparticles with the fluid cell STEM in situ, Sci. Rep. 5 (2015) 1–7. https://doi.org/10.1038/srep09830.

APPENDICES

A. Rheological Behavior Modelling of Suspensions

Table A.1 The power law parameters obtained from the rheological behavior of electrode suspensions.

Sample	K (Pa·s^n)	n	Sample	K (Pa·s^n)	n
30LFP-A	4	0.01	**30LFP-D**	0.5	0.20
40LFP-A	13	0.04	**40LFP-D**	1.8	0.007
50LFP-A	28	0.004	**50LFP-D**	1.2	0.03
1KB–30LFP-A	14	0.05	-	-	-
1KB–40LFP-A	71	0.05	**1KB–40LFP-D**	11	0.06
1KB–45LFP-A	2368	0.002	-	-	-
			1KB–50LFP-D	35	0.07
2KB–20LFP-A	28	0.05	-	-	-
2KB–30LFP-A	166	0.05	**2KB–30LFP-D**	18	0.06
			2KB–40LFP-D	63	0.05
			2KB–45LFP-D	241	0.04

* ***Power law:*** $\eta = K \cdot \dot{\gamma}^{n-1}$ *where η is the suspension viscosity, K is the consistency coefficient and n is the power law index.* R^2 *values for fitting the rheological behavior of suspensions were higher than 0.99.*

B. Potentiostatic Electrochemical Impedance Spectra Curve Fitting of Suspension Electrodes

Table B.1 PEIS Fitting parameters for electrode suspensions prepared with agglomerated and dispersible LFP particles. The used model for fitting is: R1 (R2 // Q2)

Sample	**R_1 (Ω)**	**R_2 (Ω)**	**Q_2 (x10^{-6} F)**	**α_2**
1KB – 30 LFP-A	1.86	39,807	19.89	0.84
1KB – 40 LFP-A	1.97	10,226	19.76	0.81
1KB – 45 LFP-A	2.25	12,685	16.14	0.84
2KB – 20 LFP-A	1.24	2,090	17.95	0.85
2KB – 30 LFP-A	1.37	3,930	15.47	0.87
1KB – 40 LFP-D	1.66	873,839	29.86	0.86
1KB – 50 LFP-D	1.86	1,610,000	23.62	0.89
2KB – 30 LFP-D	1.36	8,152	19.26	0.84
2KB – 40 LFP-D	1.47	7,566	18.74	0.91
2KB – 45 LFP-D	1.47	2,604	15.60	0.91

C. The Variation in the Electrochemical Performance of 2KB – 20LFP-A Suspension Electrode Regarding Fructose Content

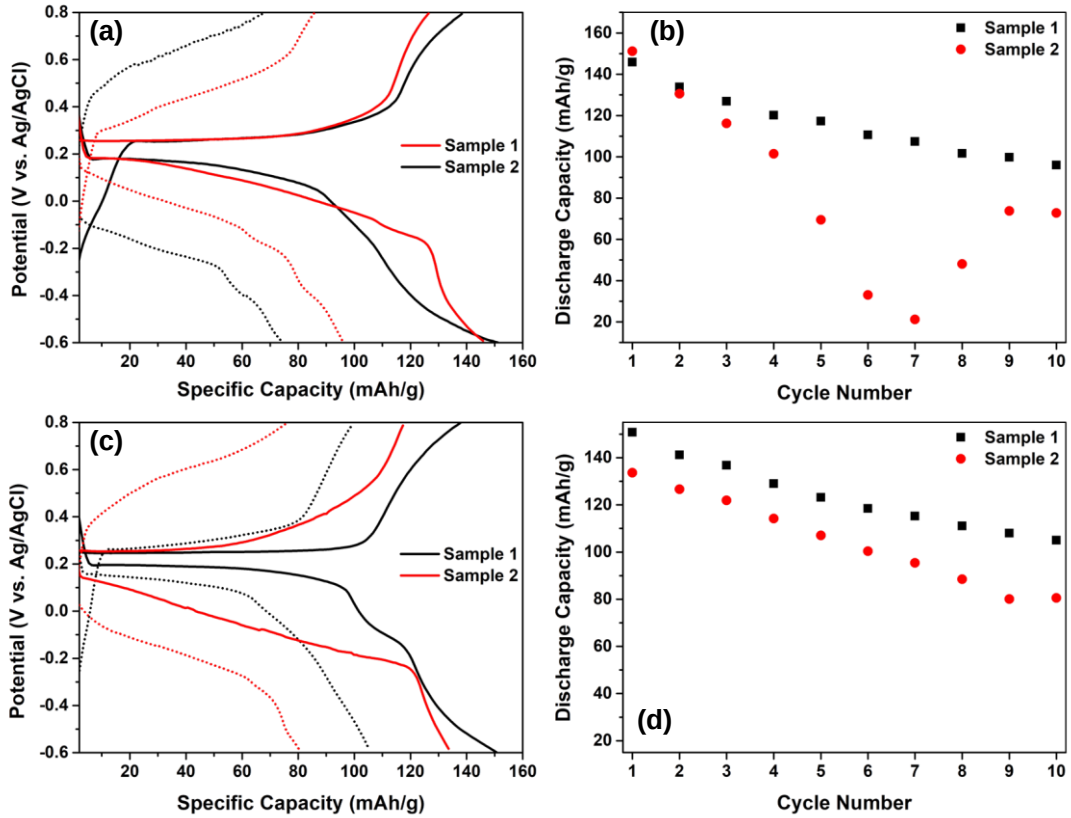

Figure C.1 The charge and discharge profiles of aqueous 2KB – 20LFP-A suspension electrode prepared with (a) 2% Fructose, (c) 4% Fructose (solid lines represent the 1st cycle while dashed lines represent the 10th cycle), the impact of dissolved fructose content on the cyclic stability of aqueous 2KB – 20LFP-A suspension electrode prepared with (b) 2% Fructose, (d) 4% Fructose.

CURRICULUM VITAE (ONLY FOR DOCTORAL THESIS)

Surname, Name: Yıldız, Bayram

EDUCATION

Degree	Institution	Year of Graduation
MS	PAU Mechanical Engineering	2016
BS	DEU Physics	2012

FOREIGN LANGUAGES

Advanced English

PUBLICATIONS

ARTICLES

1. Yıldız, B., Aşkar, Y., Coşkun, E., Durukan, M.B., Ulgüt, B., Unalan, H.E., Maviş, B., Çınar Aygün, S., ”Influence of Agglomeration State of Electroactive Material on the Rheological and Electrical Properties of Aqueous Electrode Suspensions” (Submitted, under review).
2. Aşkar, Y., Yıldız, B., Coşkun, E., Aydınol, M.K., Maviş, B., Çınar Aygün, S., “Utilization of Colloidal Principles in Carbon Coating of Electroactive Materials” (to be submitted).
3. Coşkun, E., Kurşun, E., Yıldız, B., Aşkar, Y., Bahtiyar, D., Aydınol, M.K., Maviş, B., Çınar Aygün, S. (2024) “Size and Morphology Controlled Polyol Synthesis of LiFePO4 Nanoparticles with Addition of Organic Acid Combinations” (Ceramics International, available online 7 February 2024).
4. Durukan, M. B., Keskin, D., Tufan, Y., Dincer, O., Cicek, M. O., Yıldız, B., ... & Unalan, H. E. (2023). ”An Edible Supercapacitor Based on Zwitterionic Soy Sauce-Based Gel Electrolyte”, Advanced Functional Materials, 2307051.

5. Cicek, M. O., Durukan, M. B., Yıldız, B., Keskin, D., Doganay, D., Çınar Aygün, S., Çakir M. P., Unalan, H. E. (2023). ”Ultra-Sensitive Bio-Polymer Iontronic Sensors for Object Recognition from Tactile Feedback”, Advanced Materials Technologies, 8(16), 2300322.
6. Yıldız, B., Balkanci, A., Ovali, I., and Unlü, C. G. (2018). ”Investigation of tribological behaviors of graphene-coated journal ¨bearing”, Tribology-materials, surfaces & interfaces, 12(4), 177-185.

CONFERENCE PROCEEDINGS

Yıldız, B., Aşkar, Y., Coşkun, E., Maviş, B., and Çınar Aygün, S., "Significance of Electroactive Material Selection in Suspension Based Electrochemical Energy Storage Systems" (oral presentation, presenter), 7th International Symposium on Materials for Energy Storage and Conversion (mESC-IS 2023), 17-21 July 2023, Muğla, Türkiye.

Durukan, M.B., Görür, M.C., Ozturk, G., Keskin, D., Bolukbası, T., Yıldız, B., Çınar Aygün S., and Unalan, H.E., “Direct Ink Writing of 1T-MoS2/Ag NW Inks for the Fabrication of Interdigitated Microsupercapacitors” (poster), e-MRS 2022 Fall Meeting, 19-22 September 2022, Warsaw, Poland

Yıldız, B., Aşkar, Y., Coşkun, E., Maviş, B., and Çınar, S., “Investigation of the Performance of Colloidal $LiFePO_4$ Particles in Suspension Flow Battery” (oral presentation, presenter), 20th International Metallurgy and Materials Congress (IMMC 2021) 10-12 June 2021, “in Digital Platform”

Ulusel, M., Şahin, O., Dinçer, O., Yıldız, B., Çınar, S., “Synthesis of Metallic Striped and Janus Particles” (oral presentation), 20th International Metallurgy and Materials Congress (IMMC 2021) 10-12 June 2021, “in Digital Platform”

Aşkar, Y., Yıldız, B., Maviş, B., Çınar, S., “Fabrication of Colloidal and Conductive $LiFePO_4$ Particles for Suspension Flow Batteries” (poster), 20th International Metallurgy and Materials Congress (IMMC 2021) 10-12 June 2021, “in Digital Platform”

Coşkun, E., Yıldız, B., Aşkar, Y., Maviş, B., Çınar, S, "Synthesis of Lithium Iron Phosphate with Controlled Size and Shape" (poster), 20th International Metallurgy and Materials Congress (IMMC 2021) 10-12 June 2021, "in Digital Platform"

Yıldız, B., Aşkar, Y., Maviş, B., and Çınar, S., **"**Synthesis of Electroactive Materials for Suspension-based Flow Assisted Batteries" (oral presentation, presenter), 4th Int. Symposium on Materials for Energy Storage and Conversion (mESC-IS 2019), 11-13 September 2019, Akyaka, Muğla, Türkiye.

Yıldız, B., Aşkar, Y., and Çınar, S., "A new concept in flow assisted energy storage: suspension electrode approach" (poster), 4th Int. Symposium on Materials for Energy Storage and Conversion (mESC-IS 2019), 11-13 September 2019, Akyaka, Muğla, Türkiye.

Aşkar, Y., Yıldız, B., Maviş, B., and Çınar, S., "Fabrication of Conductive Electroactive Materials for Next-Generation Suspension Flow Batteries" (poster), 4th Int. Symposium on Materials for Energy Storage and Conversion (mESC-IS 2019), 11-13 September 2019, Akyaka, Muğla, Türkiye.

Yıldız, B., Balkancı, A., Tanış, Y.E., Ünlü, C.G., Can, A.Ç., Baykara, M.Z., "Investigation of Tribological Properties of Metal Surface Coated with Monolayer Graphene" (poster), 2016 Graphene & Related Materials Conference (GRM-2016) 13-15 July 2016, Ankara, Turkey.

Ünlü, C.G., Yıldız, B., Tanış, Y.E., Acet, M., "Synthesis and Functionalization of Large Area CVD Graphene with Cu Nanoparticles for Biosensor" (poster), 2016 Graphene & Related Materials Conference (GRM-2016) 13-15 July 2016, Ankara, Turkey.

Yıldız, B., Tanış, Y.E., Satılmıs, H., Ünlü, C.G., Özmen, Y., "Synthesis of Graphene Layers for Biomedical Applications" (poster), 1st Conference of Medical and Biological Engineering in Bosnia and Herzegovina (CMBEBIH 2015) 13-15 March 2015, Sarajevo, Bosnia and Herzegovina.